Development of Drug Delivery Vehicles for Biomedical Applications

By

Kelly Anne Gilmore

Dissertation

Submitted to the Faculty of the

Graduate School of Vanderbilt University

in partial fulfillment of the requirements

for the degree of

DOCTOR OF PHILOSOPHY

in

Chemistry

August 11, 2017

Nashville, Tennessee

Approved:

Eva M. Harth, Ph.D.
David W. Wright, Ph.D.
Timothy P. Hanusa, Ph.D.
Leon Bellan, Ph.D.

To Mom and Dad

ACKNOWLEDGMENTS

I would like to acknowledge the financial support for this research from the Warren Graduate Fellowship, the Juvenile Diabetes Research Foundation, and the Vanderbilt Department of Chemistry.

First and foremost, I would like to express my gratitude to Dr. Eva Harth for her guidance, mentorship and advice over these past few years. Thank you for being willing to take on a student with no background in polymer chemistry and giving me the tools I needed to become a polymer scientist. I will carry this knowledge base with me beyond Vanderbilt and it will become the basis for my success.

I would also like to thank my committee members: Dr. David Wright, Dr. Timothy Hanusa, and Dr. Leon Bellan, for gifting to me their time, energy, and advice over the course of my graduate career. Your guidance has helped me to think in new ways and helped me tremendously to grow as a scientist. I am incredibly grateful for the input and critical analysis that you have provided of my research.

I would like to extend a special thank you to Dr. Tara Todd, who I have had the pleasure of working with these past few years. You have helped to shape me into a better teacher and your confidence and trust in me is truly empowering. I am grateful for the creative freedom you have allowed me and it has been wonderful to work with you during my time at Vanderbilt.

None of this work would have been possible without the constant support and encouragement of my incredible family. To my parents, Diane and Patrick Gilmore, thank you for providing me with the opportunities I have had to pursue my passions and for valuing my education. To my siblings, Connor and Meghan, thank you for being there for me and offering a helping hand and an encouraging word when I needed it the most. I would also like to thank Dr.

Sarah Petty, who inspired my interest in research as an undergraduate at Holy Cross and helped to shape my decision to pursue graduate education.

To the members of the Harth lab, both past and present, thank you for walking this path with me. I am incredibly lucky to work with a group of such wonderful people. The friendships I have forged while here will be one of the most potent lasting memories of my graduate education, and I hope that they continue in the years to come.

Lastly, to Nick: Thank you for your unfailing love and support over these past few years at Vanderbilt. I would not have been able to accomplish this without you by my side. Words cannot express how blessed I am to have you in my life.

LIST OF FIGURES

LIST OF TABLES

TABLE OF CONTENTS

Page

CHAPTER I

INTRODUCTION

Polymeric Nanoparticles in Drug Delivery

Polymeric networks have been utilized extensively over the last several years to create a wide array of functional macromolecular materials intended for use in biomedical applications.[1-10] These types of materials range in size from bulk materials to discrete micron or nanoscale structures, and have been utilized in applications such as drug delivery,[2-3, 9] tissue engineering,[10] and diagnostics.[1, 6-7] Of these, perhaps the most prominent field of application for these types of materials is in drug delivery. Polymeric nanoparticles in particular have emerged as valuable tools for the solubilization and delivery of small molecule hydrophobic drugs.[11-18] Entrapping a hydrophobic drug inside of a nanoparticle matrix can aid in both solubility and bioavailability of the drug, usually by decreasing the crystallinity of the entrapped cargo. However, many of these structures suffer from limitations including non-degradability, uncontrolled release rates of the cargo, and untargeted action.

There are multiple examples that can be found in the literature of nanoparticle structures that aim to address one or sometimes two of these shortcomings, but structures that are able to overcome all three are much more limited. Biodegradable nanoparticles have been successfully constructed from polymers such as polyamides,[19-20] polyurethanes,[21-22] and polycarbonates.[23] Another prominent class of polymer used to construct biodegradable structures is polyesters. Polyesters have long been used as materials for biomedical applications due to their well demonstrated biocompatibility and hydrolytic degradation mechanism and have been shown to

be useful for the formation of biodegradable nanoparticles.[24-26] A nanoparticle platform synthesized from polyester precursors that exhibits control over the release rate of its cargo as well as targeted delivery could prove to be a desirable structure for multiple applications. For example, much of the current research for diabetes treatment involves the search for small molecules that can successfully aid in the regeneration of beta-cell (insulin producing cell) function. However, clinical use of many of these small molecules is not practical because of unacceptable off-target effects, or solubility concerns. Delivery of these therapeutics inside of a specifically targeted nanoparticle platform that could provide a sustained release of the drug at the beta-cell surface would be an invaluable resource in the treatment of diabetes.

Another field of research that could benefit greatly from this type of platform is in the treatment of unstable arterial plaques. Therapies aimed at preventing plaque rupture usually involve the systemic administration of broad spectrum metalloproteinase inhibitors, which suffer from multiple side effects and therefore a decreased efficacy. Encapsulation of one of these inhibitors into a nanoparticle structure that has specific homing ability towards unstable plaques in the arteries would serve to greatly enhance the efficacy of the currently available drugs while modulating the adverse effects caused by action of the drug at multiple sites.

Such a structure should ideally have multiple reactive handholds on the surface for the attachment of targeting units such as peptide agonists that would impart homing ability to the particle. A mechanism should also be present for controlling and tailoring the release rate of an entrapped cargo from these carriers. Polyesters that are made using a ring-opening polymerization method and then crosslinked via amine-epoxide chemistry to form degradable nanoparticles have the unique property of being able to control the diffusion of encapsulated cargo based upon the functionalization of the polymer precursor.[24] Functional groups that serve

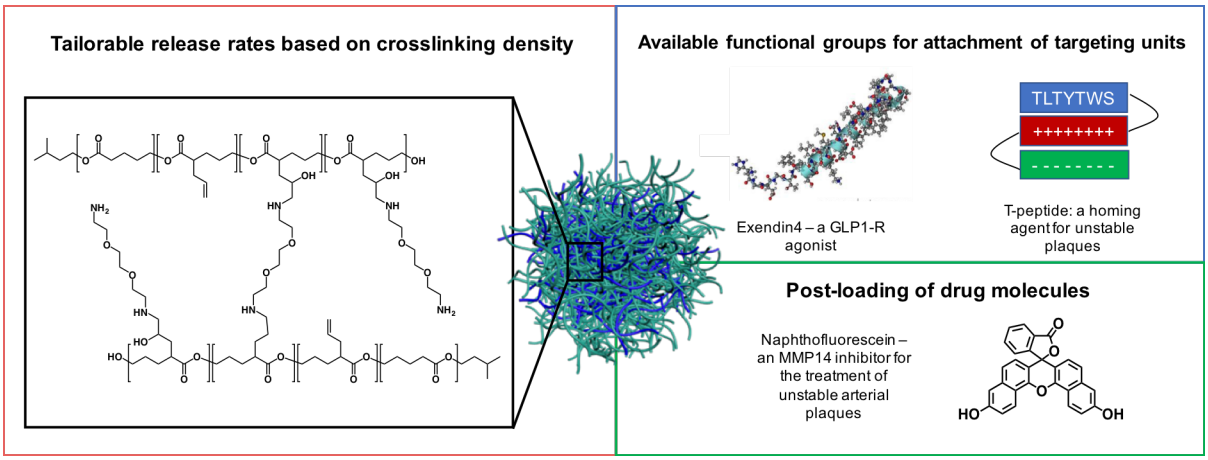

Figure I-1. An outline of the desirable properties of the proposed nanoparticle platform for applications in the treatment of diabetes and unstable arterial plaques.

as reactive handles for conjugation of targeting units to the surface are also present after the nanoparticle formation reaction. This particle platform shows great promise as a degradable, targeted delivery vehicle capable of sustained release of a therapeutic at a specific site.

Hydrogel Structures for Protein Delivery

Biodegradable polymeric nanoparticles have shown great success for the delivery of small molecule drugs. However, this type of structure is not the most ideal delivery system for larger therapeutics, such as proteins or peptides, as entrapment of these moieties on the nanoscale has proven to be difficult. The polymeric scaffolds that have been most widely utilized for the delivery of large hydrophilic biological structures include microparticles[27-29] and hydrogels.[30-32] Hydrogels are materials that can swell to many times their weight when placed in an aqueous solution, which provides an excellent environment for the entrapment of large hydrophilic structures for drug delivery. However, this high degree of swelling is often accompanied by a rapid rate of diffusion of the entrapped cargo, leading to a burst-like rather than a sustained

release profile. Several conditions that are treated using protein drugs, including cystic fibrosis, thrombosis, and even certain types of cancer,[33] could benefit from the delivery of these therapeutics over a more sustained period of time. Entrapment of these drugs within a hydrogel structure that could deliver them in a sustained way could lead to benefits such as lower toxicity, reduced side effects, and decreased dosage requirements.

One specific example of a treatment that could be improved by this kind of material is the delivery of bone morphogenetic protein 2 (BMP2) for the treatment of fractures in patients with neurofibromatosis 1. BMP2 is a growth factor intended to aid in the calcification of bone following a fracture. Previous work has shown that delivery of BMP2 by injection into the fracture site leads to rapid diffusion and undesired calcification of the surrounding muscle tissue.[34] Therefore, it follows that there is a need for a suitable delivery system that can provide a more controlled release of this protein into the treatment site. Another desirable characteristic of this hydrogel system is that the properties of the matrix be tunable, so that the release rate of the BMP2 from the system can be easily modulated where necessary.

The high degree of swelling and subsequent burst release of proteins from typical hydrogel structures mainly derives from the polymeric precursor used to construct the gel matrix. PEG-based crosslinkers are the most commonly used molecules to construct these matrices, but the limited functionality (2-4 functional groups per molecule) leads to large pore sizes and poor entrapment of the protein. A more highly functionalized hydrophilic polymer such as polyglycidol would be more suitable as a crosslinker over these linear PEG structures for sequestration and sustained release of proteins.

Polyglycidol has traditionally been synthesized as a hyperbranched structure, and has been well-studied in this form.[35-37] Applications of this polymer are numerous, due to the high

biocompatibility and similarity in structure and properties to PEG. Hyperbranched polyglycidol and its derivatives have proven to be of great use for biological applications. For example, surface modified hyperbranched polyglycidol has been used as an inverted micelle for the entrapment of hydrophilic cargos including therapeutics and diagnostic agents.[38-39] Nanoparticle structures based on dendritic polyglycidol have also been shown to be useful for applications in metal binding and catalysis.[40] However, for the construction of hydrogels for the purpose of drug delivery, a hyperbranched, globular-shaped structure is expected to provide poor entrapment and sequestration of the desired protein. A semi-branched form of this polymer could provide a tighter network structure for sequestration (Figure 2), while maintaining the high functionality

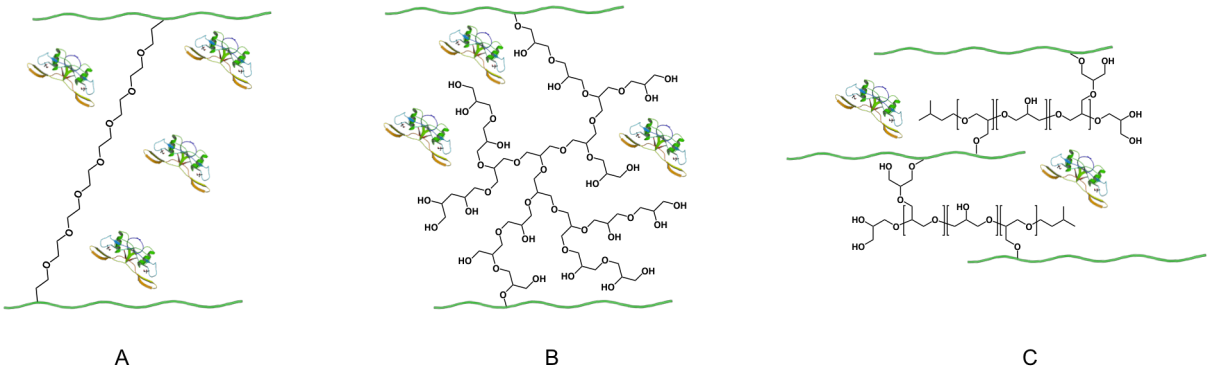

Figure I-2. Both bifunctional linear PEG (A) and globular hyperbranched polyglycidol (B) offer poor sequestration of proteins within a hydrogel network. C) The semi-branched polyglycidol creates tighter networks providing better sequestration and a more controlled release of a protein from the hydrogel matrix.

needed to overcome the obstacles seen in PEG based hydrogels. A tunable hydrogel structure created using this semi-branched polymer along with a ketone functionalized linear polyester shows great promise as a system for the sustained delivery of BMP2.

Dual Drug Delivery: Towards More Sophisticated Systems

Although both polymeric nanoparticles and hydrogels each have their own distinct

advantages for the delivery of small hydrophobic and large hydrophilic structures respectively, many applications require the use of multiple drugs, which often have vastly different physiochemical properties. Dual delivery of these kinds of therapies require more sophisticated delivery systems capable of providing a suitable environment for both therapeutics simultaneously.[41] Successful dual delivery of proteins and small molecule drugs has been demonstrated using unique matrices of nanoparticles embedded in hydrogel structures held together via electrostatic[42] or hydrophobic[43] interactions between the two materials. Utilization of this semi-branched functional polyglycidol allows for the formation of covalent bonds between the hydrogel components, which may have advantages over these non-covalent interactions for this application. These hydrogels presented in this work have been made using oxime click chemistry, which is completely biorthogonal, leaving the possibility of entrapment of other structures such as nanoparticles open without fear of side reaction or interference. In this way, these structures have the potential to serve as platforms for dual drug delivery.

Highly Functional Polymers for Prodrug Applications

Highly functionalized polymers such as the polyglycidol described above are also widely sought after for prodrug applications. Traditional small molecule prodrugs involve the addition of an additional cleavable chemical group to the drug molecule, usually for the purposes of decreased rate of metabolism or increased solubility.[44-45] Polymeric prodrugs offer these advantages as well, usually to a greater extent, along with other benefits such as the ability to attach other functionalities to the polymer backbone besides the drug, such as targeting moieties or imaging agents.[46-47] Previous work has focused on the construction of polymeric prodrugs using a "drug-initiated" approach where one drug molecule is used to initiate a polymer chain,

resulting in a ratio of one active drug molecule per prodrug moiety.[48] Recently interest has grown concerning polymer scaffolds for prodrugs that provide multiple points of attachment for the drug molecule, to create prodrugs that that do not require high doses to obtain the correct dosage of the active drug.

Classes of small molecule therapeutics that have benefited from the use of prodrugs include but are not limited to: cancer therapeutics,[49] anti-inflammatory medications,[50] and antibiotics[51] (Figure 3). Another group of small molecules that have recently garnered interest in prodrug delivery is the class of otherwise toxic small molecules such as hydrogen sulfide, carbon monoxide, nitric oxide, and formaldehyde. These small molecules have been found to be useful

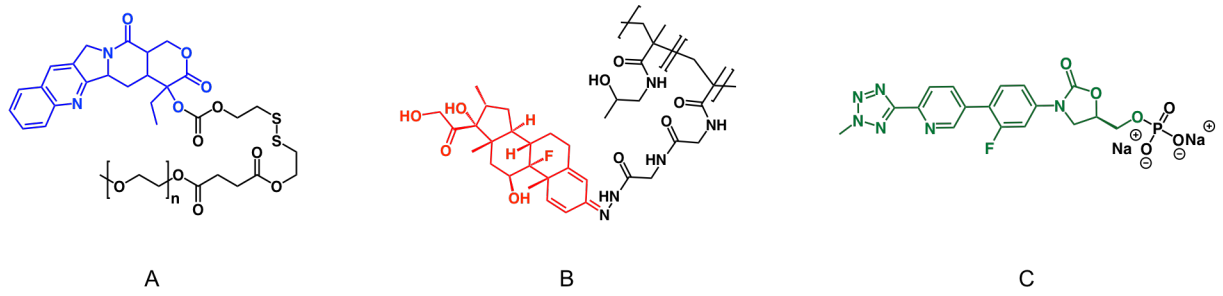

Figure I-3. Examples of some prodrug constructs for the treatment of A) cancer, B) inflammation, and C) infection. The active form of the drug is shown in color.

for synergistic therapy in applications ranging from muscular dystrophy[52] to cardiac ischemia.[53] Formaldehyde specifically has been found to have a synergistic effect for the treatment of cancer when co-administered with a drug from the class of anthracyclines. Because of the innate toxicity of these small molecules, a delivery vehicle allowing for slow sustained release is necessary for administration. Polyglycidol and its functional derivatives could serve as excellent scaffolds for the creation of formaldehyde based prodrugs due to the large abundance of functional groups on the polymer backbone. The types of linkages that can be formed with

formaldehyde also allow for tailoring of the release of the small molecule based upon the rate of hydrolysis.

Dissertation Overview

Ring-opening polymerization was used to construct functional polyester and polyglycidol scaffolds that were used as building blocks for a range of macromolecular materials. These bulk-scale and nanoscale materials were studied for the purpose of drug delivery for applications in the treatment of neurofibromatosis 1, diabetes, cardiovascular disease, and cancer.

Polyesters containing ketone functional groups in the backbone were synthesized successfully using a 2-oxepane-1,5-dione monomer. Ideal reaction conditions were investigated and established for the incorporation of a 13% functionality of the ketone into the backbone structure. Before attempts were made to use this polymer to construct crosslinked hydrogels, model reactions using O-hydroxylamine (tetra ethylene) glycol were conducted using various reaction times to study the feasibility and the kinetics of the oxime click reaction at the ketone site. The oxime click reaction at this site was found to be both rapid and efficient, and led to the construction of hydrogel structures using this linear ketone-functionalized polyester and an amino-oxy functionalized semi-branched polyglycidol. By varying the composition of the hydrogel structure based on the ratio of the two components, the tunability of properties such as swelling ratio, degradation profile, and mechanical strength was investigated. It was discovered that these properties could be easily tuned based on the synthesis conditions, making these an attractive tailorable delivery system for BMP2 to aid in the treatment of fractures in NF1 patients.

Polyesters containing epoxide and allyl groups were used to create a functional

nanoparticle platform containing surface functional groups that could be utilized to attach both targeting peptides and imaging dyes. An orthogonal chemistry scheme was developed so that both units could be successfully conjugated to the surface without interfering with the function of the other. Two constructs were synthesized and characterized: a nanoparticle containing the GLP1 agonist Exendin4 and a near infrared imaging dye, and a nanoparticle containing a collagen homing peptide (T-peptide) and a cyanine dye, and loaded with napthofluorescein. The Exendin4 tagged construct was shown to effectively target human islet grafts in a mouse model, making them a highly desirable delivery system targeted towards beta cell drug delivery for diabetes treatment. The second nanoparticle construct was shown to increase the efficacy of the encapsulated drug almost two-fold over its free counterpart due to the targeted action of the delivery system, making them an exciting treatment option for the prevention of unstable plaque rupture and the decreased occurrence of myocardial infarctions.

The semi-branched polyglycidol used to construct the hydrogel materials mentioned above was also utilized to create a novel prodrug of formaldehyde for synergistic cancer therapy. Semi-branched polyglycidol was utilized to form formaldehyde prodrugs by trapping the small molecule using an acetal linkage, and the resulting construct was extensively characterized. The rate of hydrolysis of the formaldehyde off of the backbone of the acetal prodrug was studied using a dialysis method with colorimetric detection at two separate pH levels and found to be pH dependent. The apoptosis-inducing efficacy of this prodrug towards a breast cancer cell line when used in combination with doxorubicin was found to be superior to treatment with only doxorubicin and treatment with doxorubicin and unbound formaldehyde together. Another prodrug utilizing amino-oxy functionalized polyglycidol was also explored by conjugating formaldehyde to the backbone via an oxime linkage, and again the resulting construct was

extensively characterized. These prodrugs should prove to be interesting materials for the sustained delivery of formaldehyde for synergistic cancer therapy.

References

1. Song, X.; Gong, H.; Yin, S.; Cheng, L.; Wang, C.; Li, Z.; Li, Y.; Wang, X.; Liu, G.; Liu, Z., Ultra-Small Iron Oxide Doped Polypyrrole Nanoparticles for In Vivo Multimodal Imaging Guided Photothermal Therapy. *Advanced Functional Materials* **2014,** *24* (9), 1194-1201.

2. Tian, Y.; Bian, S.; Yang, W., A redox-labile poly(oligo(ethylene glycol)methacrylate)-based nanogel with tunable thermosensitivity for drug delivery. *Polymer Chemistry* **2016,** *7* (10), 1913-1921.

3. Concheiro, A.; Alvarez-Lorenzo, C., Chemically cross-linked and grafted cyclodextrin hydrogels: from nanostructures to drug-eluting medical devices. *Advanced Drug Delivery Reviews* **2013,** *65* (9), 1188-203.

4. Zhang, X.; Malhotra, S.; Molina, M.; Haag, R., Micro- and nanogels with labile crosslinks - from synthesis to biomedical applications. *Chemical Society Reviews* **2015,** *44* (7), 1948-73.

5. Jonker, A. M.; Löwik, D. W. P. M.; van Hest, J. C. M., Peptide- and Protein-Based Hydrogels. *Chemistry of Materials* **2012,** *24* (5), 759-773.

6. Canfarotta, F.; Whitcombe, M. J.; Piletsky, S. A., Polymeric nanoparticles for optical sensing. *Biotechnology Advances* **2013,** *31* (8), 1585-99.

7. Elsabahy, M.; Heo, G. S.; Lim, S. M.; Sun, G.; Wooley, K. L., Polymeric Nanostructures for Imaging and Therapy. *Chemical Reviews* **2015,** *115* (19), 10967-1011.

8. Appel, E. A.; del Barrio, J.; Loh, X. J.; Scherman, O. A., Supramolecular polymeric hydrogels. *Chemical Society Reviews* **2012,** *41* (18), 6195-214.

9. Eswaramma, S.; Rao, K. S., Synthesis of dual responsive carbohydrate polymer based IPN microbeads for controlled release of anti-HIV drug. *Carbohydrate Polymers* **2017,** *156*, 125-134.

10. Nazir, R., Collagen–hyaluronic acid based interpenetrating polymer networks as tissue engineered heart valve. *Materials Science and Technology* **2016,** *32* (9), 871-882.

11. Kadari, A.; Gudem, S.; Kulhari, H.; Bhandi, M. M.; Borkar, R. M.; Kolapalli, V. R. M.; Sistla, R., Enhanced oral bioavailability and anticancer efficacy of fisetin by encapsulating as inclusion complex with HPβCD in polymeric nanoparticles. *Drug Delivery* **2017,** *24* (1), 224-232.

12. Jain, A. K.; Thanki, K.; Jain, S., Co-encapsulation of tamoxifen and quercetin in polymeric nanoparticles: implications on oral bioavailability, antitumor efficacy, and drug-induced toxicity. *Molecular Pharmaceutics* **2013,** *10* (9), 3459-74.

13. Graf, N.; Bielenberg, D. R.; Kolishetti, N.; Muus, C.; Banyard, J.; Farokhzad, O. C.; Lippard, S. J., alpha(V)beta(3) integrin-targeted PLGA-PEG nanoparticles for enhanced anti-tumor efficacy of a Pt(IV) prodrug. *ACS Nano* **2012,** *6* (5), 4530-9.

14. Ang, C. Y.; Tan, S. Y.; Teh, C.; Lee, J. M.; Wong, M. F.; Qu, Q.; Poh, L. Q.; Li, M.; Zhang, Y.; Korzh, V.; Zhao, Y., Redox and pH Dual Responsive Polymer Based Nanoparticles for In Vivo Drug Delivery. *Small* **2017,** *13* (7).

15. He, C.; Cai, P.; Li, J.; Zhang, T.; Lin, L.; Abbasi, A. Z.; Henderson, J. T.; Rauth, A. M.; Wu, X. Y., Blood-brain barrier-penetrating amphiphilic polymer nanoparticles deliver docetaxel

for the treatment of brain metastases of triple negative breast cancer. *Journal of Controlled Release* **2017,** *246*, 98-109.

16. Yousry, C.; Elkheshen, S. A.; El-Laithy, H. M.; Essam, T.; Fahmy, R. H., Studying the influence of formulation and process variables on Vancomycin-loaded polymeric nanoparticles as potential carrier for enhanced ophthalmic delivery. *European Journal of Pharmaceutical Sciences* **2017,** *100*, 142-154.

17. Zhang, Y.; Lu, Y.; Wang, F.; An, S.; Zhang, Y.; Sun, T.; Zhu, J.; Jiang, C., ATP/pH Dual Responsive Nanoparticle with d-[des-Arg10]Kallidin Mediated Efficient In Vivo Targeting Drug Delivery. *Small* **2017,** *13* (3).

18. Ramezanli, T.; Zhang, Z.; Michniak-Kohn, B. B., Development and characterization of polymeric nanoparticle-based formulation of adapalene for topical acne therapy. *Nanomedicine* **2017,** *13* (1), 143-152.

19. Crespy, D.; Landfester, K., Anionic polymerization of epsilon-caprolactam in miniemulsion: Synthesis and characterization of polyamide-6 nanoparticles. *Macromolecules* **2005,** *38* (16), 6882-6887.

20. Hrubý, M.; Koňák, Č.; Ulbrich, K., Poly(ethylene oxide)-coated polyamide nanoparticles degradable by glutathione. *Colloid and Polymer Science* **2006,** *285* (5), 569-574.

21. Fu, H.; Gao, H.; Wu, G.; Wang, Y.; Fan, Y.; Ma, J., Preparation and tunable temperature sensitivity of biodegradable polyurethane nanoassemblies from diisocyanate and poly(ethylene glycol). *Soft Matter* **2011,** *7* (7), 3546.

22. Ou, C. W.; Su, C. H.; Jeng, U. S.; Hsu, S. H., Characterization of biodegradable polyurethane nanoparticles and thermally induced self-assembly in water dispersion. *ACS Applied Materials and Interfaces* **2014,** *6* (8), 5685-94.

23. Stevens, D. M.; Tempelaar, S.; Dove, A. P.; Harth, E., Nanosponge formation from organocatalytically-synthesized poly(carbonate) copoplymers. *ACS Macro Letters* **2012,** *1* (7), 915-918.

24. Stevens, D. M., Gilmore, K. A., Harth, E., An assessment of nanosponges for intravenous and oral drug delivery of BCS class IV drugs: Drug delivery kinetics and solubilization. *Polymer Chemistry* **2014,** *5* (11), 3551-3554.

25. van der Ende, A. E.; Kravitz, E. J.; Harth, E., Approach to formation of multifunctional polyester particles in controlled nanoscopic dimensions. *Journal of the American Chemical Society* **2008,** *130* (27), 8706-13.

26. Wang, Q.; Zai, Y.; Yang, D.; Qiu, L.; Niu, C., Bio-based elastomer nanoparticles with controllable biodegradability. *RSC Advances* **2016,** *6* (104), 102142-102148.

27. Joshi, R. V.; Nelson, C. E.; Poole, K. M.; Skala, M. C.; Duvall, C. L., Dual pH- and temperature-responsive microparticles for protein delivery to ischemic tissues. *Acta Biomater* **2013,** *9* (5), 6526-34.

28. Rinker, T. E.; Philbrick, B. D.; Temenoff, J. S., Core-shell microparticles for protein sequestration and controlled release of a protein-laden core. *Acta Biomaterialia* **2016**.

29. Mizushima, Y.; Ikoma, T.; Tanaka, J.; Hoshi, K.; Ishihara, T.; Ogawa, Y.; Ueno, A., Injectable porous hydroxyapatite microparticles as a new carrier for protein and lipophilic drugs. *Journal of Controlled Release* **2006,** *110* (2), 260-5.

30. Vermonden, T.; Censi, R.; Hennink, W. E., Hydrogels for protein delivery. *Chemical Reviews* **2012,** *112* (5), 2853-88.

31. Hiemstra, C.; Zhong, Z.; Van Tomme, S. R.; van Steenbergen, M. J.; Jacobs, J. J.; Otter, W. D.; Hennink, W. E.; Feijen, J., In vitro and in vivo protein delivery from in situ forming

poly(ethylene glycol)-poly(lactide) hydrogels. *Journal of Controlled Release* **2007,** *119* (3), 320-7.

32. Leach, J. B.; Schmidt, C. E., Characterization of protein release from photocrosslinkable hyaluronic acid-polyethylene glycol hydrogel tissue engineering scaffolds. *Biomaterials* **2005,** *26* (2), 125-35.

33. Leader, B.; Baca, Q. J.; Golan, D. E., Protein therapeutics: a summary and pharmacological classification. *Nature Reviews Drug Discovery* **2008,** *7* (1), 21-39.

34. Shields, L. B.; Raque, G. H.; Glassman, S. D.; Campbell, M.; Vitaz, T.; Harpring, J.; Shields, C. B., Adverse effects associated with high-dose recombinant human bone morphogenetic protein-2 use in anterior cervical spine fusion. *Spine (Phila Pa 1976)* **2006,** *31* (5), 542-7.

35. Rainer Haag, A. S., and Jean-Francois Stumbe, An Approach to Glycerol Dendrimers and Pseudo-Dendritic Polyglycerols. *Journal of the American Chemical Society* **2000,** *122*, 2954-2955.

36. Wilms, D.; Stiriba, S. E.; Frey, H., Hyperbranched Polyglycerols: From the Controlled Synthesis of Biocompatible Polyether Polyols to Multipurpose Applications. *Accounts of Chemical Research* **2010,** *43* (1), 129-141.

37. Sunder, A.; Hanselmann, R.; Frey, H.; Mulhaupt, R., Controlled synthesis of hyperbranched polyglycerols by ring-opening multibranching polymerization. *Macromolecules* **1999,** *32* (13), 4240-4246.

38. Xu, S.; Luo, Y.; Graeser, R.; Warnecke, A.; Kratz, F.; Hauff, P.; Licha, K.; Haag, R., Development of pH-responsive core-shell nanocarriers for delivery of therapeutic and diagnostic agents. *Bioorganic & Medicinal Chemistry Letters* **2009,** *19* (3), 1030-4.

39. Stiriba, S. E.; Kautz, H.; Frey, H., Hyperbranched molecular nanocapsules: Comparison of the hyperbranched architecture with the perfect linear analogue. *Journal of the American Chemical Society* **2002,** *124* (33), 9698-9699.

40. Zimmerman, S. C.; Quinn, J. R.; Burakowska, E.; Haag, R., Cross-linked glycerol dendrimers and hyperbranched polymers as ionophoric, organic nanoparticles soluble in water and organic solvents. *Angewandte Chemie International Edition* **2007,** *46* (43), 8164-7.

41. Gilmore, K. A.; Lampley, M. W.; Boyer, C.; Harth, E., Matrices for combined delivery of proteins and synthetic molecules. *Advanced Drug Delivery Reviews* **2016,** *98*, 77-85.

42. Appel, E. A.; Tibbitt, M. W.; Greer, J. M.; Fenton, O. S.; Kreuels, K.; Anderson, D. G.; Langer, R., Exploiting Electrostatic Interactions in Polymer–Nanoparticle Hydrogels. *ACS Macro Letters* **2015,** *4* (8), 848-852.

43. Appel, E. A.; Tibbitt, M. W.; Webber, M. J.; Mattix, B. A.; Veiseh, O.; Langer, R., Self-assembled hydrogels utilizing polymer-nanoparticle interactions. *Nature Communications* **2015,** *6*, 6295.

44. Huang, P.; Wang, D.; Su, Y.; Huang, W.; Zhou, Y.; Cui, D.; Zhu, X.; Yan, D., Combination of small molecule prodrug and nanodrug delivery: amphiphilic drug-drug conjugate for cancer therapy. *Journal of the American Chemical Society* **2014,** *136* (33), 11748-56.

45. Testa, B., Prodrugs: bridging pharmacodynamic/pharmacokinetic gaps. *Current Opinion in Chemical Biology* **2009,** *13* (3), 338-44.

46. Larson, N.; Ghandehari, H., Polymeric conjugates for drug delivery. *Chemistry of Materials* **2012,** *24* (5), 840-853.

47. Neeraj Agrawal, R.; Alok Mukerji, A. J., Polymeric Prodrugs: Recent Achievements and General Strategies. *Journal of Antivirals & Antiretrovirals* **2013,** *s15*.

48. Tong, R.; Cheng, J., Drug-Initiated, Controlled Ring-Opening Polymerization for the Synthesis of Polymer-Drug Conjugates. *Macromolecules* **2012,** *45* (5), 2225-2232.

49. Zhang, L.; Wang, Y.; Zhang, X.; Wei, X.; Xiong, X.; Zhou, S., Enzyme and Redox Dual-Triggered Intracellular Release from Actively Targeted Polymeric Micelles. *ACS Applied Materials and Interfaces* **2017,** *9* (4), 3388-3399.

50. Quan, L.; Zhang, Y.; Crielaard, B. J.; Dusad, A.; Lele, S. M.; Rijcken, C. J.; Metselaar, J. M.; Kostkova, H.; Etrych, T.; Ulbrich, K.; Kiessling, F.; Mikuls, T. R.; Hennink, W. E.; Storm, G.; Lammers, T.; Wang, D., Nanomedicines for inflammatory arthritis: head-to-head comparison of glucocorticoid-containing polymers, micelles, and liposomes. *ACS Nano* **2014,** *8* (1), 458-66.

51. Burdette, S. D.; Trotman, R., Tedizolid: The First Once-Daily Oxazolidinone Class Antibiotic. *Clinical Infectious Diseases* **2015,** *61* (8), 1315-21.

52. Sciorati, C.; Buono, R.; Azzoni, E.; Casati, S.; Ciuffreda, P.; D'Angelo, G.; Cattaneo, D.; Brunelli, S.; Clementi, E., Co-administration of ibuprofen and nitric oxide is an effective experimental therapy for muscular dystrophy, with immediate applicability to humans. *British Journal of Pharmacology* **2010,** *160* (6), 1550-60.

53. Kang, J.; Li, Z.; Organ, C. L.; Park, C. M.; Yang, C. T.; Pacheco, A.; Wang, D.; Lefer, D. J.; Xian, M., pH-Controlled Hydrogen Sulfide Release for Myocardial Ischemia-Reperfusion Injury. *Journal of the American Chemical Society* **2016,** *138* (20), 6336-9.

CHAPTER II

AN OXIME CLICK HYDROGEL PLATFORM FOR THE SUSTAINED RELEASE OF BONE MORPHOGENETIC PROTEIN 2

Introduction

Neurofibromatosis type 1 (NF1) is a genetic disorder that is caused by a mutation in one of the genes that controls bone growth. One of the major symptoms of this disorder is dysplasia, or abnormal growth, of the bones. Particularly in children, this often leads to fracture of the bone from only minor trauma. As another result of this disorder, these fractures oftentimes are unable to heal, sometimes requiring amputation of the limb. The most common treatment for fractures sustained in an NF1 individual is the administration of the growth factor bone morphogenetic protein 2 (BMP2), however, this method has met with limited success.[1-2] Recently, in collaboration with the Elefteriou group, we have demonstrated that trametinib, a MEK inhibitor, when co-administered with BMP2, results in callus formation in the broken bone of an NF1 mouse model.[3] These two drugs were delivered together in a novel polymeric delivery system outlined in Fig. 1. Briefly, the trametinib was encapsulated in a polyester nanoparticle structure and both the particles and the BMP2 were suspended in a viscous polymeric matrix made from polyglycidol.

While this treatment method proved to be very successful in healing the broken bones, calcification of the surrounding muscle tissue at the fracture site was also observed. What this indicates is that the diffusion of the BMP2 from the polymer matrix is too rapid, and needs to be better controlled. We postulated that this could be achieved by substituting the polyglycidol

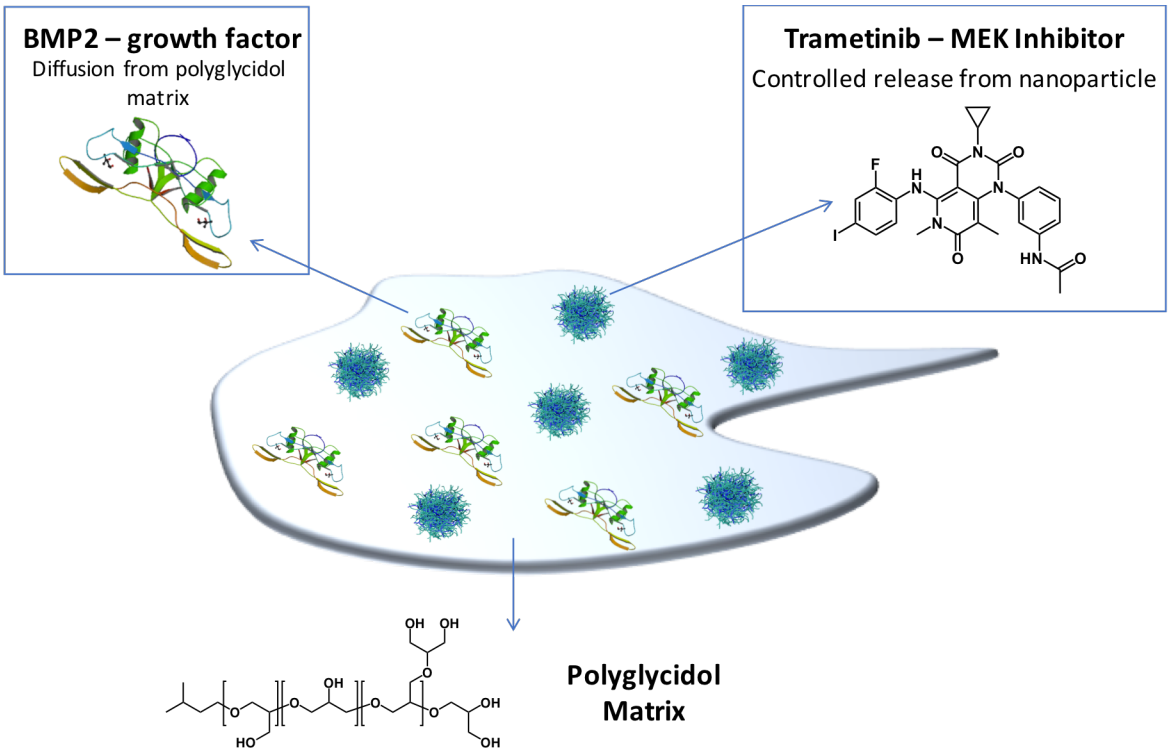

Figure II-1. The previously developed dual drug delivery system for the co-delivery of trametinib and BMP2 to increase bone healing.

instead with a crosslinked hydrogel matrix that could better modulate the diffusion of the BMP2. When considering the chemistry to be used to construct this matrix, it was necessary to choose a type of chemistry that would be rapid, efficient, and bio-orthogonal, so as to not interfere with the function of the BMP2. The class of chemistries known as click reactions, such as tetrazine-alkene,[4-6] Diels-Alder,[7-8] and thiol-based reactions[9-10] (thiolene, thiolyne, thiol-maleimide) have long been utilized to construct a wide range of functional macromolecular materials. In recent years, the oxime click reaction has emerged as a powerful new tool for the construction of such materials.[11-19] This chemistry has been most widely utilized in applications for bioconjugation that range from selective extraction of glycopeptides from a proteome[16] to use as tethers for attachment of a drug to a delivery vehicle.[12] The advantages of this chemistry over others such as

Diels-Alder or thiolene are that the reaction is kinetically rapid and does not require the use of potentially toxic photoinitiators or an external stimulus. The oxime reaction produces a biologically benign byproduct, water, and exhibits the high efficiency typically associated with a click reaction. The use of this chemistry has recently expanded to include other valuable macromolecular structures such as branched star architectures[15] and three-dimensional hydrogel networks.[13-14, 20]

For our application, hydrogel materials formed using oxime click chemistry are of particular interest. These types of hydrogels have been demonstrated to be useful for a vast number of biomedical applications including use as surgical adhesives,[19] scaffolds for wound healing,[21] and drug delivery vehicles[22-24] to name a few. The complete bio-orthogonality of the oxime click reaction, aqueous byproduct, and lack of a need for any stimulus, makes this chemistry rather attractive for use in the synthesis of a hydrogel drug delivery platform. The bio-orthogonal nature of the reaction and the non-toxic byproduct help ensure that the BMP2 will retain activity after entrapment in the hydrogel matrix, and the lack of a need for a stimulus opens the possibility for this delivery system to be delivered via injection.

In order for a hydrogel to act as a successful drug delivery platform, it must ideally exhibit controlled release of the entrapped therapeutic and be constructed in such a way that the release rate of the therapeutic can be modulated.[25-26] Current examples of hydrogels formed by oxime click chemistry almost exclusively utilize polyethylene glycol (PEG) derivatives as a component of the gel due to their well-demonstrated biocompatibility and hydrophilicity.[13-14, 20] However, PEG derivatives are limited in the number and distribution of functional groups along the polymer, often leading to networks with large pore sizes and poor control over the diffusion of entrapped drug cargo.

In this work, we utilize an amino-oxy functionalized semi-branched polyglycidol crosslinker[27-28] in place of linear or multi-arm PEG in an effort to produce oxime click hydrogels that exhibit tighter networks and therefore improved sequestration of entrapped therapeutics. This crosslinker is reacted with a ketone-functionalized linear polyester to form an exciting new class of oxime click hydrogel materials. The synthesis route of these polymer precursors as well as the synthesis of the hydrogel structures allow for not only the functionality of each polymer to be tuned, but also the properties of the resulting hydrogel material to be modulated based upon the ratio of polyester to polyglycidol used. Here we will demonstrate the formation of a group of biocompatible oxime click hydrogels that exhibit varied swelling, degradation, and mechanical properties, based upon their composition.

Each of the properties studied here are crucial to the performance of the material as a drug delivery system. The swelling capability of the hydrogels will dictate the initial amount of entrapped cargo that is released from the system, while the degradation profiles will dictate long-term behavior. It has been demonstrated in the literature that the two most prominent pathways for degradation of a biologically relevant material are via oxidative species, or by enzymes,[29-31] which is why they are studied here. The mechanical strength of the hydrogel is an important property to consider when determining the placement of the hydrogel in a biological system and what forces it must withstand. Furthermore, being able to tune the mechanical strength of a material has been shown to be very beneficial for biological applications.[32] The tunability and unique structure of these hydrogels makes them exciting new additions to the growing field of macromolecular tools made by oxime click chemistry.

Results and Discussion

Poly(δ-valerolactone-2-oxepane-1,5-dione) was synthesized with a 13% incorporation of the OPD monomer into the chain. This polymer was shown to react successfully with a model substrate to form oxime bonds. The reaction of this polyester with an amino-oxy functionalized polyglycidol was used to form hydrogel structures. Gels were constructed using ratios of 30/70, 50/50, and 70/30 by weight of polyester to polyglycidol and shown to have tunable swelling, degradation, and mechanical properties. Biocompatibility of the material was demonstrated using NIH 3T3 cells.

Design and Synthesis of a Hydrogel Platform using Oxime Click Chemistry

Poly (δ-valerolactone-2-oxepane-1,5-dione) was synthesized by ring opening polymerization with a tin triflate catalyst using a modified version of a procedure previously developed by our group.[33] The synthesis procedure had to be modified after initial synthesis attempts presented challenges, namely that a high degree of polymerization could not be achieved concurrently with a high incorporation of the OPD monomer into the backbone. Analysis of crude ^{1}H NMR spectra revealed that degradation of the OPD during the synthesis was a likely reason for the low incorporation of the monomer. Lowering the temperature of the reaction to 0^{o}C during the initial stages of the polymerization successfully reduced the occurrence of the competing degradation reaction and allowed for a total incorporation of 13 wt% OPD into the polymer backbone. This 13% poly (VL/OPD) was utilized for all studies presented in this work.

As the reaction of this polyester with the amino-oxy functionalized polyglycidol was expected to produce a crosslinked hydrogel material, incapable of being studied by traditional

solution state NMR, we developed a model system in order to confirm the formation of the oxime bond. One of the most advantageous aspects of oxime click chemistry is the ability for the reaction to occur in aqueous media. As such, a hydrogel system constructed using this chemistry has the potential to be formed *in vivo* by injection of each of the components into a target site. We were interested in investigating not only if oxime bond formation would occur at the ketone group of the polyester, but also if this chemistry was efficient enough to allow for the reaction to occur in aqueous buffer. The compound that was chosen as a model substrate is one that has been

A

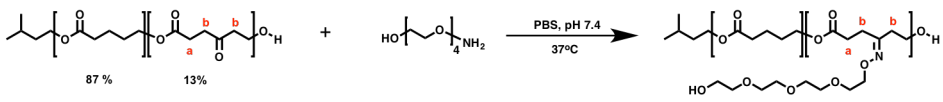

B

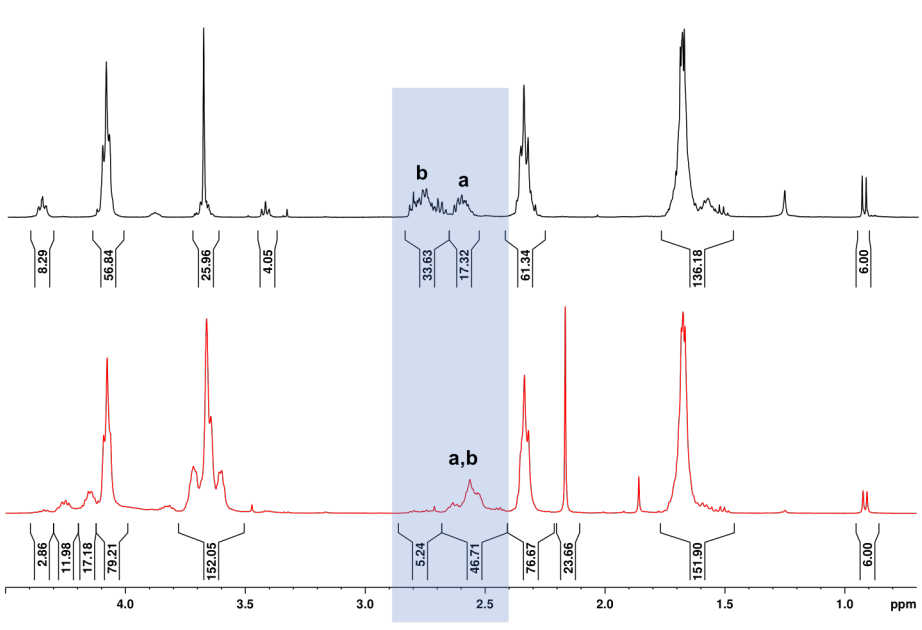

C

Time (min)	5	10	30	60
% Conversion	91.9	89.8	88.5	89.0

Figure II-2. A) Reaction scheme for the model reaction between poly (VL/OPD) and O-hydroxylamine tetra (ethylene glycol). B) The spectrum of the poly (VL/OPD) (black, top) shows a signal at 2.73 ppm for those protons directly adjacent to the ketone group. After 5 minutes of reaction in PBS (red, bottom), an upfield shift is seen, indicating successful formation of the oxime bond. C) High conversions are observed for all reaction times.

successfully synthesized previously by Maynard and coworkers. This O-hydroxylamine tetra (ethylene glycol) has a structure similar to that of polyglycidol due to the PEG backbone, and was expected to react with the ketone on the polyester backbone without causing crosslinking. The resulting product was soluble in organic solvent and could easily be characterized by ^{1}H NMR.

Model studies of the reaction between a VL/OPD polymer (13% OPD) and O-hydroxylamine tetra (ethylene glycol) were performed in PBS buffer at a temperature of 37^{o}C, and a pH of 7.4. ^{1}H NMR analysis of the reaction mixture was performed after 5, 10, 30, 60, and 120 minutes of reaction, to monitor the kinetics of the oxime bond formation. In the ^{1}H NMR spectrum of the poly (VL/OPD), the signal for the OPD protons directly adjacent to the ketone group is present at 2.73 ppm. Upon successful formation of the oxime bond, this peak is shifted upfield to 2.55 ppm where it overlaps with the signal for the OPD protons alpha to the carbonyl. Using the integration values of these two regions, a percent conversion of the ketone group was calculated for each time point. As shown in Figure 2, high conversions are observed after only 5 minutes of reaction in aqueous buffer.

In light of these promising results, hydrogel formation reactions were attempted in PBS by bringing together a VL/OPD polymer (13% OPD) and a 60% functionalized amino-oxy polyglycidol (AOPG) under the same experimental conditions as those used in the model reactions. Although these reactions did result in some amount of crosslinking, the gels were not well formed due to the higher dilution required to sufficiently suspend the polyester. As a result, gelation reactions were run in DMSO to achieve consistently reproducible hydrogel structures more suitable for characterization. In DMSO at higher concentrations, the poly (VL/OPD) and the AOPG can be mixed to form a solid, but flexible hydrogel structure (see Figure 4).

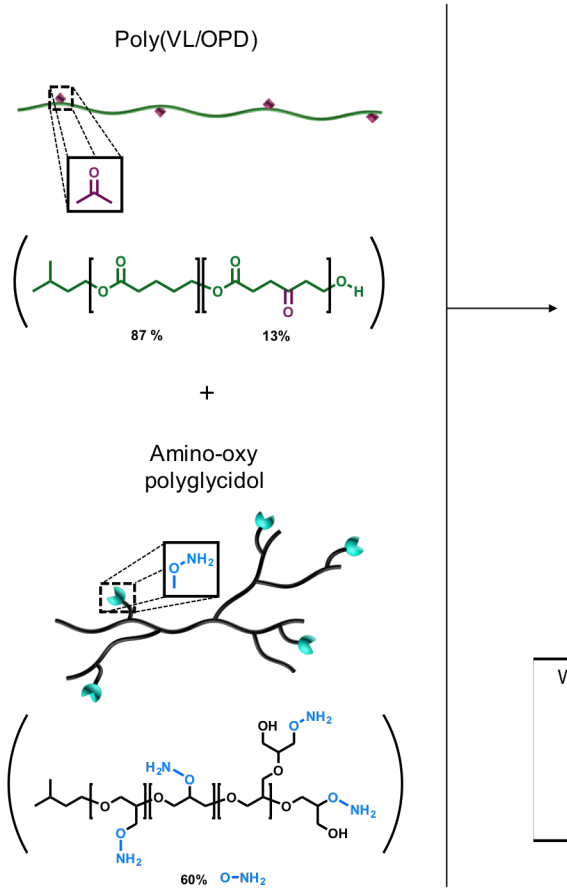

Wt % Poly(VL/OPD)	Wt% Amino-oxy polyglycidol	Name of hydrogel product
30	70	PE30
50	50	PE50
70	30	PE70

Figure II-3. Synthesis of an oxime click hydrogel via the reaction between poly (VL/OPD) and amino-oxy functionalized polyglycidol (AOPG).

As we were interested in tuning the properties of this hydrogel system, gels were formed using three different ratios of the two components by weight (30/70, 50/50, and 30/70 poly (VL/OPD):AOPG, Figure 3). Following formation and purification, gels of each composition were studied for swelling ability, rate of degradation, mechanical strength, and biocompatibility, all of which are crucial aspects for the performance of the material as a drug delivery vehicle.

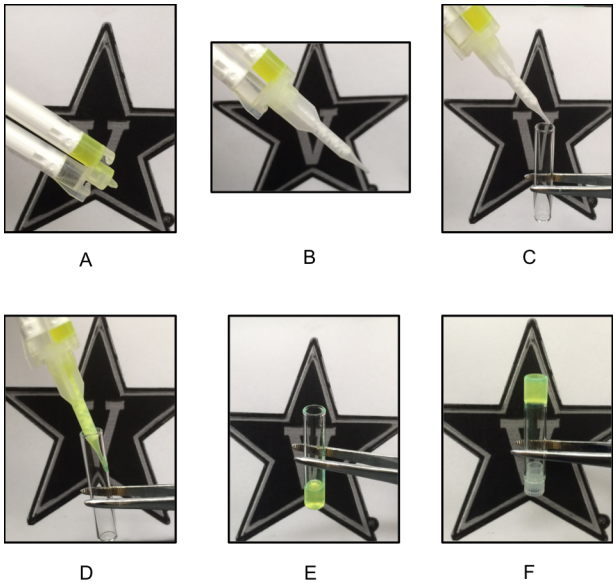

Figure II-4. A) Amino-oxy functionalized polyglycidol (left chamber, clear solution) and VL/OPD polymer (right chamber, yellow-green solution) are loaded into the double-barreled syringe. The VL/OPD polymer is dyed using a small amount of Coumarin 30 for visualization purposes. B) The mixing tip is attached to the syringe. C) A vial is prepared for injection of the two hydrogel components. D) The plunger on the syringe is pushed downward and the components are mixed in the tip and then injected into the vial. E) The gel solution is allowed to sit at room temperature in the vial. F) After 15 minutes at room temperature, a solid hydrogel has formed.

Tuning the Properties of Oxime Click Hydrogels

It is well known that the swelling properties of a hydrogel play an important role in maintaining the integrity of the cargo trapped inside the gel, and can also be a factor in the rate of release of the cargo. In general, hydrogels are constructed to absorb multiple times their weight in water, to provide a suitably hydrated inner environment for the therapeutic. Gels made from hydrophilic polymers typically exhibit pronounced swelling ability,[34-35] while hydrogels such as those presented here that contain a hydrophobic polymer might be expected to exclude water. The swelling properties of the oxime click hydrogels were studied by immersing dry gel samples in PBS at pH 7.4 for 24 hours and then calculating the ratio between the swollen weight and the dry weight. As shown in Figure 5, hydrogel samples composed of 30, 50 and 70 percent poly

(VL/OPD) gave average swelling ratios of 4.41, 1.92, and 2.03 respectively. Because of the high percentage of hydrophilic polyglycidol in the network, the PE30 product exhibits the highest swelling ratio of all three materials. Dropping the polyglycidol content to 50% leads to an approximately two-fold decrease in swelling ability. Finally, it is worth noting that even gels containing only 30% polyglycidol by weight still exhibit swelling behavior, indicating that any of the three ratios tested could be used to create a gel structure suitable for protein delivery.[36]

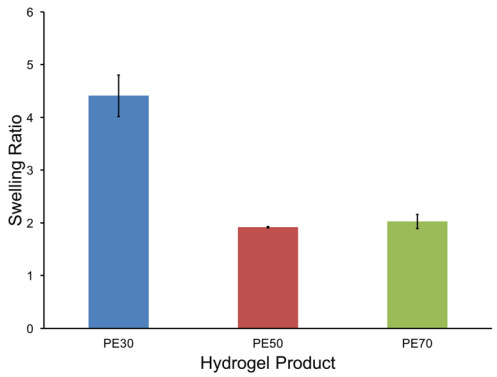

Figure II-5. Swelling profiles for oxime click hydrogels with a poly (VL/OPD):AOPG weight ratio of 30/70, 50/50, and 70/30.

The rate of degradation of these hydrogel materials is of critical importance to their performance as delivery vehicles, as this rate will play a role in the long term release behavior of these materials. The two major pathways by which polymeric devices are degraded *in vivo* are through oxidation or by enzymatic activity. Oxidation occurs mainly via peroxides and other reactive oxygen species naturally found in the bloodstream, while enzymatic activity differs by location. While these hydrogel structures would also be susceptible to hydrolytic degradation, this process is extremely slow and is expected to have little overall effect on the degradation profile of these materials compared to other pathways.

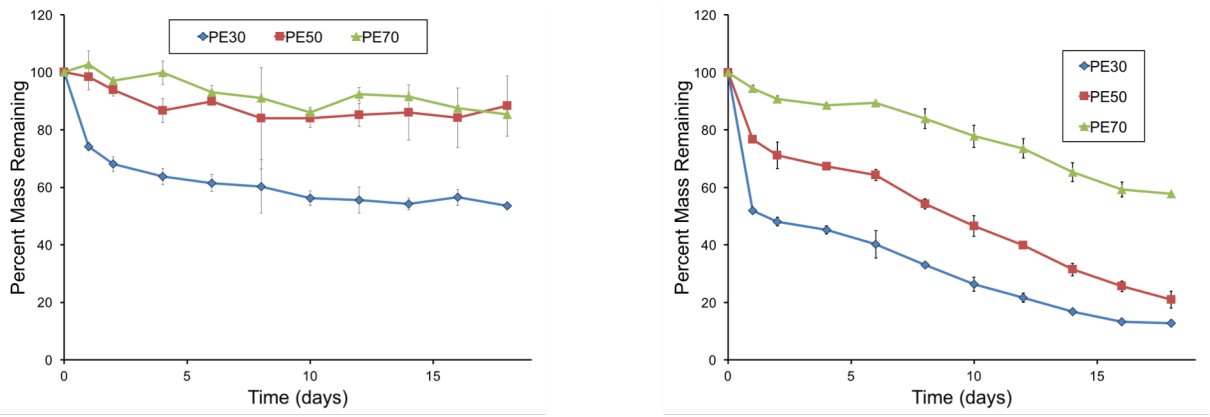

Figure II-6. Degradation profiles for oxime click hydrogels under both A) enzymatic and B) oxidative conditions.

To study the enzymatic degradation profile of these hydrogels, we used a solution of cholesterol esterase and a method modified from Christenson et. al. wherein hydrogels were submerged in this enzymatic media and then removed and weighed every two days to determine mass loss from enzymatic activity. As shown in Figure 6A, the PE30 hydrogel is seen to degrade the fastest, while the PE70 gel exhibits the slowest enzymatic degradation profile. To mimic the oxidative degradation process, we again modified a method used by Christenson et. al. wherein hydrogen peroxide was mixed with a solution of cobalt chloride to generate oxidative radical species.[37] Just as in the enzymatic study, the hydrogels were subjected to this oxidative media solution and removed and weighed every two days to determine mass loss. As shown in Figure 6B, the oxidative degradation follows the same trends as those seen in the enzymatic degradation, where the PE30 hydrogel is seen to degrade fastest, followed by the PE50, and the PE70 in turn. What this suggests is that an increasing percentage of polyester makes the hydrogel less susceptible to both enzymatic and oxidative degradation processes. The degradation profiles shown here, taken together with the swelling ratios shown above, suggest that an increasing

polyester content leads to a smaller pore size and a lower permeability of the material. For example, as the PE30 hydrogel exhibits the highest swelling ratio, it is expected to be the most permeable to the degradative solutions and is therefore expected to degrade fastest. The range of degradation rates we are able to achieve by altering the composition of these gels gives us a way to tune the properties for a specific application, and is expected to be of great importance in carrying these forward as drug delivery vehicles.

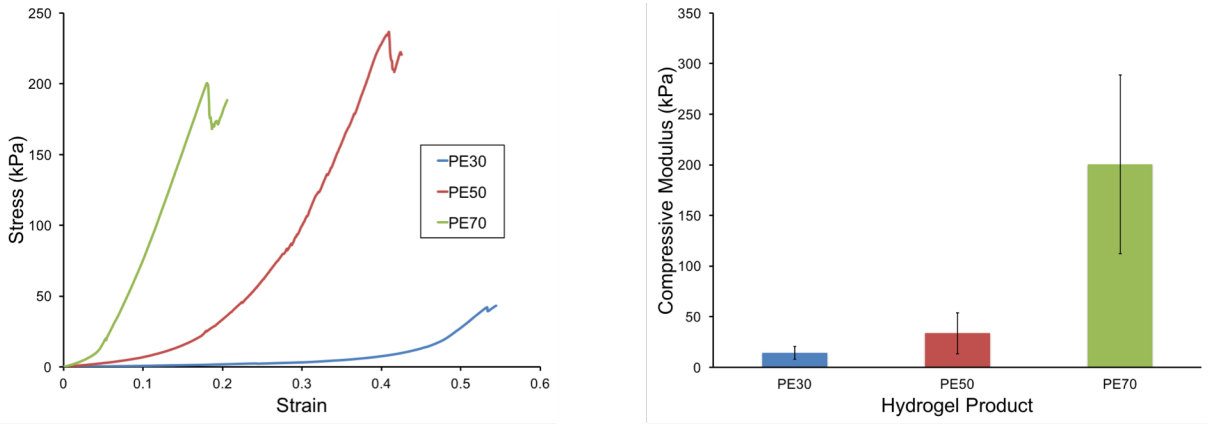

Figure II-7. A) Representative stress-strain curves from hydrogels of each of the three compositions. B) Compressive modulus results of unconfined compression testing of hydrogel materials. The value for the modulus was obtained using the initial linear portion of the stress-strain curve.

The range of properties achieved is also supported by the mechanical compression data, the results of which are shown in Figure 7. As seen in the stress-strain curves, again here a range of properties is achieved. The PE30 hydrogel exhibits the lowest modulus of 14.1 ± 6.3 kPa, while the PE50 and PE70 hydrogels have compressive modulus values of 33.6 ± 20.2 kPa and 200.6 ± 88.1 kPa respectively. All three of these values fall within a range that has been demonstrated to be acceptable for drug delivery applications.[38-40] The significantly higher modulus value of the PE70 gel suggests that the material is much stiffer than the hydrogels of the

other two weight ratios, which will be an important aspect to consider for future use in biomedical applications.

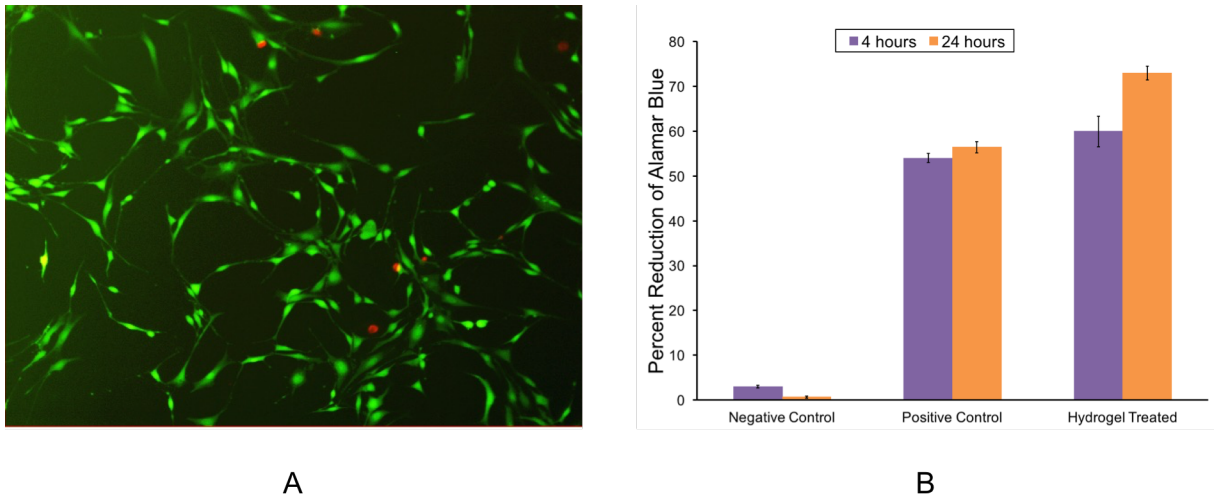

Figure II-8. A) LIVE/DEAD staining of NIH 3T3 cells after incubation with the hydrogel for 24 hours. B) Cells incubated with hydrogel show comparable viability to cells cultured on TCPS as quantified by Alamar Blue assay.

In order to assess the biocompatibility of these hydrogel materials, gel samples were incubated with NIH 3T3 cells for a period of 4 hours or 24 hours. A high viability of cells after incubation is essential if this platform is to be used for biomedical applications. Cells were analyzed qualitatively by LIVE/DEAD staining and quantitatively using an Alamar Blue assay. As shown in Figure 8, cells incubated with PE30 for 4 hours (not shown) or 24 hours show a significantly higher abundance of living cells (green) than dead cells (red). The results of the Alamar Blue assay agree with these qualitative observations (see Figure 8). At both time points, cells incubated with PE30 show comparable reduction of the Alamar Blue reagent as compared to the positive control cells grown on TCPS. These analyses together suggest that these hydrogels exhibit little to no toxicity and could potentially serve as a suitable platform for future biomedical applications.

Conclusions

We have demonstrated that degradable hydrogels can be synthesized using a polyester precursor and a functionalized polyglycidol crosslinker. These hydrogels have demonstrated swelling and mechanical properties that are suitable for protein delivery. Furthermore, the properties of these gels can be tuned based upon the ratio of the two components in the gel network. The tunable nature, along with their demonstrated biocompatibility, makes these materials an excellent candidate as a platform for applications in the controlled delivery of BMP2. Ongoing work with these materials is focused on increasing the incorporation of the OPD monomer into the polyester backbone for the purposes of increased aqueous solubility. Based on the success of our initial model reactions, we postulate that this system could potentially be developed into an injectable system for delivery purposes.

Experimental

Materials

All reagent materials were purchased from Sigma-Aldrich, Acros Chemicals, Fisher Scientific, or EMD Chemicals and were used as received unless otherwise specified. All materials used in the biocompatibility studies were purchased from Life Technologies. Spectra/Por® dialysis membrane was purchased from Spectrum Laboratories Inc. m-CPBA (<77%) was purified as previously described in the literature, and δ-valerolactone was purified after receipt by vacuum distillation.

Characterization

All ^{1}H and ^{13}C spectra were obtained using a Bruker DPX 300 MHz, a Bruker AV-I 400 MHz or a Bruker AV-III 600 MHz spectrometer. Fluorescence imaging was performed using an AZ100 fluorescence microscope equipped with a Nikon DS-Ri1 camera. Mechanical properties were assessed using an Instron 5944 Single Column Testing System.

Purification of m-CPBA

m-CPBA (17.5 g) was dissolved in diethyl ether (125 mL) and transferred to a separatory funnel. The ether layer was then washed 3x with 100 mL portions of buffer solution (410 mL 0.1M NaOH, 250 mL 0.2M KH_2PO_4 made up to 1 L, pH 7.5). The ether layer was dried over $MgSO_4$ and then carefully evaporated using a rotary evaporator to yield the pure (>99%) m-CPBA product.[41] Yield: 11.5 g (65.7%) ^{1}H NMR (300 MHz, $CDCl_3$) δ: 7.46 (1H, t, CH), 7.63 (1H, m, CH), 7.89 (1H, m, CH), 7.99 (1H, m, CH). ^{13}C NMR (100MHz, $CDCl_3$) δ: 126.9, 127.3, 129.3, 130.2, 134.4, 135.1, 166.8.

Synthesis of 2-oxepane-1, 5-dione (OPD)

This reaction was performed as previously described in the literature[42-44] with the exception of the use of purified m-CPBA rather than using the purchased purity. Yield: 3.23 g (70.7%) ^{1}H NMR (300 MHz, $CDCl_3$) δ: 2.72 (2H, m, CH_2), 2.84 (4H, m, CH_2), 4.42 (4H, t, CH_2). ^{13}C NMR (100 MHz, $CDCl_3$) δ: 27.9, 38.6, 44.7, 63.4, 173.2, 204.9

Synthesis of VL/OPD (75/25) Linear Polymer

A 25 mL round-bottom flask was flame-dried and purged with nitrogen. A catalytic amount (2.5 mg, 5.97 x 10^{-6} mol, 3.2 x 10^{-4} eq.) of tin triflate was added to the bottom of the round-bottom flask, and then the flask was again purged with nitrogen. The 3-methyl-1-butanol initiator (54.48 µL, 0.50 mmol, 0.026 eq.) and the dichloromethane were added to the flask to achieve a final monomer concentration of 5.6M. The mixture was stirred for 30 minutes at room temperature and then cooled to 0^{o}C. The OPD (598 mg, 4.67 mmol, 1.0 eq) and δ-valerolactone (1.30 mL, 14.00 mmol, 3.0 eq.) were then added to the flask, and the reaction was allowed to stir at 0^{o}C for 6 hours. The reaction was then warmed to room temperature and stirred overnight before being quenched with methanol. Methanol was removed by rotary evaporation, and excess catalyst was removed by stirring the resulting mixture with a SiliaMetS® Cysteine scavenger (40-63 µm, Silicycle, Inc., Quebec, Canada) for 2.5 hours in DCM. The scavenger was removed by filtration and the product was then purified by dialysis against a 50:50 (v/v) DCM/MeOH solution using Spectra/Por Dialysis Tubing with a 1K MWCO. ^{1}H NMR (400 MHz, CDCl3) δ: 0.92 (6H, d, CH3), 1.53 (2H, q, CH2), 1.58-1.78 (4H, m, CH2), 1.86 (1H, m, CH), 2.34 (2H, m, CH2), 2.52-2.88 (4H, m, CH2), 3.68 (2H, m, CH2), 3.88 (2H, t, CH2), 4.08 (2H, m, CH2), 4.36 (2H, t, CH2). ^{13}C NMR (100 MHz, CDCl3) δ: 21.3, 21.4, 22.5, 25.1, 28.1, 32.1, 33.5, 33.7, 33.9, 37.5, 41.4, 59.1, 62.1, 63.9, 173.4, 209.5

Synthesis of Polyglycidol (PG)

A 25 mL round-bottom flask was flame-dried and purged with nitrogen. A catalytic amount (9.0 mg, 2.16 x 10^{-5} mol, 3.2 x 10^{-4} eq.) of tin triflate was added to the bottom of the round-bottom flask, and then the flask was again purged with nitrogen. The flask was equipped with a nitrogen

balloon, and the 3-methyl-1-butanol initiator (90.8 μL, 0.833 mmol, 1.0 eq.) was then added to the flask and the mixture was allowed to stir at room temperature for 30 minutes. The reaction flask and the distilled glycidol monomer were then cooled to 0^{o}C. The glycidol monomer (4.50 mL, 67.5 mmol, 90.0 eq) was added to the reaction mixture at 0^{o}C dropwise over the course of 20 minutes. After monomer addition was complete, the reaction was allowed to come to room temperature and then stirred overnight. The reaction was quenched with excess methanol and then purified by precipitation into ethyl acetate. ^{1}H NMR (400 MHz, MeOD) δ: 0.92 (6H, d, CH3), 1.48 (2H, q, CH2), 1.72 (1H, m, CH), 3.39-3.98 (5H, m, CH_2CHCH_2). ^{13}C-IG NMR (150 MHz, MeOD) δ: 61.3, 61.8, 63.0, 69.3, 69.6, 70.5-71.9, 72.6, 78.6, 80.1, 81.8.

Synthesis of Phthalimide Functionalized Polyglycidol

The phthalimide functionalized glycidol was synthesized using a previously published procedure, with minor modifications.[27] A 100 mL round-bottom flask was flame-dried and purged with nitrogen, then equipped with a nitrogen balloon. Purified polyglycidol (2.31 g, 7.36 x 10^{-4} mol, 1.0 eq) was dissolved in anhydrous DMF to a concentration of 0.0444 M, and then added to the reaction flask via syringe. N-hydroxyphthalimide (2.84 g, 0.0173 mol, 23.5 eq.) and triphenylphosphine (4.57 g, 0.0173 mol, 23.5 eq.) were added to the reaction flask sequentially. Diisopropyl azodicarboxylate (3.39 mL, 0.0173 mol, 23.5 eq.) was then added dropwise through the septum and the reaction mixture was allowed to stir at room temperature overnight. After reaction completion, DMF was removed via high vacuum rotary evaporator. The concentrated reaction mixture was resuspended in dichloromethane and precipitated twice into a 50/50 (v/v) mixture of ethyl acetate and diethyl ether. Percent functionalization of the polyglycidol was calculated by comparing the integration of the polyglycidol backbone peaks from 3.17-4.95 ppm

to the aromatic proton peak from the phthalimide at 7.72 ppm. ^{1}H NMR (600 MHz, $CDCl_3$) δ: 0.92 (6H, d, CH3), 1.48 (2H, q, CH2), 1.72 (1H, m, CH), 3.17-4.95 (5H, m, CH_2CHCH_2), 7.57-7.85 (4H, m, CH). ^{13}C-IG NMR (150 MHz, $CDCl_3$) δ: 63.7, 68.0, 69.4, 70.6-72.3, 72.8, 78.3, 79.8, 123.5, 128.7, 134.6, 163.3, 163.7, 171.1

Synthesis of Amino-oxy Functionalized Polyglycidol (AOPG)

The final amino-oxy polyglycidol product was also synthesized using an adapted literature procedure.[27] A 200 mL round-bottom flask was flame-dried and purged with nitrogen, then equipped with a nitrogen balloon. The phthalimide functionalized polyglycidol (1.46 g, 4.65 x 10^{-4} mol, 1.0 eq.) was dissolved in anhydrous tetrahydrofuran and added to the reaction flask through the septum. An equivalent volume of anhydrous methanol was then added to the reaction flask. An excess of hydrazine (1.04 mL, 71.0 eq) was then added to the flask dropwise and the reaction was allowed to stir overnight. Unreacted hydrazine was removed via high vacuum rotary evaporator. The phthalimide byproduct was removed by filtration through a 0.45 micron syringe filter followed by dialysis against distilled water, and then methanol using Spectra/Por Dialysis Tubing with a 1K MWCO. ^{1}H NMR (600 MHz, MeOD) δ: 0.87 (6H, d, CH3), 1.42 (2H, q, CH2), 1.66 (1H, m, CH), 3.34-3.93 (5H, m, CH_2CHCH_2). ^{13}C-IG NMR (150 MHz, d-DMSO) δ: 61.2, 61.7, 63.4, 68.1, 68.9, 69.2, 70.0, 70.8, 71.2, 71.8, 73.3, 75.6, 77.3, 78.4, 80.3

Synthesis of O-hydroxylamine tetra (ethylene glycol)

This reaction was performed as previously described in the literature[14] with a modified purification procedure. The intermediate product was adsorbed onto silica gel and then purified by column chromatography. A hexanes:ethyl acetate gradient was used to separate the intermediate from the DIAD byproduct and the triphenyl phosphine oxide. An additional column

using a methanol:ethyl acetate gradient was needed to separate the intermediate product from the remaining tetra(ethylene glycol). ^{1}H NMR (400 MHz, CDCl3) δ: 3.61-3.75 (12H, m, CH2), 3.83 (4H, m, CH2). ^{13}C NMR (100 MHz, CDCl3) δ: 61.0, 69.1, 70.0, 72.4, 74.2

Studying Oxime Click Reaction Kinetics Using a Model Reaction

The VL/OPD polymer (40.0 mg, 11-13% OPD) was dissolved in PBS at pH 7.4 in an Eppendorf tube and then sonicated until a suspension was achieved. The O-hydroxylamine tetra(ethylene glycol) (1.2 eq/ketone) was added and the mixture was diluted further with PBS to achieve a final concentration of 3.0 wt% of the VL/OPD polymer. The Eppendorf tube was then submerged in an oil bath at 37^{o}C and stirred for the indicated amount of time, before being immediately frozen in dry ice. Reactions were lyophilized to remove the PBS, dissolved in deuterated chloroform, and then immediately analyzed by ^{1}H NMR.

Synthesis of Oxime Click Hydrogels

The necessary amount of VL/OPD polymer (13% OPD) was dissolved in DMSO to a concentration of 1.0 mg/μL and then transferred into the well of an 8-well glass slide (Lab-Tek Chamber Slide). The amino-oxy functionalized polyglycidol (1.0 mg/μL in DMSO) was then added via pipette to the well and the reaction mixture was sonicated with a probe sonicator for no more than 30 seconds. The mixture was allowed to sit at room temperature overnight to allow the gel to form. Gels were purified by consecutive 30-minute washes in dichloromethane and methanol followed by a final wash in methanol and then distilled water. Water was removed via lyophilization.

Swelling of Oxime Click Hydrogels

Lyophilized gels were weighed (M_d) and then subsequently submerged in 5.0 mL of PBS at pH 7.4 and kept at 37°C. After 24 hours, the gel was removed and excess water was blotted gently using a Kim Wipe. The gel was then weighed again to determine the swollen weight (M_s). The swelling ratio was calculated for each gel by dividing the swollen weight by the dry weight. All measurements were performed in triplicate.

Oxidative Degradation of Oxime Click Hydrogels

Lyophilized gels were weighed and then placed in 2.0 mL of an oxidative solution (0.1 M $CoCl_2 \bullet 6H_2O$ in 20% H_2O_2) at 37°C. Every two days, gels were removed, rinsed with distilled water, lyophilized, and then weighed. Gels were then returned to the oil bath with a fresh aliquot of oxidative solution and this process was repeated for a total study length of 18 days.[37]

Enzymatic Degradation of Oxime Click Hydrogels

Lyophilized gels were weighed and then placed in 1.0 mL of an enzymatic solution (0.279 U/mL cholesterol esterase in distilled water, filtered through a 0.45 μm PTFE filter) at 37°C. Every two days, gels were removed, rinsed with distilled water, lyophilized, and then weighed. Gels were then returned to the oil bath with a fresh aliquot of enzymatic solution and this process was repeated for a total study length of 18 days.[37]

Unconfined Compression Testing of Oxime Click Hydrogels

Hydrogel samples for mechanical testing were synthesized as previously described and tested directly after formation. The resulting hydrogels were tested in triplicate at a rate of 1 mm min^{-1}

on an Instron 5944. The compressive modulus was determined using the initial linear region for each sample on the stress-strain curve.

Cell Culture

Mouse embryonic fibroblasts (NIH 3T3, Sigma Aldrich, St. Louis, MO) were cultured in Dulbecco's modified eagle's medium (DMEM) supplemented with 10% bovine serum and 1% penicillin/streptomycin. Cells were cultured at 37^{o}C and 5% CO_2 using standard protocols.

LIVE/DEAD Staining

NIH 3T3 cells were grown to 75% confluency and then trypsinized to remove cells from the surface of the flask. Cells were resuspended in full culture media and then seeded onto a 60 x 15 mm tissue culture plate at a density of 2.5 x 10^5 cells/plate. Cells were then allowed to adhere for 20 hours before being overlaid with the gel. After the specified incubation time (4 hours or 24 hours), the gel and media were removed, and the cells were washed with PBS. Cells were stained using a LIVE/DEAD® Viability/Cytotoxicity Kit and visualized using a fluorescence microscope.

Alamar Blue Assay

NIH 3T3 cells were prepared as for the LIVE/DEAD assay, and then overlaid with the hydrogel. After 4 hours of incubation, gel and media were removed, and replaced with a solution of 10% Alamar Blue in culture medium. Cells were then incubated with the Alamar Blue reagent for 20 hours at 37^{o}C and 5% CO_2. The absorbance of the resulting medium was read at 562 nm and 600 nm using a microplate reader. The media was then replenished and the gel was again overlaid

with the cells. After incubation for an additional 24 hours, the gel was again removed and the viability was determined as above. Cells grown on TCPS at the same density were used as a positive control and full culture medium containing no cells was used as a negative control.

References

1. Lee, F. Y.; Sinicropi, S. M.; Lee, F. S.; Vitale, M. G.; Roye, D. P., Jr.; Choi, I. H., Treatment of congenital pseudarthrosis of the tibia with recombinant human bone morphogenetic protein-7 (rhBMP-7). A report of five cases. *Journal of Bone and Joint Surgery American Volume* **2006,** *88* (3), 627-33.

2. Fabeck, L.; Ghafil, D.; Gerroudj, M.; Baillon, R.; Delince, P., Bone morphogenetic protein 7 in the treatment of congenital pseudarthrosis of the tibia. *Journal of Bone and Joint Surgery British Volume* **2006,** *88* (1), 116-8.

3. de la Croix Ndong, J.; Stevens, D. M.; Vignaux, G.; Uppuganti, S.; Perrien, D. S.; Yang, X.; Nyman, J. S.; Harth, E.; Elefteriou, F., Combined MEK inhibition and BMP2 treatment promotes osteoblast differentiation and bone healing in Nf1Osx -/- mice. *Journal of Bone and Mineral Research* **2015,** *30* (1), 55-63.

4. Truong, V. X.; Ablett, M. P.; Richardson, S. M.; Hoyland, J. A.; Dove, A. P., Simultaneous orthogonal dual-click approach to tough, in-situ-forming hydrogels for cell encapsulation. *Journal of the American Chemical Society* **2015,** *137* (4), 1618-22.

5. Peng, T.; Hang, H. C., Site-Specific Bioorthogonal Labeling for Fluorescence Imaging of Intracellular Proteins in Living Cells. *Journal of the American Chemical Society* **2016,** *138* (43), 14423-14433.

6. Kim, K.; Park, J. H.; Park, S. H.; Lee, H. Y.; Kim, J. H.; Kim, M. S., An Injectable, Click-Cross-Linked Small Intestinal Submucosa Drug Depot for the Treatment of Rheumatoid Arthritis. *Advanced Healthcare Materials* **2016**.

7. Zhang, G. G.; Zhao, Q.; Yang, L. P.; Zou, W. K.; Xi, X. Y.; Xie, T., Exploring Dynamic Equilibrium of Diels-Alder Reaction for Solid State Plasticity in Remoldable Shape Memory Polymer Network. *ACS Macro Letters* **2016,** *5* (7), 805-808.

8. Bapat, A. P.; Ray, J. G.; Savin, D. A.; Hoff, E. A.; Patton, D. L.; Sumerlin, B. S., Dynamic-covalent nanostructures prepared by Diels-Alder reactions of styrene-maleic anhydride-derived copolymers obtained by one-step cascade block copolymerization. *Polymer Chemistry* **2012,** *3* (11), 3112-3120.

9. Kharkar, P. M.; Kloxin, A. M.; Kiick, K. L., Dually degradable click hydrogels for controlled degradation and protein release. *Journal of Materials Chemistry B* **2014,** *2* (34), 5511-5521.

10. Li, G. L.; Yu, R.; Qi, T.; Mohwald, H.; Shchukin, D. G., Double-Shelled Polymer Nanocontainers Decorated with Polyethylene glycol) Brushes by Combined Distillation Precipitation Polymerization and Thiol-Yne Surface Chemistry. *Macromolecules* **2016,** *49* (3), 1127-1134.

11. Feldborg, L. N.; Jolck, R. I.; Andresen, T. L., Quantitative evaluation of bioorthogonal chemistries for surface functionalization of nanoparticles. *Bioconjugate Chemistry* **2012,** *23* (12), 2444-50.

12. Ferris, D. P.; McGonigal, P. R.; Witus, L. S.; Kawaji, T.; Algaradah, M. M.; Alnajadah, A. R.; Nassar, M. S.; Stoddart, J. F., Oxime ligation on the surface of mesoporous silica nanoparticles. *Organic Letters* **2015,** *17* (9), 2146-9.

13. Grover, G. N.; Garcia, J.; Nguyen, M. M.; Zanotelli, M.; Madani, M. M.; Christman, K. L., Binding of Anticell Adhesive Oxime-Crosslinked PEG Hydrogels to Cardiac Tissues. *Advanced Healthcare Materials* **2015,** *4* (9), 1327-31.

14. Grover, G. N.; Lam, J.; Nguyen, T. H.; Segura, T.; Maynard, H. D., Biocompatible hydrogels by oxime Click chemistry. *Biomacromolecules* **2012,** *13* (10), 3013-7.

15. Mukherjee, S.; Bapat, A. P.; Hill, M. R.; Sumerlin, B. S., Oximes as reversible links in polymer chemistry: dynamic macromolecular stars. *Polymer Chemistry* **2014,** *5* (24), 6923-6931.

16. Zhang, Y.; Yu, M.; Zhang, C.; Ma, W.; Zhang, Y.; Wang, C.; Lu, H., Highly selective and ultra fast solid-phase extraction of N-glycoproteome by oxime click chemistry using aminooxy-functionalized magnetic nanoparticles. *Analytical Chemistry* **2014,** *86* (15), 7920-4.

17. Olsen, T. R.; Davis, L. L.; Nicolau, S. E.; Duncan, C. C.; Whitehead, D. C.; Van Horn, B. A.; Alexis, F., Non-invasive deep tissue imaging of iodine modified poly(caprolactone-co-1-4-oxepan-1,5-dione) using X-ray. *Acta Biomaterialia* **2015,** *20*, 94-103.

18. Collins, J.; Xiao, Z. Y.; Mullner, M.; Connal, L. A., The emergence of oxime click chemistry and its utility in polymer science. *Polymer Chemistry* **2016,** *7* (23), 3812-3826.

19. Ghosh, S.; Cabral, J. D.; Hanton, L. R.; Moratti, S. C., Strong poly(ethylene oxide) based gel adhesives via oxime cross-linking. *Acta Biomaterialia* **2016,** *29*, 206-214.

20. Mukherjee, S.; Hill, M. R.; Sumerlin, B. S., Self-healing hydrogels containing reversible oxime crosslinks. *Soft Matter* **2015,** *11* (30), 6152-61.

21. Hassan, W.; Dong, Y. X.; Wang, W. X., Encapsulation and 3D culture of human adipose-derived stem cells in an in-situ crosslinked hybrid hydrogel composed of PEG-based hyperbranched copolymer and hyaluronic acid. *Stem Cell Research & Therapy* **2013,** *4*.

22. Anjum, F.; Lienemann, P. S.; Metzger, S.; Biernaskie, J.; Kallos, M. S.; Ehrbar, M., Enzyme responsive GAG-based natural-synthetic hybrid hydrogel for tunable growth factor delivery and stem cell differentiation. *Biomaterials* **2016,** *87*, 104-117.

23. Reid, R.; Sgobba, M.; Raveh, B.; Rastelli, G.; Sali, A.; Santi, D. V., Analytical and Simulation-Based Models for Drug Release and Gel-Degradation in a Tetra-PEG Hydrogel Drug-Delivery System. *Macromolecules* **2015,** *48* (19), 7359-7369.

24. Wang, N. X.; Sieg, S. F.; Lederman, M. M.; Offord, R. E.; Hartley, O.; von Recum, H. A., Using glycosaminoglycan/chemokine interactions for the long-term delivery of 5P12-RANTES in HIV prevention. *Molecular Pharmaceutics* **2013,** *10* (10), 3564-73.

25. Burdick, J. A.; Murphy, W. L., Moving from static to dynamic complexity in hydrogel design. *Nature Communications* **2012,** *3*.

26. Angelo S. Mao, J.-W. S., Stefanie Utech, Huanan Wang, Oktay Uzun, Weiwei Li, Madeline Cooper, Yuebi Hu, Liyuan Zhang, David A. Weitz, and David J. Mooney, Deterministic encapsulation of single cells in thin tunable microgels for niche modelling and therapeutic delivery. *Nature Materials* **2017,** *16*, 236-243.

27. Beezer, D. B.; Harth, E., Post-Polymerization Modification of Branched Polyglycidol with N-Hydroxy Phthalimide to Give Ratio-Controlled Amino-Oxy Functionalized Species. *Journal of Polymer Science Part A: Polymer Chemistry* **2016,** *54* (17), 2820-2825.

28. Spears, B. R.; Waksal, J.; McQuade, C.; Lanier, L.; Harth, E., Controlled branching of polyglycidol and formation of protein-glycidol bioconjugates via a graft-from approach with "PEG-like" arms. *Chemical Communications* **2013,** *49* (24), 2394-2396.

29. Adak, A.; Das, G.; Barman, S.; Mohapatra, S.; Bhunia, D.; Jana, B.; Ghosh, S., Biodegradable Neuro-Compatible Peptide Hydrogel Promotes Neurite Outgrowth, Shows

Significant Neuroprotection, and Delivers Anti-Alzheimer Drug. *ACS Applied Materials and Interfaces* **2017,** *9* (6), 5067-5076.

30. Koetting, M. C.; Guido, J. F.; Gupta, M.; Zhang, A.; Peppas, N. A., pH-responsive and enzymatically-responsive hydrogel microparticles for the oral delivery of therapeutic proteins: Effects of protein size, crosslinking density, and hydrogel degradation on protein delivery. *Journal of Controlled Release* **2016,** *221*, 18-25.

31. Aran, K.; Parades, J.; Rafi, M.; Yau, J. F.; Acharya, A. P.; Zibinsky, M.; Liepmann, D.; Murthy, N., Stimuli-responsive electrodes detect oxidative stress and liver injury. *Advanced Materials* **2015,** *27* (8), 1433-6.

32. Zhao, W. F.; Han, Z. Y.; Ma, L.; Sun, S. D.; Zhao, C. S., Highly hemo-compatible, mechanically strong, and conductive dual cross-linked polymer hydrogels. *Journal of Materials Chemistry B* **2016,** *4* (48), 8016-8024.

33. Stevens, D. M.; Watson, H. A.; LeBlanc, M. A.; Wang, R. Y.; Chou, J.; Bauer, W. S.; Harth, E., Practical polymerization of functionalized lactones and carbonates with Sn(OTf)(2) in metal catalysed ring-opening polymerization methods. *Polymer Chemistry* **2013,** *4* (8), 2470-2474.

34. Zhou, C.; Heath, D. E.; Sharif, A. R.; Rayatpisheh, S.; Oh, B. H.; Rong, X.; Beuerman, R.; Chan-Park, M. B., High water content hydrogel with super high refractive index. *Macromolecular Bioscience* **2013,** *13* (11), 1485-91.

35. Glisoni, R. J.; Garcia-Fernandez, M. J.; Pino, M.; Gutkind, G.; Moglioni, A. G.; Alvarez-Lorenzo, C.; Concheiro, A.; Sosnik, A., beta-Cyclodextrin hydrogels for the ocular release of antibacterial thiosemicarbazones. *Carbohydrate Polymers* **2013,** *93* (2), 449-57.

36. Xu, W.; He, X.; Zhong, M.; Hu, X.; Xiao, Y., A novel pH-responsive hydrogel based on natural polysaccharides for controlled release of protein drugs. *RSC Advances* **2015,** *5* (5), 3157-3167.

37. Christenson, E. M.; Patel, S.; Anderson, J. M.; Hiltner, A., Enzymatic degradation of poly(ether urethane) and poly(carbonate urethane) by cholesterol esterase. *Biomaterials* **2006,** *27* (21), 3920-6.

38. Fajardo, A. R.; Silva, M. B.; Lopes, L. C.; Piai, J. F.; Rubira, A. F.; Muniz, E. C., Hydrogel based on an alginate-Ca2+/chondroitin sulfate matrix as a potential colon-specific drug delivery system. *RSC Advances* **2012,** *2* (29), 11095-11103.

39. Han, S.; Ham, T. R.; Haque, S.; Sparks, J. L.; Saul, J. M., Alkylation of human hair keratin for tunable hydrogel erosion and drug delivery in tissue engineering applications. *Acta Biomaterialia* **2015,** *23*, 201-213.

40. Chun, Y. Y.; Wang, J. K.; Tan, N. S.; Chan, P. P. Y.; Tan, T. T. Y.; Choong, C., A Periosteum-Inspired 3D Hydrogel-Bioceramic Composite for Enhanced Bone Regeneration. *Macromolecular Bioscience* **2016,** *16* (2), 276-287.

41. Aggarwal, V. K.; Gultekin, Z.; Grainger, R. S.; Adams, H.; Spargo, P. L., (1R,3R)-2-methylene-1,3-dithiolane 1,3-dioxide: a highly reactive and highly selective chiral ketene equivalent in cycloaddition reactions with a broad range of dienes. *Journal of the Chemical Society-Perkin Transactions 1* **1998,** (17), 2771-2781.

42. van der Ende, A.; Croce, T.; Hamilton, S.; Sathiyakumar, V.; Harth, E., Tailored polyester nanoparticles: post-modification with dendritic transporter and targeting units via reductive amination and thiol-ene chemistry. *Soft Matter* **2009,** *5* (7), 1417-1425.

43. van der Ende, A. E.; Kravitz, E. J.; Harth, E., Approach to formation of multifunctional polyester particles in controlled nanoscopic dimensions. *Journal of the American Chemical Society* **2008,** *130* (27), 8706-13.

44. van der Ende, A. E.; Sathiyakumar, V.; Diaz, R.; Hallahan, D. E.; Harth, E., Linear release nanoparticle devices for advanced targeted cancer therapies with increased efficacy. *Polymer Chemistry* **2010,** *1* (1), 93-96.

CHAPTER III

TARGETING THE ISLETS OF LANGERHANS USING A POLYESTER NANOPARTICLE SCAFFOLD

Introduction

The Islets of Langerhans are discrete groups of cells contained within the pancreas, and contain the β-cells responsible for the secretion of insulin. In both type 1 and type 2 diabetes, the functional capacity of these β-cells is reduced as a result of inflammation or apoptosis, leading to a loss of glycemic control, among other symptoms.[1-3] At present, most therapies used to treat diabetes are focused on insulin replacement, rather than on restoring the function of the β-cells.[4-7] Recently, multiple small molecules have emerged as potential therapies and have shown great promise as inhibitors of β-cell death, both *in vitro* and *in vivo*.[8-10] However, these small molecules are often not effective in practice due to the high risk of severe off-target effects. It is clear that the efficacy of many of these therapeutics could be drastically improved by entrapping them within a targeted delivery vehicle that could carry and then subsequently release the drug at the surface of the β-cells.

Nanoparticles have long been utilized as delivery systems of small molecule drugs ranging from chemotherapeutic agents[11-15] to anti-retroviral[16-17] and anti-inflammatory[18-19] medications. One of the most prevalent polymers used in these types of applications is poly (lactic-co-glycolic acid) (PLGA),[20-23] due to its well-demonstrated biocompatibility, and ability to self-assemble into particles in aqueous solution. These particles have shown great success in increasing both the solubility and the bioavailability of many hydrophobic drugs, but are limited in their ability to be

post-modified after formation.

Our lab has shown that polyester nanoparticles can be synthesized via an amine-epoxide crosslinking reaction,[24-25] and that the rate of release of a therapeutic from these particles can be modulated based upon the crosslinking density.[26] These nanoparticles offer multiple advantages over traditional PLGA-based particles, the most significant being the availability of functional groups on the surface that can undergo post-modification reactions. Unlike PLGA-based nanoparticles which are self-assembled, these polyester particles are chemically crosslinked, so post-modification reactions can be performed in organic solvent without inducing dissolution of the particle structure. In this work, we will demonstrate that the functional groups on the particle surface can be utilized to conjugate both a targeting moiety and a dye molecule to create a fluorescently tagged nanoparticle intended for specific therapeutic delivery to the β-cells.

One of the most well-studied interactions at the surface of the β-cells is that of glucagon-like peptide (GLP1) and its corresponding receptor, GLP1-R. This interaction gives GLP1 the potential to be used a targeting unit for specific therapeutic delivery to the β-cell surface. However, GLP1 is highly prone to degradation and has a very short plasma half-life (1-2 minutes),[27-28] both of which preclude it from being viable for therapeutic use. Exendin4 is a well-studied GLP1 agonist with similar efficacy and a much longer half-life, making this peptide much more applicable for clinical use than GLP1.[29] In this work, we utilize a modified version of this peptide as the targeting unit that is covalently attached to the surface of the nanoparticle.

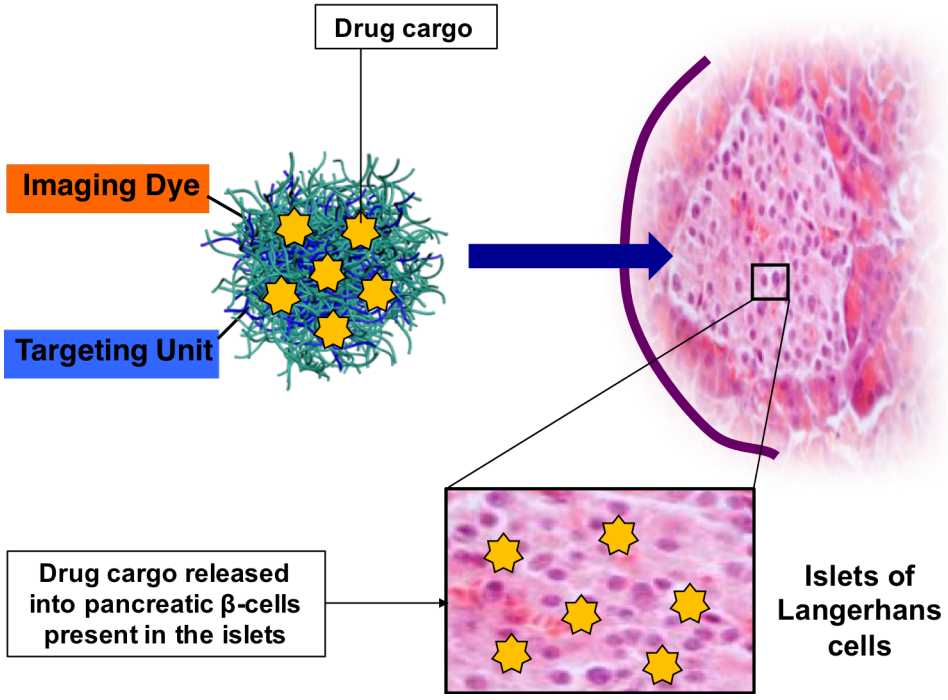

Figure III-1. A peptide labeled, fluorescently tagged nanoparticle capable of delivering therapeutics directly to pancreatic β-cells.

The goal of this work is to construct a nanoparticle platform using Exendin4 as a targeting moiety that could be used to deliver therapeutics directly to the pancreatic β-cells (Figure 1). As we wished to be able to track the location of this delivery system in an *in vivo* model to establish targeting ability, a fluorescent dye was also conjugated to the surface. Because of the wide range of functional groups contained in the Exendin4 sequence, conjugating both the peptide and an imaging dye to the particle surface without comprising the function of either molecule presented synthetic challenges. We will demonstrate in this work the successful development of an orthogonal synthesis scheme to conjugate both an imaging dye and a peptide targeting unit to the surface of the particle delivery vehicle. We will also show that this nanoparticle delivery system is capable of successfully targeting GLP1-R using both a tumor model, and subcutaneous human islet grafts.

Results and Discussion

Polyester nanoparticles formed by amine-epoxide crosslinking were synthesized and then surface-modified with both an Exendin4 targeting peptide and a near infrared dye molecule. An orthogonal synthesis scheme was developed so that both surface units could be successfully attached without inducing any undesirable side reactions. A CRE-Luc assay was used to demonstrate that the activity of the Exendin4 agonist is maintained *in vitro* after attachment to the nanoparticle surface. The fully targeted nanoparticle labeled with Exendin4 and a suitable imaging dye was shown to successfully target GLP1-R *in vivo* using both a tumor model and subcutaneous human islet grafts.

Synthesis of a Cys40-Exendin4 Labeled, Fluorescently Tagged Nanoparticle for Targeting the Islets of Langerhans

Polyester nanoparticles were formed using previously developed protocols[26] to create a macromolecular structure with both allylic and amine functional groups present on the surface of the carrier. Briefly, this synthesis involves the crosslinking of polyester chains that contain both allyl and epoxide functional groups, with a diamine linker. The diamine linker reacts with the epoxide groups on the linear polymer, leaving the allyl groups free on the surface of the particle. As the diamine is added in excess to the epoxides, there are also free amine groups present on the particle surface. Proton NMR of the nanoparticles shows a high incorporation of the diamine linker, as evidenced by the peak at 3.50 ppm, providing an abundance of attachment sites on the surface, and TEM analysis of the particles shows an average size of approximately 100 nm. Previous work in our lab has led to successful nanoformulations that are surface-conjugated to both an imaging dye and a targeting unit.[24, 30] In these protocols, thiolene click chemistry is used to attach the targeting unit to the surface of the nanoparticle via the allyl group on the surface,

followed by conjugation of the imaging dye to the amines on the surface using NHS-ester chemistry. However, as the Exendin4 contains free amine groups as part of its structure, using this synthesis scheme would result in undesired labeling of the peptide with the NHS-ester dye, rendering the peptide inactive. This obstacle required the construction of a new synthesis scheme for conjugation using orthogonal chemistries for the attachment of each component.

To this end, the amine functional group on the surface of the particle was converted to an aldehyde by use of the small molecule linker, N-hydroxysuccinimidyl-p-formylbenzoate. The NHS ester group on the small molecule linker reacts with the amine on the particle surface, leaving

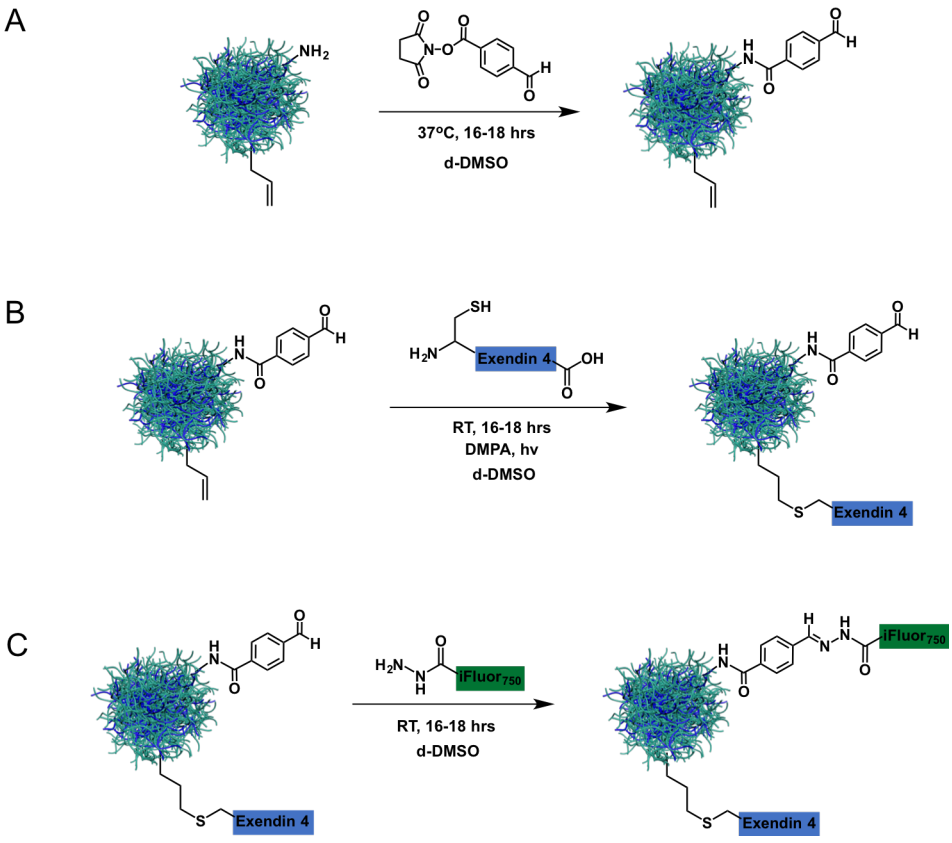

Figure III-2. The orthogonal synthesis scheme for attachment of both an Exendin4 peptide targeting unit and an imaging dye to the surface of the nanoparticle. A) Amines on the surface of the particle are transformed into aldehyde groups by reaction with an N-succinimidyl-p-formylbenzoate linker. B) The peptide is attached using a thiolene click reaction via the free thiol on the cysteine residue. C) The imaging dye is attached to the surface via a hydrazine linkage that does not interfere with any of the functional groups in the peptide.

the aldehyde group free. This linker was successfully conjugated to the surface of the nanoparticle using the conditions shown in Fig. 2. Following attachment of the N-succinimidyl-p-formylbenzoate to the surface of the nanoparticle, the ^{1}H NMR spectrum of the purified material shows peaks in both the aromatic region and at 10.1 ppm for the free aldehyde as expected. The peaks for the aromatic protons and the free aldehyde proton of the linker that appear in the spectrum of the purified material are shifted slightly upfield from those of the free linker, as would be expected upon attachment to a macromolecular structure. Conjugation of this linker successfully transformed the free amines on the vehicle surface into free aldehyde groups, allowing for attachment of the imaging dye to the surface via hydrazide chemistry. As there are no free aldehyde or ketone groups present in the Exendin4 peptide, this conjugation eliminated the possibility of undesired peptide labeling.

The allyl functional group on the surface of the particle allows for attachment of a peptide unit via the free thiol of a cysteine group. As Exendin4 does not contain a native cysteine residue, one was installed just before the N-terminus of the peptide. The cysteine was installed here specifically because the active binding domain of Exendin4 to GLP1-R is located on the C-terminus of the peptide. The Cys40-Exendin4 peptide was conjugated to the particle surface via a thiolene click reaction using DMPA as a photoinitiator. A reduction of the allyl peaks at 5.04 and 5.73 ppm in the crude spectrum of the attachment product indicates a successful attachment of the peptide. In this work, a near infrared dye molecule was utilized (λ_{em} = 750 nm) as this wavelength of light most easily penetrates skin and would be most easily visualized using *in vivo* imaging. The hydrazide dye was attached to the nanoparticle via the free aldehyde on the linker molecule that was previously installed on the surface. The attachment of the hydrazide dye was run under ambient conditions in the absence of light and again monitored by ^{1}H NMR. Both

shape changes in the aromatic region as well as the disappearance of the free aldehyde peak at 10.06 ppm confirms the attachment of the dye. Integration of the aromatic region from 6.5-7.4 ppm following the attachment of the dye and the subsequent purification shows an increase in the region of 3.87 protons. The protons in this region should almost exclusively be the result of aromatic residues on the peptide backbone, so it is possible to estimate the number of peptides on each particle using the integration value. Each Exendin4 peptide contains four aromatic residues which contribute a total of 16 protons to the specified region. A calculation based on this integration increase shows a total of 11.7 Exendin4 peptides attached to each nanoparticle, which

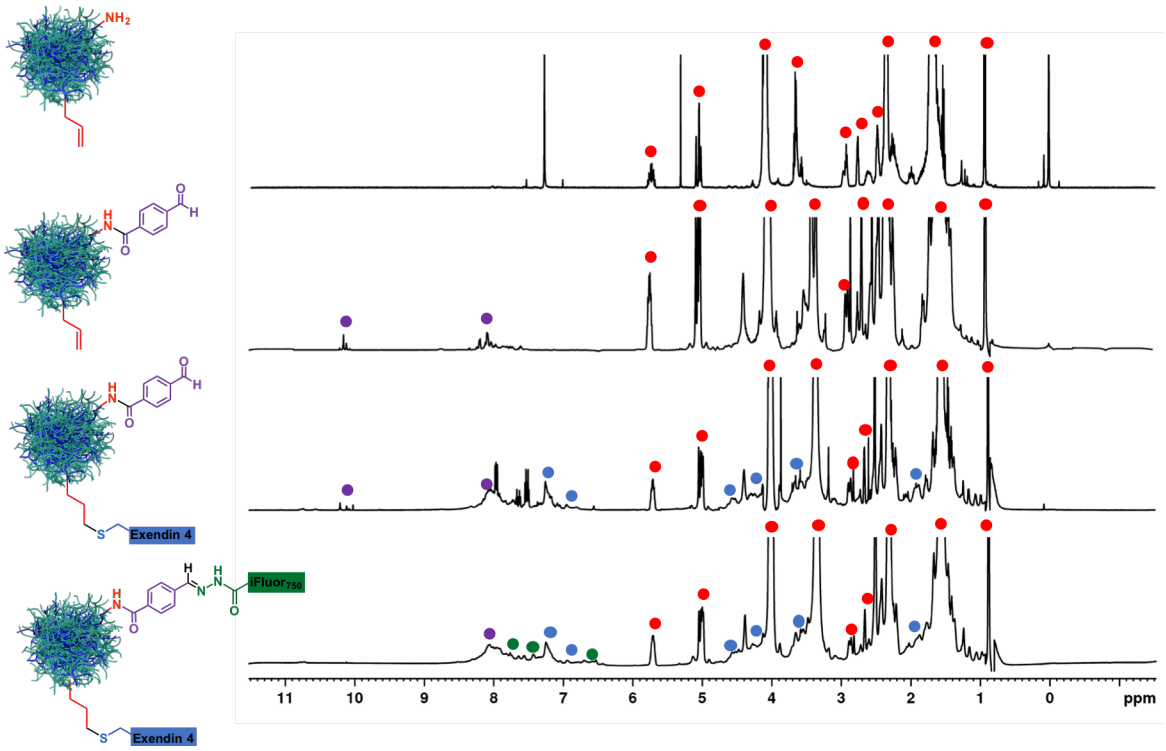

Figure III-3. An overlay of NMR spectra showing each step of the orthogonal synthesis scheme to construct a nanoparticle with both a peptide targeting unit and an imaging dye attached. Polyester nanoparticles show a good incorporation of the diamine linker (top). Attachment of the N-succinimidly-p-formylbenzoate to the surface of the particles (top center). Attachment of the Cys40-Exendin4 peptide to the particle surface (bottom center). Attachment of the iFluor750 hydrazide dye to the surface (bottom). Attached moieties on the surface are colored to correspond to the labeled peaks in the NMR.

is consistent with the experimental conditions. Figure 3 shows an overlay of the ^{1}H NMR data from all of the attachments to the nanoparticle surface.

Cys40-Exendin4 as a Targeting Unit

Before the targeted, dye labeled nanoparticle could be tested *in vivo,* it was necessary to confirm that the addition of the cysteine residue as well as conjugation of the peptide to the particle structure did not affect the binding affinity of the Exendin4 to GLP1-R. Two separate assays were utilized in order to test each of these conditions. To analyze the effect of the cysteine residue addition on the binding affinity of the peptide, an HEK293:GLP1-R cell line was developed by the Powers lab. The expression of GLP1-R on the surface of these cells was confirmed by incubating the cells with a fluorescein labeled Exendin4 and then washing extensively. As can be seen in Figure 4, when analyzed under a fluorescent microscope, the control cell line of HEK293 cells shows no fluorescence, while the modified cell line shows strong fluorescence signal in the fluorescein channel, indicating binding of the Exendin4 peptide

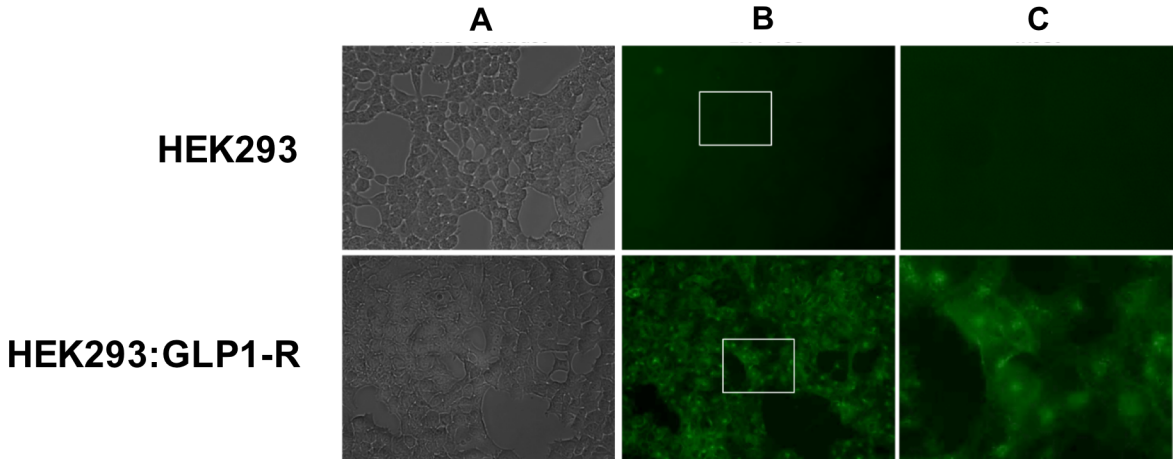

Figure III-4. Fluorescently labeled Exendin4 binds to the GLP1-R modified HEK293 cells, indicating a successfully incorporation of the receptor on the surface. A) Phase contrast microscope image of HEK293 (top) and HEK293:GLP1-R (bottom) cells. B) Fluorescence microscope image of HEK293 (top) and HEK293:GLP1-R (bottom) cells. C) Magnified images of the insets shown in B). Imaging experiments were performed by Neil Phillips of the Powers lab.

and the successful incorporation of GLP1-R onto the surface of the cells.

Using this same HEK293:GLP1-R cell line, the activity of the Cys40-Exendin4 peptide was compared to that of the native Exendin4 peptide using a CRE-Luc assay. Cells were modified to express luciferase in response to an elevated cyclic AMP level caused by the binding

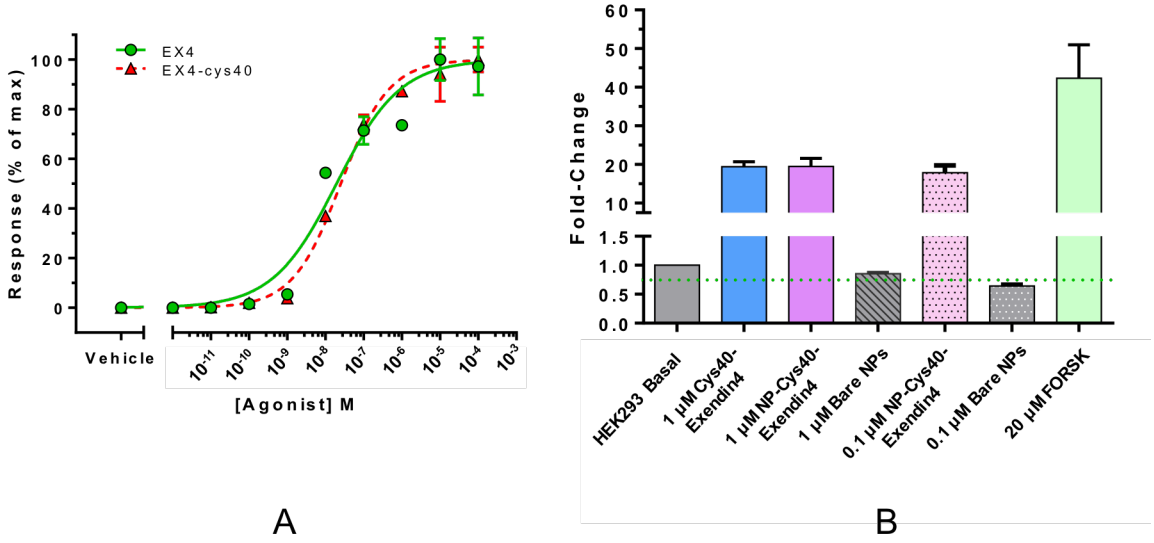

Figure III-5. A) The dose-response curve for Cys40-Exendin4 versus the native sequence using a CRE-Luc assay and HEK293:GLP1-R cells. The nearly identical curves show that the addition of the cysteine residue has no detrimental effect on the binding affinity. B) The results of the same CRE-Luc assay using HEK293:GLP1-R cells showing that the binding affinity of the peptide is not altered upon attachment to the particles. At both 1 µM and at 0.1 µM Exendin4, the peptide conjugated particles show the same increase in luminescence as the 1 µM Cys40-Exendin4 alone. CRE-Luc assays were performed by Neil Phillips of the Powers lab.

of Exendin4 to GLP1-R, and then incubated with either unmodified Exendin4 or Cys40-Exendin4 for several hours at varied concentrations. After incubation, cells were dosed with a luciferase substrate, and the luminescence was measured. In this way, the luminescence signal seen can be correlated to the binding affinity of Exendin4. Figure 5 shows that the dose response curve for the Cys40-Exendin4 is nearly identical to the native, unmodified peptide, indicating that the addition of the cysteine residue has no effect on the binding affinity.

To test the effect of conjugation to the nanoparticle surface on the binding affinity of the Cys40-Exendin4, this peptide was conjugated to bare nanoparticles using a thiolene click reaction. Using the same CRE-Luc assay, these peptide-labeled nanoparticles were tested for binding affinity to GLP1-R. The measured luminescence signal for Cys40-Exendin4 alone and peptide labeled nanoparticles at two concentrations was compared; bare nanoparticles were used a negative control, and forskolin (FORSK) was used as a positive control for the assay. As shown in Figure 5, the Cys40-Exendin4 conjugated to the nanoparticles exhibits comparable binding to the free Cys40-Exendin4 at both concentrations. From this we can conclude that the particle conjugation has no detrimental effect on the function of the peptide.

Studying the Targeting Ability of Cys40-Exendin4 Conjugated Nanoparticles using a PC9:GLP1-R Model

After confirming the binding ability of the Cys40-Exendin4 labeled nanoparticle *in vitro,* we wished to test the ability of this construct to target GLP1-R *in vivo*. For initial *in vivo* experiments, we chose to use a model system in place of human islet grafts, due to the large variability and unpredictability of the islet donor pool.[31] Because islet grafts come from human donors, each group of islets will have varied expression of GLP1-R, as well as varied viability ratios. Therefore, for these experiments, we instead utilized a PC9 lung carcinoma cell line modified to express GLP1-R developed by the Powers lab. Unmodified PC9 cells, which do not express GLP1-R were utilized as a negative control. Aliquots of either PC9 or PC9:GLP1-R cells were engrafted onto the hind legs of mice and allowed to form a tumor mass over the course of 5 weeks.

To confirm the validity of the tumor model, we synthesized an iFluor750-labeled version

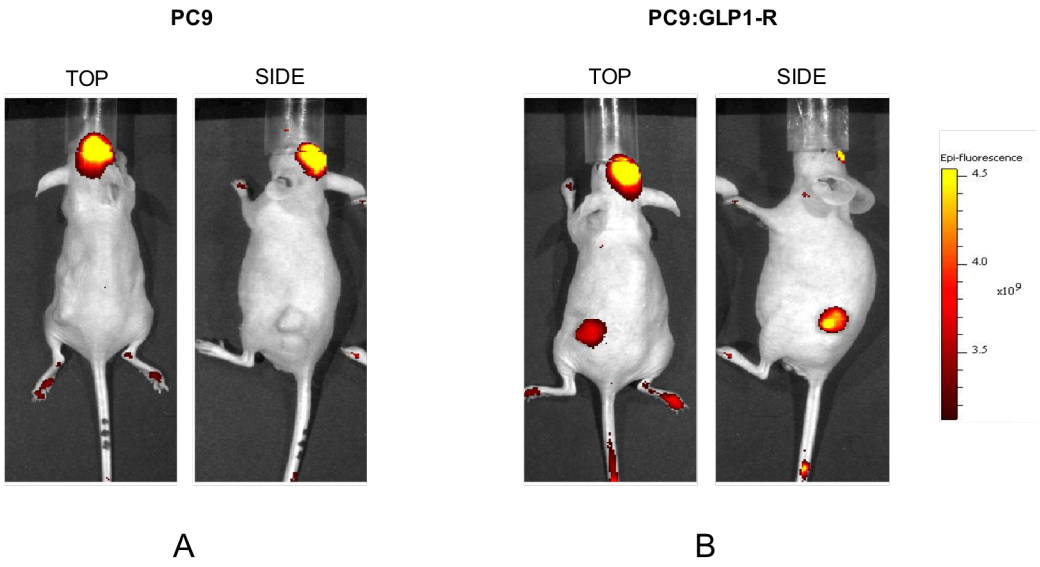

Figure III-6. Mice imaged 70 minutes post injection of 450 µg of Cys40-Exendin4 conjugated to a maleimide functionalized iFluor750 dye. A) The top and side view of the PC9 mouse, showing no fluorescence accumulation in the tumor. B) The top and side view of the PC9:GLP1-R mouse, showing an accumulation of the fluorescently labeled peptide in the tumor, indicating a successful binding of Exendin4 to the GLP1-R. Injections and *in vivo* imaging were performed by Neil Phillips in the Powers lab.

of the Cys40-Exendin4 by conjugating a maleimide functionalized dye to the peptide via the free thiol of the cysteine residue. Both PC9 and PC9:GLP1-R mice were then injected with this fluorescently labeled peptide (450 µg, 150 µL), and imaged 70 minutes after injection. Figure 6 shows that an accumulation of fluorescence is only observed in the PC9:GLP1-R mouse, which demonstrates the binding capability of the Cys40-Exendin4 to the receptor at the tumor site, and acts as a positive control to which the targeted nanoparticle construct can be compared.

Following confirmation of the validity of the model, mice bearing either PC9 or PC9:GLP1-R tumors were each injected with nanoparticles labeled with both Cys40-Exendin4 and an iFluor750 dye (2.2 mg, 450 µg peptide per mouse) which were synthesized as described in the sections above. Figure 7 shows the resulting images taken 24 hours post-injection. As clearly shown, the targeted nanoparticles accumulate readily in the PC9:GLP1-R tumor, while no

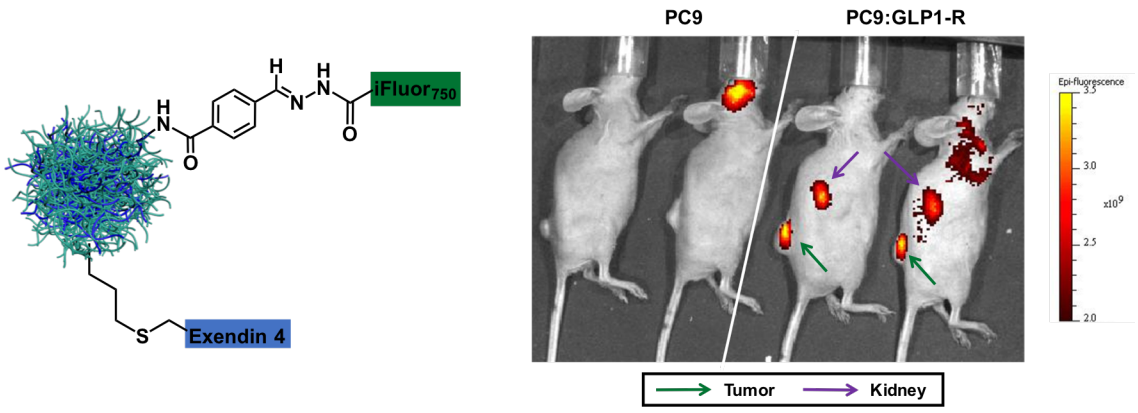

A B

Figure III-7. A) The nanoparticle construct that the mice were injected with prior to imaging, bearing both Cys40-Exendin4 and an iFluor750 imaging dye. B) Imaging results 24 hours post-injection. Mice from the PC9 group (left) are separated from mice from the PC9:GLP1-R group (right) by the white solid line. PC9 mice show no accumulation of fluorescence in the tumor, while PC9:GLP1-R mice show a clear accumulation of the targeted nanoparticle in the tumor mass as indicated by the green arrows. Signal that can be attributed to the degradation of the nanoparticles is seen in the kidneys and indicated by the purple arrows. The *in vivo* imaging shown in B) was performed by Neil Phillips of the Powers lab.

signal is seen from the PC9 tumor. These results help to establish that the fluorescence localization at the PC9:GLP1-R tumor site is a result of the nanoparticle construct successfully binding to GLP1-R, and not a false positive signal due to the EPR effect. Signal is also observed in the kidneys, as labeled in Figure 7. Kidney signal is to be expected due to the degradable nature of the nanoparticles. It is important to note that no accumulation is seen in the liver of the mouse, indicating little to no buildup or toxicity of the fully labeled nanoparticle.

As a second control experiment, one mouse was also engrafted with contralateral tumors, with only one of the tumors bearing the GLP1 receptor. This mouse acted as an internal control and allowed us to test whether the fully labeled nanoparticle would preferentially target the PC9:GLP1-R tumor over the PC9 tumor under the same physiological conditions. Figure 8 shows a comparison of a mouse from the PC9 group and the mouse engrafted with contralateral

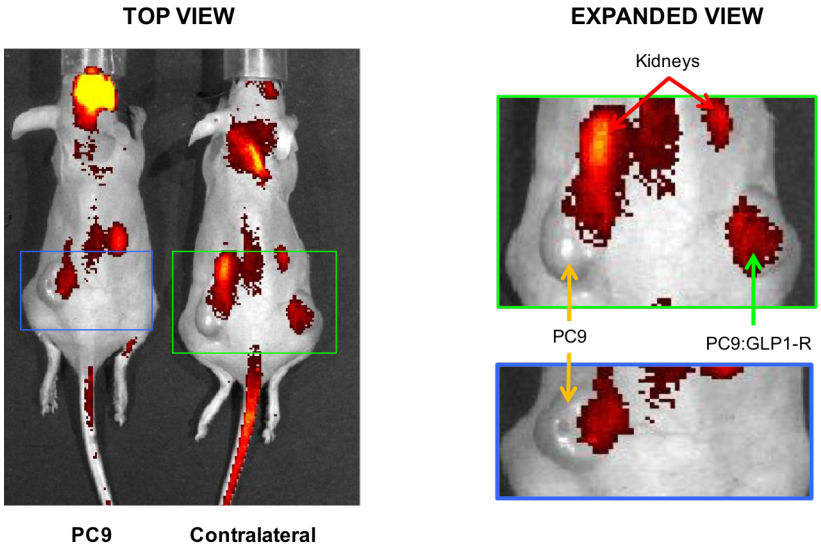

Figure III-8. A) A top down view of a PC9 mouse (left) and a mouse engrafted with contralateral PC9 and PC9:GLP1-R tumors (right), imaged 24 hours post injection of the Cys40-Exendin4 labeled, iFluor750 dye tagged nanoparticles. The contralateral mouse has a PC9 tumor on the left hind limb and a PC9:GLP1-R tumor on the right hind limb. B) Insets from A showing the contralateral mouse (green inset, top) and a PC9 mouse for comparison (blue inset, bottom). The contralateral mouse shows that accumulation of the targeted nanoparticles is only seen in the PC9:GLP1-R tumor. The fluorescence signal seen in close proximity to the PC9 tumor is due to the kidney of the mouse. *In vivo* imaging was performed by Neil Phillips of the Powers lab.

tumors. Insets demonstrate the 1.5-fold increase in signal that is observed in the PC9:GLP1-R tumor over the PC9 tumor, indicating that the nanoparticle construct preferentially targets the receptor-bearing tumor. It is important to note here that as indicated in Figure 8, the left kidney on these mice is lower than the right, which contributes to the signal seen in the PC9 tumor. A comparison to a PC9 mouse from the experimental group shows the location of the kidney signal that is expected to be observed. Because of this signal slightly obscuring the PC9 tumor, the difference between the two signals may in fact be even higher.

Studying the Targeting Ability of Cys40-Exendin4 Conjugated Nanoparticles using Human Islet Cells

After the targeting ability of the Cys40-Exendin4 and iFluor750 dye labeled nanoparticle was confirmed in the tumor model, we began to test the ability of this construct to target human islet grafts *in vivo*. Initial studies were conducted using human islet grafts placed in the fat pad of a mouse. Mice were then injected with a suspension of Cys40-Exendin4 and iFluor750 dye labeled nanoparticles and then subsequently imaged 24 hours after injection. Both *in vivo* imaging and *ex vivo* imaging of the pancreas, kidneys, and fat pad were performed to determine if a localized fluorescence signal could be seen in the fat pad. These initial experiments showed no fluorescence signal in the fat pad after 24 hours, making it clear that optimization of experimental conditions was necessary. It was hypothesized that the fatty composition of the tissue around the islet graft may be contributing to the attenuation of the fluorescence signal, making detection of the nanoparticles much more difficult. In order to combat this, we worked to increase our fluorescence signal by encapsulating the fluorophore Nile Red in the matrix of the nanoparticles following surface modification with the Cys40-Exendin4 and the iFluor750 dye. Mice injected with this Nile Red-loaded nanoparticle construct show a strong fluorescence signal in the fat pad after 24 hours when imaged using the Nile Red fluorescence channel (650 nm), indicating localization of the targeted nanoparticles to the islet graft. Figure 9 shows images of the pancreas, kidneys, and fat pad of two mice injected with this targeted, Nile-Red loaded nanoparticle construct.

An additional set of *in vivo* studies utilizing a different location of the islet graft was also carried out. Grafts for these studies were implanted subcutaneously in the quadricep muscle of the mice, and then monitored for several weeks to ensure suitable viability of the grafts. This

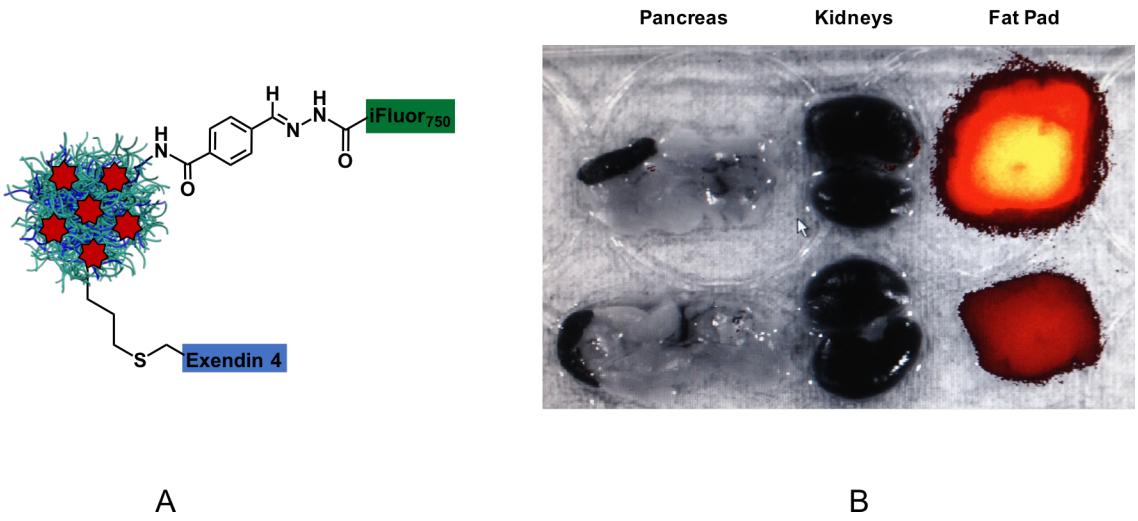

Figure III-9. A) Structure of the nanoparticles labeled with Cys40-Exendin4 and iFluor750 dye, and loaded with Nile Red (red starbursts). B) *Ex vivo* imaging of mice injected with the nanoparticle construct in A) 24 hours post-injection. Clear fluorescence signal from the Nile Red is seen in the fat pad, indicating localization of the targeted particles to the islet graft. No fluorescence is seen in either the kidneys or the pancreas of the mice. *Ex vivo* imaging was performed by Neil Phillips of the Powers lab.

location of the islet graft offers several benefits over the fat pad location including longer viability and ease of *in vivo* imaging. Because of the subcutaneous nature of the graft, *in vivo* fluorescence signal should be easily seen, as there is only a thin skin layer which the light must pass through to be detected. Because of this benefit, experiments utilizing this graft location were performed first without the incorporation of the Nile Red into the nanoparticles, to see if the signal from the dye alone was strong enough to indicate localization. When testing this graft location, a negative control for the *in vivo* studies was also developed and implemented.

For these studies, a control within the mouse model itself as used for our tumor model system was not possible, as all human islet grafts will contain GLP1-R. Therefore, it was necessary to establish a nanoparticle control. Rather than use bare nanoparticles as a control, we chose instead to develop a construct that was very similar to the Cys40-Exendin4 and dye

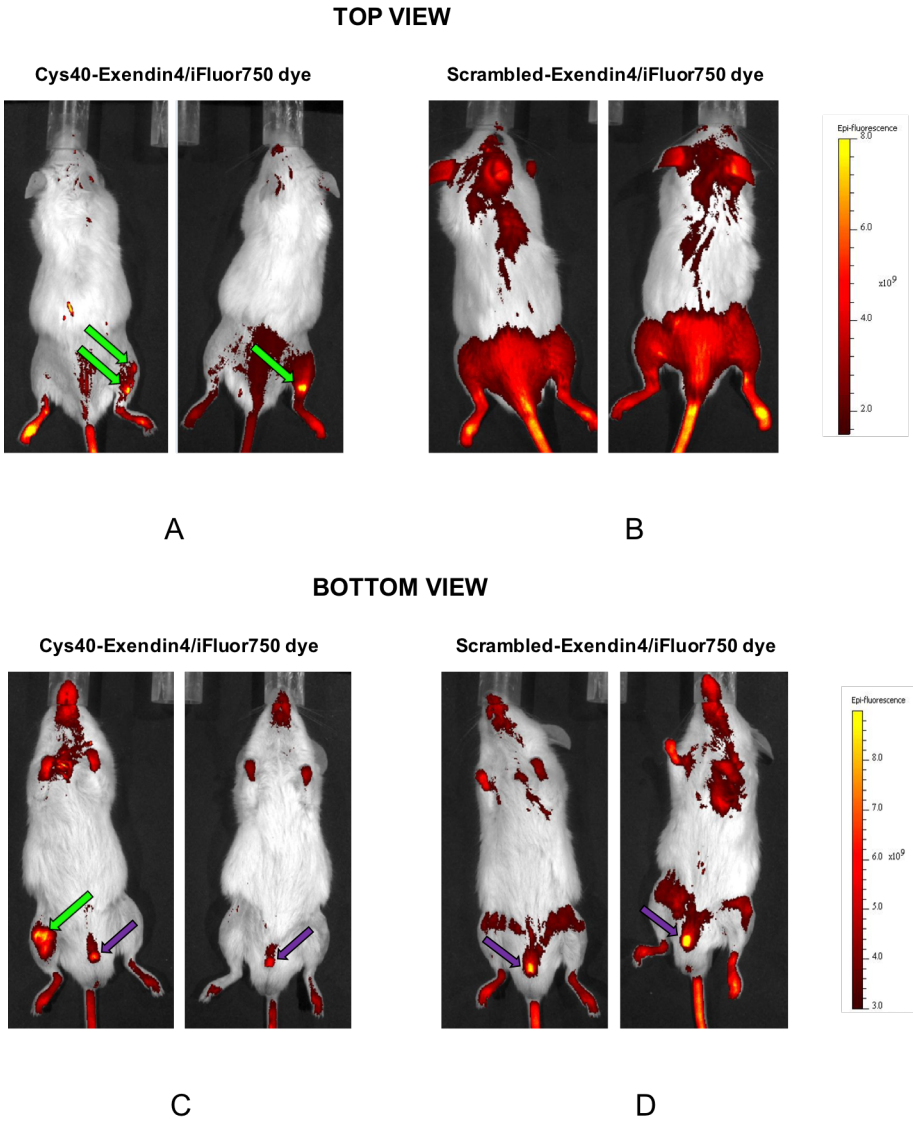

Figure III-10. A) A top down view of two mice injected with nanoparticles labeled with Cys40-Exendin4 and iFluor750 dye, imaged 18 hours post injection. The strongest fluorescence signal is observed at the location of the islet graft as indicated by the green arrows, indicating successful targeting. B) Mice injected with nanoparticles labeled with the scrambled control sequence and iFluor750 dye show only background fluorescence. C) A flipped view of the two mice in A). The purple arrows indicate signal seen in the bladder due to degradation and clearance of the nanoparticles. D) A flipped view of the two mice in B). Here significant signal is only seen in the bladder indicating no targeting ability of the negative control as expected. All *in vivo* imaging was performed by Neil Phillips in the Powers lab.

labeled particles. For the control nanoparticles, in place of the Cys40-Exendin4, we instead attached a peptide having the same 40 amino acids, in a different order. As the function of the

Cys40-Exendin4 peptide is highly dependent on the order of the amino acids, this "scrambled" version of the peptide should exhibit no binding to GLP1-R. By using this scrambled peptide, we ensure that both the experimental group and the control group of nanoparticles will have similar solubility and circulation kinetics in the mouse model. Mice containing quadricep islet grafts were injected with either nanoparticles labeled with Cys40-Exendin4 and iFluor750 dye, or nanoparticles labeled with the scrambled Exendin4 sequence and iFluor750 dye and then imaged 18 hours post injection. Figure 10 shows the imaging results of these studies. The two mice injected with the scrambled Exendin4 nanoparticle construct show no signal in the location of the islet graft, while those injected with the Cys40-Exendin4 nanoparticle construct show clear localization of the material after 18 hours at the islet graft in the quadricep muscle. The fluorescence signal seen in the control mice is due to circulation of the nanoparticle material through the bloodstream before clearance through the kidneys and bladder. Signal from the circulation is only seen on the lower half of the mice due to the presence of hair on the upper part of the animals which obscures the signal. We can conclude then that our peptide labeled, iFluor750 dye tagged nanoparticles are capable of successfully targeting human islet grafts *in vivo*. Future work will be focused on repeating these successful results. These results show that there is great promise for these vehicles to be used as a targeted delivery system to the pancreatic β-cells.

Conclusions

In collaboration with the Powers group, we have developed a polyester nanoparticle delivery system made to specifically target and deliver therapeutics to pancreatic islet cells. An orthogonal synthesis scheme has been developed to covalently conjugate a modified version of

the GLP1 agonist Exendin4 and an imaging dye to the surface of a nanoparticle. Successful attachments of all functional units to the surface has been confirmed by NMR. The activity of the Cys40-Exendin4 particles towards the GLP1 receptor has been demonstrated *in vitro* using a CRE-Luc assay and found to be comparable to the free, unconjugated Cys40-Exendin4. The targeting ability towards GLP1-R has been demonstrated *in vivo* using a PC9:GLP-1R mouse model. Preliminary work using human islet grafts has shown promising *in vivo* targeting ability of the Exendin4 conjugated particles. These data suggest that this nanoparticle construct could be utilized as a drug carrier targeted specifically to pancreatic β-cells.

Experimental

Materials

All peptides used as well as the N-succinimidyl-p-formylbenzoate were custom synthesized by Chem-Impex International (Wood Dale, IL). The iFluor750 hydrazide dye was obtained from AAT Bioquest (Sunnyvale, CA). Spectra/Por® dialysis membrane was purchased from Spectrum Laboratories Inc. m-CPBA (<77%) was purified as previously described in the literature, and δ-valerolactone was purified after receipt by vacuum distillation. All other reagents were obtained from Sigma Aldrich (St. Louis, MO) and used as received unless otherwise specified.

Characterization

All NMR spectra of polymer precursors were obtained using a Bruker AV-I 400 MHz spectrometer. NMR spectra of all attachments to the nanoparticle surface were obtained using a Bruker AV-III 600 MHz spectrometer and a 3mm NMR tube.

Synthesis of α-allyl-δ-valerolactone

This reaction was performed as previously described in the literature[25] with the following exceptions: vacuum distilled **δ**-valerolactone was used in place of the purchased purity, and an equivalent amount of diisopropylamine (DIPA) was used in place of diisopropylethylamine (DIPEA). ^{1}H NMR (300 MHz, $CDCl_3$) **δ**: 1.51-2.17 (4H, m, CH2), 2.33 (1H, m, CH2), 2.59 (2H, m, CH2, CH), 4.31 (2H, m, CH2), 5.07 (2H, m, CH2), 5.80 (1H, m, CH).

General Procedure for Synthesis of a VL/AVL Linear Polymer

A 25 mL round-bottom flask was flame-dried and purged with nitrogen. A catalytic amount (2.5 mg, 6.0 mmol, 3.2 x 10^{-4} eq/total monomer) of tin triflate was added to the bottom of the round-bottom flask, and then the flask was again purged with nitrogen. The 3-methyl-1-butanol initiator (72.64 μL, 0.67 mmol) was added to the flask, along with the DCM (0.88 mL), and the mixture was stirred for 30 minutes to allow the catalyst to coordinate to the alcohol group on the initiator. The **δ**-valerolactone (1.37 mL, 14.80 mmol, 4.0 eq) and the **α**-allyl-**δ**-valerolactone (0.48 mL, 3.70 mmol, 1.0 eq) were added to the reaction mixture and the reaction was allowed to stir for 16-18 hours at room temperature. The reaction was quenched with excess methanol and then stirred with an excess (100 mg) of SiliaMetS® Cysteine scavenger (40-63 μm) to remove excess catalyst. The scavenger was removed by filtration and the product was purified by precipitation in cold methanol. ^{1}H NMR (400 MHz, $CDCl_3$) **δ**: 0.92 (6H, d, CH3), 1.47-1.78 (8H, m, CH2), 1.86 (1H, m, CH), 2.14-2.52 (5H, m, CH2, CH), 3.65 (2H, t, CH2), 4.08 (4H, m, CH2), 5.04 (2H, m, CH2) 5.73 (1H, m, CH).

General Procedure for Synthesis of a VL/AVL/EVL Linear Polymer

To a 6-dram vial equipped with a stir bar, the VL/AVL polymer (0.300 g, 0.4621 mmol allyl) was added along with m-CPBA (56.3 mg, 0.326 mmol, 0.7 eq/allyl). Dichloromethane was added to a final epoxide concentration of 0.065 M. The vial was capped and parafilmed, then allowed to stir at room temperature for 48 hours. Oxidized polymer was purified by washing three times with an equal volume of saturated sodium bicarbonate followed by an extraction of the product three times in dichloromethane. ^{1}H NMR (400 MHz, $CDCl_3$): The significant change seen in the ^{1}H NMR is a reduction of the allylic peaks at 5.04 and 5.73 ppm and the emergence of small broad peaks at 2.47, 2.76, and 2.94 ppm due to the epoxide ring.

General Procedure for Nanoparticle Formation

To a 100 mL round-bottom flask, the VL/AVL/EVL linear polymer (0.267 g, 0.239 mmol epoxide) was added and then dissolved in dichloromethane to a final epoxide concentration of 0.0054 M. The 2,2'(ethylenedioxy)diethylamine (35.0 μL, 2 amines/epoxide) was added to the vigorously stirring flask via microsyringe, and the solution was refluxed at 46ºC for 12 hours. The resulting nanoparticles were purified by dialysis using Snakeskin Dialysis tubing (10K MWCO) against DCM for 72 hours and then passed through a 0.45μm syringe filter. Particle size and uniformity were determined by transmission electron microscopy. ^{1}H NMR (400 MHz, d-DMSO) **δ**: 0.92 (6H, d, CH3), 1.47-1.78 (8H, m, CH2), 1.86 (1H, m, CH), 2.14-2.52 (5H, m, CH2, CH), 3.50-3.65 (14H, m, CH2), 4.08 (4H, m, CH2), 5.04 (2H, m, CH2) 5.73 (1H, m, CH)

Attachment of N-succinimidyl-p-formylbenzoate to Nanoparticle Surface

A 1-dram vial equipped with stir bar and septum was flamed dried and purged with nitrogen. Polyester nanoparticles (80.0 mg, 5.33 x 10^{-7} mol, 1.0 eq) were added to the vial, and the vial was again purged with nitrogen. Nanoparticles were dissolved by adding a minimal amount of deuterated dimethyl sulfoxide through the septum via syringe. A stock solution of N-succinimidyl-p-formylbenzoate was prepared in d-DMSO, and the linker (6.6 mg, 2.67 x 10^{-5} mol, 50.0 eq) was added through the septum via syringe. The reaction was then allowed to stir at 37ºC overnight. The resulting mixture was purified by dialysis against a 50/50 (v/v) mixture of methanol and acetonitrile using Snakeskin tubing (10K MWCO) for 24 hours. ^{1}H NMR (600 MHz, d-DMSO) **δ**: 0.92 (6H, d, CH3), 1.47-1.78 (8H, m, CH2), 1.86 (1H, m, CH), 2.14-2.52 (5H, m, CH2, CH), 3.50-3.65 (14H, m, CH2), 4.08 (4H, m, CH2), 5.04 (2H, m, CH2) 5.73 (1H, m, CH), 7.50-8.90 (4H, m, CH), 10.07 (1H, s, CH)

General Procedure for Attachment of Cys40-Exendin4 to the Nanoparticle Surface

A 1-dram vial equipped with stir bar and septum was flame-dried and purged with nitrogen. Polyester nanoparticles (13.0 mg, 8.67 x 10^{-8} mol, 8.34 x 10^{-6} mol allyl) were added to the vial, and the vial was again purged with nitrogen. Nanoparticles were dissolved by adding a minimal amount of deuterated dimethyl sulfoxide. Cys40-Exendin4 or the corresponding scrambled sequence (3.0 mg, 8 eq/nanoparticle) was dissolved in minimal d-DMSO and then added to the vial through the septum via syringe. A stock solution of 2,2-dimethoxy-2-phenylacetophenone (DMPA) was prepared in d-DMSO, and the photoinitiator (0.43 mg, 0.2 eq/allyl) was added to the reaction mixture via syringe. The reaction vial was placed under long wave UV light and allowed

to stir at room temperature overnight. Attachment of the peptide was confirmed by the observation of a reduction in the allyl peaks at 5.04 and 5.73 ppm in the crude NMR spectrum.

General Procedure for Attachment of Hydrazide Imaging Dye to the Nanoparticle Surface

To a 1-dram vial equipped with a stir bar, polyester nanoparticles previously functionalized with an N-succinimidyl-p-formylbenzoate aldehyde linker and peptide (13.0 mg, 8.67 x 10^{-8} mol, 1.0 eq) were added. Nanoparticles were transferred directly from the NMR tube to the original reaction vial used to attach the peptide. A stock solution of hydrazide dye was prepared in d-DMSO and the dye (1.13 mg, 11.4 eq/nanoparticle) was added to the reaction vial via syringe. The reaction was allowed to stir in the absence of light at room temperature overnight. The resulting mixture was purified by dialysis against a 50:50 v/v mixture of acetonitrile and methanol using Snakeskin tubing (10K MWCO) for 48 hours. Successful attachment of the dye was verified by the disappearance of the aldehyde peak at 10.06 ppm.

Development of an HEK293:GLP1-R Cell Line

Modification of HEK293 cells to express GLP1-R was performed by Neil Phillips in the Powers lab. Expression and surface localization of GLP1r was assessed by live cell imaging following incubation with a fluorescent Exendin4 peptide (FLEX, Anaspec). Briefly, cells plated in 8-well chamber slides were incubated with 1 μM FLEX in culture media (DMEM, 10% FBS) for 30 minutes at 37ºC, 5% CO_2. For blocking of GLP1-R, cells were incubated with 10-fold molar excess of unlabeled Exendin4 for 15 minutes prior to addition of FLEX. Following extensive washing with HBSS, cells where imaged using an inverted fluorescence microscope.

Testing the Binding Affinity of Cys40-Exendin4 and Cys40-Exendin4 Nanoparticles using an HEK293:GLP1-R Cell Line

Functional characterization of the cell line was performed by Neil Phillips in the Powers lab using a CRE-Luc assay. Cells were modified to express luciferase in response to elevated levels of cyclic AMP using a plasmid pCRE-luc. After 24 hours, cells were incubated with bare nanoparticles, Forskolin, Cys40-Exendin4, or Cys40-Exendin4 nanoparticles at the indicated final concentrations and incubated for 5 hours at 37ºC. An equal volume of One-Glo reagent (Promega) was added, cell lysis permitted to occur for 3 mins and luminescence was measured with a Spectramax M5 plate reader.

Studying the Targeting Ability of Cys40-Exendin4 Conjugated Nanoparticles to the Islets of Langerhans using an in-vivo Model

PC9 cells were cultured and then subsequently modified by Neil Phillips in the Powers lab to overexpress the GLP1-R present on the surface of pancreatic β-cells. These cells were then engrafted onto the hind legs of SHO mice for 5 weeks until a tumor size was reached that was suitable for imaging. Mice were then given a retro-orbital injection of 150μL of a PBS suspension of nanoparticles conjugated to both the Cys40-Exendin4 peptide, and an iFluor750 dye (2.2 mg nanoparticles, 450 μg peptide per mouse). Mice were then imaged 24 hours after injection. Mice engrafted with PC9 cells not expressing GLP1-R were used as a negative control, and 2-3 mice were used per group.

Loading of Nanoparticles with Nile Red

D-α-Tocopherol polyethylene glycol 1000 succinate (0.0256 mg, 2.6 μL), nanoparticles modified with Cys40-Exendin4 and iFluor750 dye (2.2 mg, 34.4 μL), and Nile Red (0.36 mg, 14.4 μL) were placed in an Eppendorf tube in DMSO and mixed well to obtain a homogenous solution. A 1.0 mL aliquot of cell culture water was then added to the mixture and the contents were again mixed well. The solution was then immediately frozen and lyophilized to obtain Nile Red-loaded nanoparticles.

Studying the Targeting Ability of Cys40-Exendin4 Conjugated, Nile-Red Loaded Nanoparticles to the Islets of Langerhans using Fat Pad Human Islet Grafts

Human islet cells were implanted subcutaneously onto the fat pads of mice by collaborators in the Powers lab. Grafts were allowed to stabilize in the mice for several weeks before injections were performed. Mice were then given a retro-orbital injection of 150 μL of a suspension of nanoparticles conjugated to both the Cys40-Exendin4 peptide and an iFluor750 dye and loaded with Nile Red (2.2 mg nanoparticles, 720 μg peptide, 124 μg imaging dye, and 360 μg Nile Red per mouse) in a 1% solution of D-α-Tocopherol polyethylene glycol 1000 succinate in PBS. *Ex vivo* imaging of the pancreas, kidneys, and fat pad was performed 24 hours post-injection.

Studying the Targeting Ability of Cys40-Exendin4 Conjugated Nanoparticles to the Islets of Langerhans using Subcutaneous Quadricep Human Islet Grafts

Human islet cells were implanted subcutaneously onto the hind limbs of mice by collaborators in the Powers lab. Grafts were allowed to stabilize in the mice for 9 weeks before injections were performed. Mice were then given a retro-orbital injection of 150 μL of a suspension of one of the

following constructs in a 1% solution of D-α-Tocopherol polyethylene glycol 1000 succinate in PBS: nanoparticles conjugated to both the Cys40-Exendin4 peptide and an iFluor750 dye (2.1 mg nanoparticles, 430 μg peptide, and 162 μg imaging dye per mouse), or nanoparticles conjugated to both the scrambled Exendin4 sequence and an iFluor750 dye (2.3 mg nanoparticles, 790 μg peptide, 117 μg imaging dye per mouse). Mice were imaged 18 hours following injection.

References

1. Butler, A. E.; Janson, J.; Bonner-Weir, S.; Ritzel, R.; Rizza, R. A.; Butler, P. C., beta-cell deficit and increased beta-cell apoptosis in humans with type 2 diabetes. *Diabetes* **2003,** *52* (1), 102-110.

2. Klinke, D. J., 2nd, Extent of beta cell destruction is important but insufficient to predict the onset of type 1 diabetes mellitus. *PLoS One* **2008,** *3* (1), e1374.

3. Ahren, B., Type 2 diabetes, insulin secretion and beta-cell mass. *Current Molecular Medicine* **2005,** *5* (3), 275-286.

4. Amitabh Gaur, N. L., and Conlon, P.J. Methods for Treatment of Diabetes using Peptide Analogues of Insulin. US006197926B1, 2001.

5. Lee, I. C.; Wu, Y. C.; Tsai, S. W.; Chen, C. H.; Wu, M. H., Fabrication of two-layer dissolving polyvinylpyrrolidone microneedles with different molecular weights for in vivo insulin transdermal delivery. *RSC Advances* **2017,** *7* (9), 5067-5075.

6. Ling, M. H.; Chen, M. C., Dissolving polymer microneedle patches for rapid and efficient transdermal delivery of insulin to diabetic rats. *Acta Biomaterialia* **2013,** *9* (11), 8952-8961.

7. Grunberger, G., The need for better insulin therapy. *Diabetes, Obesity and Metabolism* **2013,** *15 Suppl 1*, 1-5.

8. Lundh, M.; Scully, S. S.; Mandrup-Poulsen, T.; Wagner, B. K., Small-molecule inhibition of inflammatory beta-cell death. *Diabetes, Obesity and Metabolism* **2013,** *15 Suppl 3*, 176-84.

9. Boerner, B. P.; George, N. M.; Mir, S. U. R.; Sarvetnick, N. E., WS6 induces both alpha and beta cell proliferation without affecting differentiation or viability. *Endocrine Journal* **2015,** *62* (4), 379-386.

10. Duan, H.; Arora, D.; Li, Y.; Setiadi, H.; Xu, D.; Lim, H. Y.; Wang, W., Identification of 1,2,3-triazole derivatives that protect pancreatic beta cells against endoplasmic reticulum stress-mediated dysfunction and death through the inhibition of C/EBP-homologous protein expression. *Bioorganic and Medicinal Chemistry* **2016,** *24* (12), 2621-30.

11. Orza, A.; Soritau, O.; Tomuleasa, C.; Olenic, L.; Florea, A.; Pana, O.; Bratu, I.; Pall, E.; Florian, S.; Casciano, D.; Biris, A. S., Reversing chemoresistance of malignant glioma stem cells using gold nanoparticles. *International Journal of Nanomedicine* **2013,** *8*, 689-702.

12. Bao, W.; Liu, R.; Wang, Y.; Wang, F.; Xia, G.; Zhang, H.; Li, X.; Yin, H.; Chen, B., PLGA-PLL-PEG-Tf-based targeted nanoparticles drug delivery system enhance antitumor efficacy via intrinsic apoptosis pathway. *International Journal of Nanomedicine* **2015,** *10*, 557-66.

13. Martinez-Carmona, M.; Lozano, D.; Colilla, M.; Vallet-Regi, M., Selective topotecan delivery to cancer cells by targeted pH-sensitive mesoporous silica nanoparticles. *RSC Advances* **2016,** *6* (56), 50923-50932.

14. Ashton, S.; Song, Y. H.; Nolan, J.; Cadogan, E.; Murray, J.; Odedra, R.; Foster, J.; Hall, P. A.; Low, S.; Taylor, P.; Ellston, R.; Polanska, U. M.; Wilson, J.; Howes, C.; Smith, A.; Goodwin, R. J. A.; Swales, J. G.; Strittmatter, N.; Takats, Z.; Nilsson, A.; Andren, P.; Trueman, D.; Walker, M.; Reimer, C. L.; Troiano, G.; Parsons, D.; De Witt, D.; Ashford, M.; Hrkach, J.; Zale, S.; Jewsbury, P. J.; Barry, S. T., Aurora kinase inhibitor nanoparticles target tumors with favorable therapeutic index in vivo. *Science Translational Medicine* **2016,** *8* (325).

15. Lockhart, J. N.; Stevens, D. M.; Beezer, D. B.; Kravitz, A.; Harth, E., Dual drug delivery of tamoxifen and quercetin: Regulated metabolism for anticancer treatment with nanosponges. *Journal of Controlled Release* **2015**.

16. Jindal, A. B.; Bachhav, S. S.; Devarajan, P. V., In situ hybrid nano drug delivery system (IHN-DDS) of antiretroviral drug for simultaneous targeting to multiple viral reservoirs: An in vivo proof of concept. *International Journal of Pharmaceutics* **2017,** *521* (1-2), 196-203.

17. Hari, B. N.; Narayanan, N.; Dhevendaran, K.; Ramyadevi, D., Engineered nanoparticles of Efavirenz using methacrylate co-polymer (Eudragit-E100) and its biological effects in-vivo. *Materials Science and Engineering C: Materials for Biological Applications* **2016,** *67*, 522-32.

18. Beloqui, A.; Coco, R.; Preat, V., Targeting Inflammatory Bowel Diseases by Nanocarriers Loaded with Small and Biopharmaceutical Anti-Inflammatory Drugs. *Current Pharmaceutical Design* **2016,** *22* (40), 6192-6206.

19. Lin, J. B.; Poh, S.; Panitch, A., Controlled release of anti-inflammatory peptides from reducible thermosensitive nanoparticles suppresses cartilage inflammation. *Nanomedicine* **2016,** *12* (7), 2095-2100.

20. Li, Q.; Wen, Y.; Wen, J.; Zhang, Y. P.; Xu, X. D.; Victorious, A.; Zavitz, R.; Xu, X., A new biosafe reactive oxygen species (ROS)-responsive nanoplatform for drug delivery. *RSC Advances* **2016,** *6* (45), 38984-38989.

21. Oh, Y. J.; Lee, J.; Seo, J. Y.; Rhim, T.; Kim, S. H.; Yoon, H. J.; Lee, K. Y., Preparation of budesonide-loaded porous PLGA microparticles and their therapeutic efficacy in a murine asthma model. *Journal of Controlled Release* **2011,** *150* (1), 56-62.

22. Patel, B.; Gupta, V.; Ahsan, F., PEG-PLGA based large porous particles for pulmonary delivery of a highly soluble drug, low molecular weight heparin. *Journal of Controlled Release* **2012,** *162* (2), 310-320.

23. Zamani, M.; Prabhakaran, M. P.; Thian, E. S.; Ramakrishna, S., Controlled delivery of stromal derived factor-1alpha from poly lactic-co-glycolic acid core-shell particles to recruit mesenchymal stem cells for cardiac regeneration. *Journal of Colloid and Interface Science* **2015,** *451*, 144-52.

24. van der Ende, A. E.; Sathiyakumar, V.; Diaz, R.; Hallahan, D. E.; Harth, E., Linear release nanoparticle devices for advanced targeted cancer therapies with increased efficacy. *Polymer Chemistry* **2010,** *1* (1), 93-96.

25. van der Ende, A. E.; Kravitz, E. J.; Harth, E., Approach to formation of multifunctional polyester particles in controlled nanoscopic dimensions. *Journal of the American Chemical Society* **2008,** *130* (27), 8706-13.

26. Stevens, D. M., Gilmore, K. A., Harth, E., An assessment of nanosponges for intravenous and oral drug delivery of BCS class IV drugs: Drug delivery kinetics and solubilization. *Polymer Chemistry* **2014,** *5* (11), 3551-3554.

27. Chia, C. W.; Egan, J. M., Biology and therapeutic potential of GLP-1 in the treatment of diabetes. *Drug Discovery Today: Disease Mechanisms* **2005,** *2* (3), 295-301.

28. Baggio, L. L.; Drucker, D. J., Biology of incretins: GLP-1 and GIP. *Gastroenterology* **2007,** *132* (6), 2131-57.

29. Thorens, B.; Porret, A.; Buhler, L.; Deng, S. P.; Morel, P.; Widmann, C., Cloning and functional expression of the human islet GLP-1 receptor. Demonstration that exendin-4 is an agonist and exendin-(9-39) an antagonist of the receptor. *Diabetes* **1993,** *42* (11), 1678-82.

30. van der Ende, A.; Croce, T.; Hamilton, S.; Sathiyakumar, V.; Harth, E., Tailored polyester nanoparticles: post-modification with dendritic transporter and targeting units via reductive amination and thiol-ene chemistry. *Soft Matter* **2009,** *5* (7), 1417-1425.

31. Kaddis, J. S.; Olack, B. J.; Sowinski, J.; Cravens, J.; Contreras, J. L.; Niland, J. C., Human pancreatic islets and diabetes research. *Journal of the American Medical Association* **2009,** *301* (15), 1580-7.

CHAPTER IV

IMPROVING THE TREATMENT OF UNSTABLE ARTERIAL PLAQUES USING A POLYESTER NANOPARTICLE SCAFFOLD

Introduction

Cardiovascular disease currently remains one of the leading causes of death in developed countries throughout the world.[1-3] One of the major risks associated with this disorder is atherosclerosis, or the buildup of plaque on the artery walls. When these plaques become unstable, they are prone to rupture and can lead to cardiac events such as heart attack or stroke.[4-6] These arterial plaques are equipped with a fibrous cap of collagen, that is meant to provide structural stability to the plaque.[7-8] Plaques become rupture-prone when this collagen cap is weakened by degradation. One of the major sources of this degradation is the activity of matrix metalloproteinases (MMPs) at the surface of the plaque.[9-12] MMP14 has been specifically linked to the presence of unstable plaques and has been found to play a significant role in activating the collagen degradative activity of several other MMPs, such as MMP2 and MMP9.[13-16] Previous clinical trials aimed at inhibiting this MMP activity have typically involved the systemic administration of broad spectrum MMP inhibitors.[17-19] These types of therapies can be problematic, as all 23 groups of MMPs are potentially affected by these drugs. Although specific MMP activity (MMP2, MMP9, and MMP14) has been linked with unstable plaque formation, other MMPs are thought to play a role in the remodeling of the plaque and to aid in structural stability.[20] This makes the administration of these broad spectrum inhibitors rather impractical, as only a small percentage has the intended effect of decreasing the MMPs collagen degradative activity.

Naphthofluorescein is a potent MMP14 inhibitor, making it a very attractive therapeutic for increasing the stability of these rupture-prone arterial plaques without interfering with the potential helpful activity of other MMPs.[21] However, systemic administration of naphthofluorescein also leads to complications and unwanted side effects, due to the wide dispersity of MMP14 throughout the body. It is therefore evident that the mechanism of this drug could be utilized to help stabilize arterial plaques and make them less prone to rupture, if a vehicle could be designed to deliver the drug specifically to the target site. Our lab has shown that polyester nanoparticles crosslinked using amine-epoxide chemistry are excellent drug delivery systems and offer properties such as tailored and sustained drug release rates, and higher drug solubility.[22-24] By conjugating these particles to a targeting unit, we aim to be able to be able to utilize this system to deliver naphthofluorescein specifically to unstable arterial plaques.

Collaborators in the Hagemeyer group have developed a novel peptide (T-peptide) capable of specifically targeting and penetrating unstable arterial plaques. This peptide is a modified version of a collagen IV homing peptide developed by Mueller et. al.[25] The peptide designed by Mueller and coworkers binds to a specific epitope on collagen IV that is exposed upon degradation by MMP2. Members of the Hagemeyer group have modified this peptide by adding a string of amino acids that allows the peptide to be taken up into the unstable plaque. Briefly, this string of amino acids contains a block polycationic sequence followed by a block polyanionic sequence to create a hairpin structure. Upon binding of the peptide to the unstable collagen epitope, the polyanionic sequence is cleaved by MMP2, leaving the polycationic arm behind and allowing the peptide to pass through the cell wall and into the plaque. An overview of the proposed process is outlined in Figure 1.

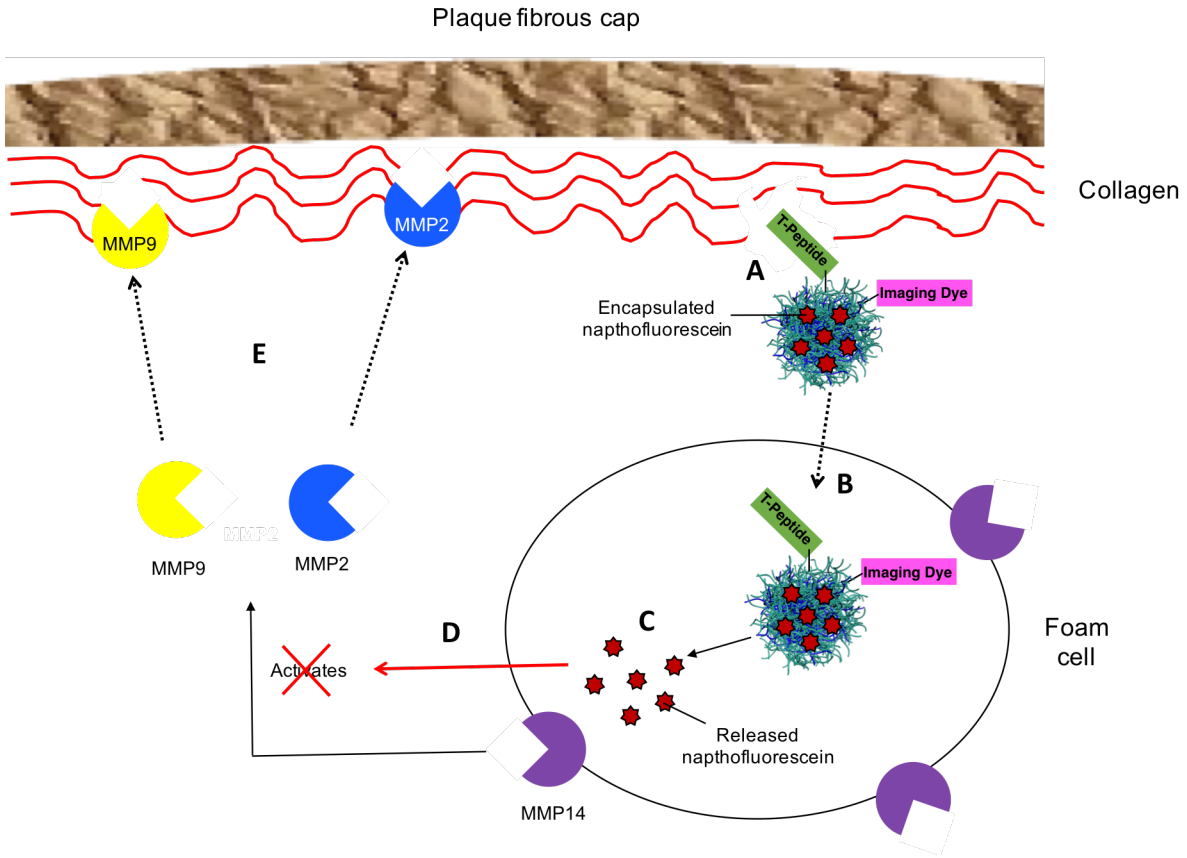

Figure IV-1. An overview of the process for the targeted delivery of naphthofluorescein to increase the stability of arterial plaques. A) A naphthofluorescein-loaded nanoparticle bearing the T-peptide targeting unit and an imaging dye binds to collagen degraded by MMP2 and MMP9. B) Upon cleavage of the polyanionic sequence, the nanoparticle construct is taken up by the foam cells in the plaque and C) releases the loaded naphthofluorescein. D) The released naphthofluorescein inhibits the activity of the membrane-bound MMP14 which in turn decreases E) the collagen degradative activity of MMP2 and MMP9, thereby increasing the stability of the plaque.

The goal of this work is to construct a polyester nanoparticle delivery system capable of delivering naphthofluorescein specifically to unstable arterial plaques using the T-peptide as a targeting unit. A synthesis scheme was developed so that a suitable fluorescent dye could also be conjugated to the surface of the nanoparticle and the construct could be tracked both *in vitro* and *in vivo*. Because of the unique chemically crosslinked structure of these particles, all surface modification could be completed before the loading of the naphthofluorescein within the matrix of the particle. We will demonstrate in this work that by loading naphthofluorescein into this

targeted delivery system, we can significantly increase the efficacy of the drug, while eliminating the off-target effects associated with systemic therapy.

Results and Discussion

Polyester nanoparticles were made via amine-epoxide chemistry and then surface modified with a T-peptide targeting unit and a cyanine3 imaging dye. An orthogonal synthesis scheme was used so that both units could be attached to the particle surface without any interfering side reactions. Nanoparticles tagged with both the T-peptide and the cyanine3 dye were shown to be taken up successfully by cells that express MMP2 *in vitro* and by unstable plaques *in vivo*. Fully labeled nanoparticles loaded with naphthofluorescein show a 1.5-fold higher efficacy in increasing the collagen content of unstable plaques over the free drug *in vivo*.

Synthesis of a T-Peptide Labeled, Fluorescently Tagged Nanoparticle for Targeting Unstable Plaques

Polyester nanoparticles were synthesized using previously developed protocols to create the template for our targeted naphthofluorescein delivery system. The polymer precursor for the nanoparticles was constructed so that only a portion of the allyl functional groups were oxidized to create the epoxides needed for the particle crosslinking reaction. This allowed for particles to be synthesized that contained both free amines and free allyls on the surface of the particles. Again here a high incorporation of the diamine linker is observed based on the peak seen at 3.50 ppm (Figure 3), providing an abundance of attachment sites for functionalization. TEM analysis of the resulting nanoparticles confirms the spherical morphology and shows an average size of the particles of approximately 150 nm. As in Chapter 3, an attachment scheme utilizing thiolene click chemistry for peptide attachment followed by NHS-ester chemistry for dye attachment is

not possible due to the amine functional groups present in the T-peptide targeting unit. Because of this obstacle, the amine groups on the surface of the particle were transformed into aldehyde groups using the same chemistry as shown in Chapter 3, by reacting the particles with N-succinimidyl-p-formylbenzoate. This linker was successfully conjugated to the surface of the nanoparticle using the conditions shown in Fig. 2. Following attachment of the N-succinimidyl-p-formylbenzoate to the surface of the nanoparticle, the ^{1}H NMR spectrum of the purified material shows the anticipated peaks in both the aromatic region and at 10.1 ppm for the free aldehyde (Fig 3), indicating a successful conjugation of the linker to the surface.

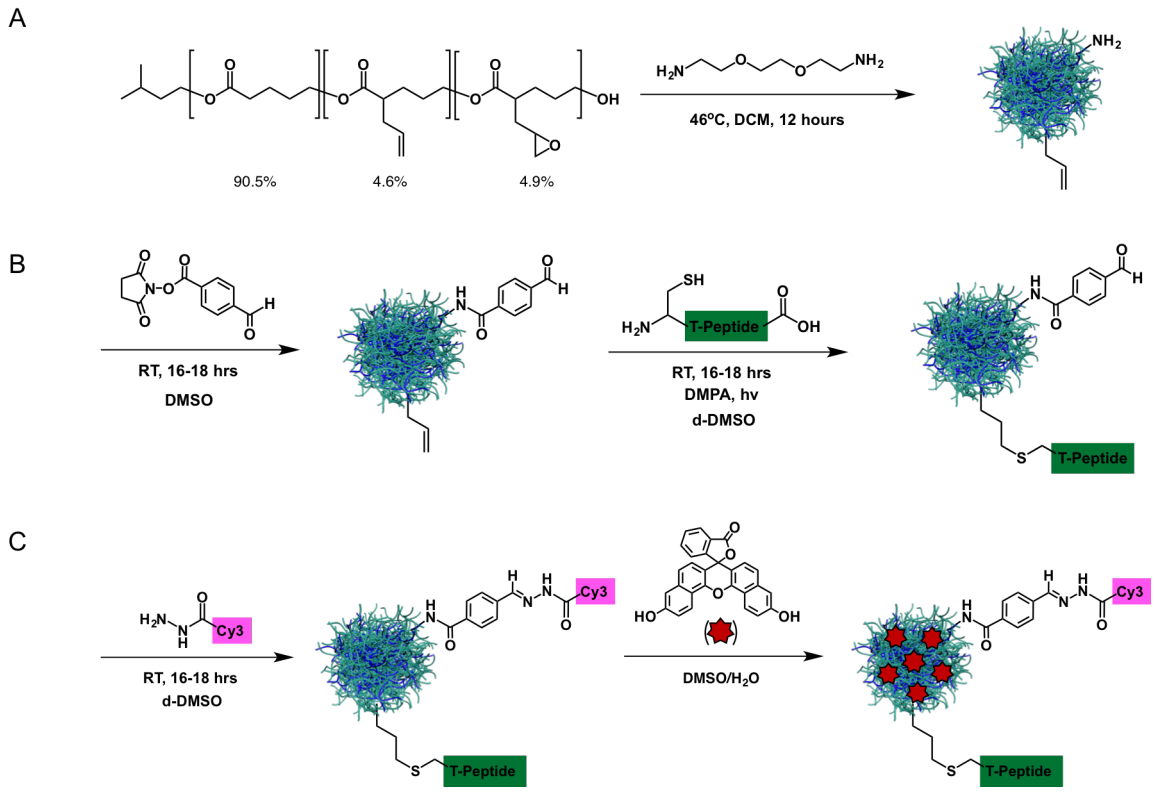

Figure IV-2. Synthesis scheme for the construction of a T-peptide labeled, fluorescently tagged, naphthofluorescein-loaded nanoparticle targeted towards unstable arterial plaques. A) Nanoparticles are constructed by crosslinking a VL/AVL/EVL polymer using a diamine linker. B) Amines on the particle surface are transformed into aldehydes by reacting the particles with N-succinimidyl-p-formylbenzoate. The T-peptide is attached to the surface of the particles by means of a thiolene click reaction. C) The cyanine3 imaging dye is attached to the surface via a hydrazine linkage formed between the hydrazide group on the dye and the aldehydes on the particle surface. After all surface functionalization is complete, particles are post-loaded with naphthofluorescein to a final loading of 14.0 wt%.

The T-peptide used in this study contains one cysteine residue, providing the free thiol needed for attachment to the particle surface via a thiolene click reaction. As such, this peptide did not need to be modified in any way before successfully attaching it to the particle surface using DMPA as a photoinitiator. A decrease in the allyl peaks at 5.04 and 5.73 ppm of the crude spectrum confirms the attachment of the peptide to the particle surface. Peaks for the backbone of the T-peptide can also be seen in the spectrum at 1.7, 4.25, and 6.8-7.2 ppm. The cyanine3 hydrazide dye used in this work was attached to the particle surface by mixing it with the peptide-functionalized particles in the absence of light under ambient conditions. The ^{1}H NMR of the product clearly shows the disappearance of the aldehyde peak and a change in the peak shape of the aromatic region after the reaction, indicating a successful dye attachment. An integration of the aromatic region from 6.5-7.45 ppm following the attachment of the dye and the subsequent purification shows an increase in the region of 12.55 protons. The protons in this region should almost exclusively be the result of aromatic residues on the peptide backbone, so it is possible to estimate the number of peptides on each particle using the integration value. It is known that at least two aromatic residues are present on the peptide, but there are likely more. Using 7-10 aromatic residues as an estimation, each containing 4 aromatic protons in the aforementioned region, we can estimate the ratio of peptides to particles as being anywhere from 13.7-19.6 peptides on each particle surface.

Following the attachment of both the T-peptide and the Cy3 imaging dye to the nanoparticle surface, we loaded this targeted delivery system with the MMP14 inhibitor naphthofluorescein. As mentioned previously, one of the largest benefits to this crosslinked polyester particle structure is the ability of the particles to be post-loaded with a therapeutic after all surface modifications are complete. In this way, we can ensure that the entire drug dose that is

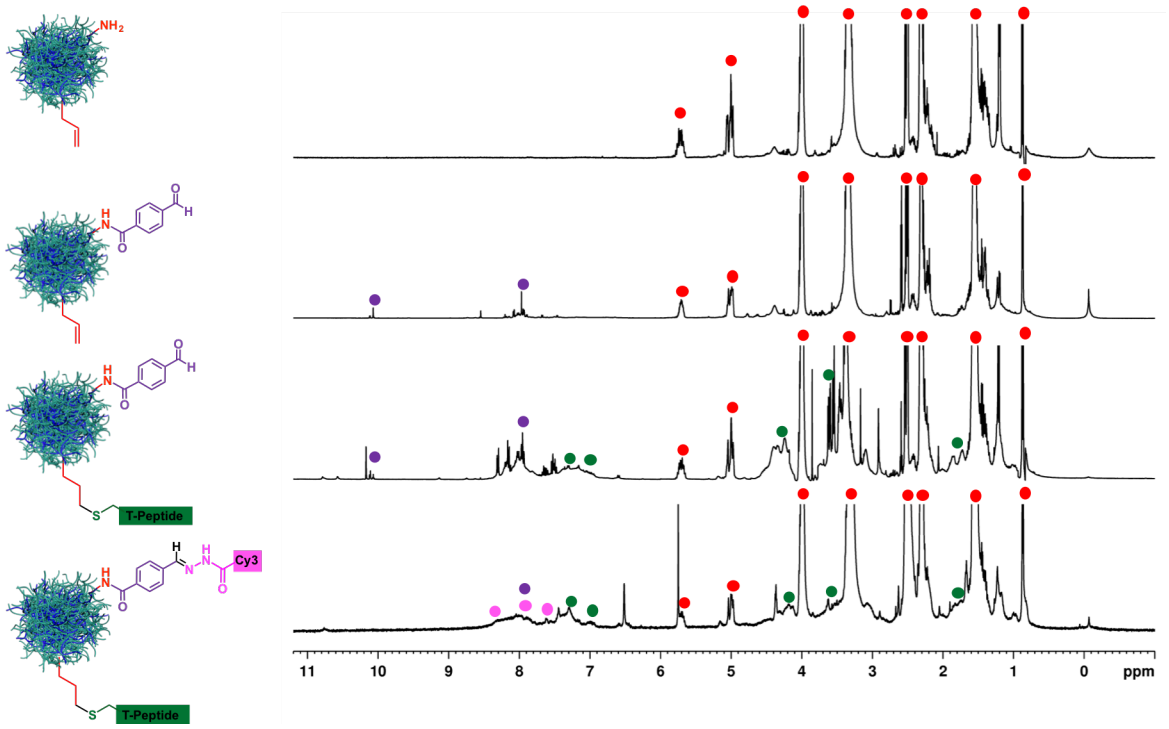

Figure IV-3. An overlay of the ^{1}H NMR spectra for the synthesis of a fluorescently tagged nanoparticle targeted to unstable plaques. A) Polyester nanoparticles show a good incorporation of the diamine linker as shown by the peak at 3.50 ppm. B) Attachment of the N-succinimidyl-p-formylbenzoate shows peaks in the aromatic region and a characteristic aldehyde peak at 10.1 ppm. C) A decrease in the allyl peaks is seen along with the emergence of the peptide peaks following attachment of the T-peptide. D) After the attachment of the Cy3 hydrazide dye, the aldehyde peak is seen to disappear, and peak shape changes are seen in the aromatic region. Attached moieties on the surface are colored to correspond to the labeled peaks in the NMR.

loaded into the particles is administered during the *in vivo* studies, and no drug is lost during subsequent synthesis steps. Briefly, to load the naphthofluorescein into the fully targeted nanoparticles, the targeted, dye labeled particles and the drug were mixed together in a concentrated solution of DMSO. A large excess of cell culture water was then added to the mixture and quickly mixed and then frozen. The large excess of water causes the naphthofluorescein to become trapped within the particle structure as a result of hydrophobic interactions.

Studying the Targeting Ability of T-Peptide Conjugated Nanoparticles *in vitro*

Before testing the naphthofluorescein loaded, fully targeted nanoparticle construct *in vivo*, we wished to determine whether the peptide maintained its action after conjugation to the particle surface. To study the activity of T-peptide conjugated nanoparticles, particles were assembled that contained both the T-peptide and a Cy3 imaging dye. Using the murine fibrosarcoma HT1080 cell line, collaborators in the Hagemeyer lab investigated cellular uptake of this construct. HT1080 cells were chosen because they naturally produce several MMPs, including MMP2. As the uptake of the peptide is dependent on the activity of MMP2, successful uptake of the construct should be accompanied by the visualization of a fluorescence signal inside the cells as a result of the Cy3 dye attached to the particle surface. These cells were incubated overnight with the targeted, dye labeled nanoparticle construct at 37ºC, and then visualized the following day using confocal live cell microscopy. In the images shown in Figure 4, the cytoplasm of the cells has been stained green, while the red signal is from the cyanine dye. Figure 4B clearly shows that the fluorescence signal from the cyanine dye is contained within the cells, indicating

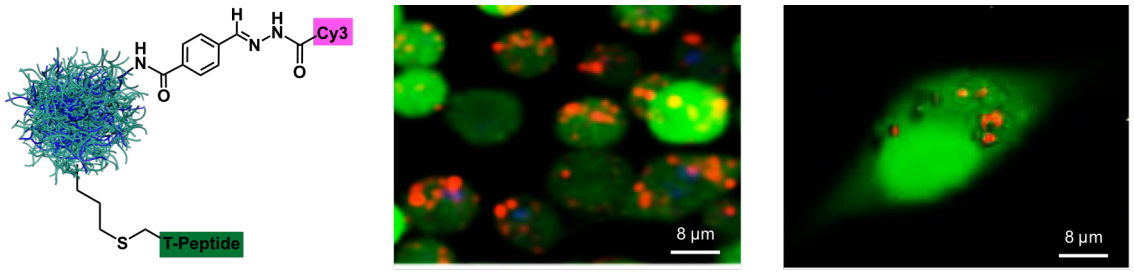

Figure IV-4. A) The nanoparticle construct that was seeded onto HT1080 cells to test the activity of the peptide following conjugation to the particle. B) 2-D reconstruction of a Z-stack image of HT1080 cells after incubation with A). The red fluorescence signal is from the Cy3 dye attached to the particle, showing the presence of the construct within the cells. C) The center of a Z-stack of one of the cells in B), showing that the red fluorescence signal is internal and not superficial surface signal. Cell imaging was performed by Mei Choy of the Hagemeyer lab. Images were taken at 60x magnification.

successful uptake of the construct. Figure 4C shows the center of a Z-stack image of one of the cells from Figure 4B. The presence of Cy3 fluorescence signal in this image confirms that the fluorescence signal seen in the 2D image is in fact internal, and not simply superficial surface signal. These results confirm not only that conjugation of the T-peptide to the particle does not negatively affect the peptides activity, but also that the particle construct is successfully taken up into the cells along with the peptide upon cleavage of the polyanionic sequence.

Studying the Targeting Ability of T-Peptide Conjugated Nanoparticles *in vivo*

After confirming successful uptake and activity of the peptide upon conjugation to the particle surface, we began to investigate the ability of these targeted nanoparticles to penetrate unstable plaques *in vivo*. Two sets of nanoparticles were constructed, one set bearing both the T-peptide targeting unit and the Cy3 imaging dye, and another tagged with just the imaging dye. Nanoparticles that were tagged with only the imaging dye were made in such a way that no allyls were present after particle formation, so as to not interfere with the solubility of the construct. These particles were tested for targeting ability using a mouse model developed by the Hagemeyer group. Briefly, these apoE knock out mice had sutures placed at the right carotid artery after 7 weeks of high fat diet to induce the formation of unstable plaques. Plaques were then allowed to develop for 5 weeks. These mice were then injected with either the targeted or non-targeted nanoparticle construct tagged with a fluorescent Cy3 dye. The plaques were then harvested and analyzed by fluorescence microscopy. As shown in Figure 5, plaques from those mice that were injected with the non-targeted nanoparticle show no evidence of fluorescence, while those that were injected with the targeted construct show localization of the nanoparticle within the plaque.

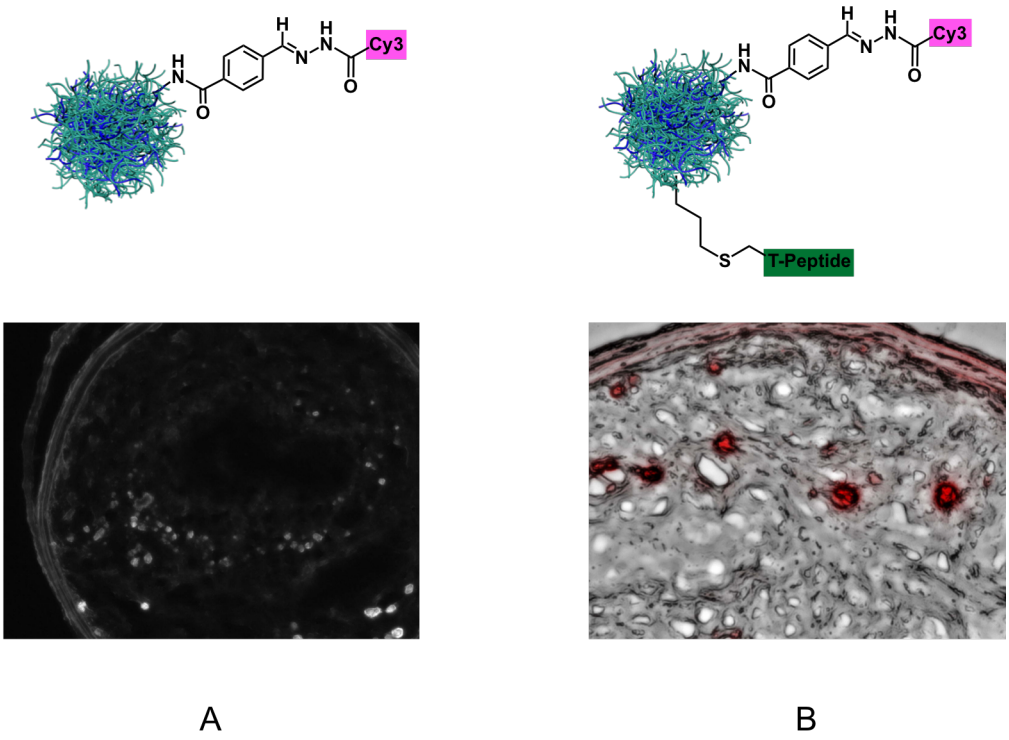

Figure IV-5. Overlay images of phase contrast image with TRITC fluorescence channel image of plaques harvested from mice after treatment with either a targeted or non-targeted nanoparticle. A) Mice treated with the untargeted nanoparticle tagged with a Cy3 dye show no fluorescence localization in the plaque. B) Mice treated with T-peptide labeled, fluorescently tagged nanoparticles show a clear accumulation of the Cy3 dye inside the unstable plaque, indicating successful *in vivo* targeting ability. *Ex vivo* imaging was performed by Mei Choy of the Hagemeyer lab.

Improving the Efficacy of Naphthofluorescein using a Targeted Nanoparticle Scaffold

After confirming the targeting ability of this T-peptide labeled nanoparticle construct *in vivo*, we investigated whether this targeted nanoparticle system could successfully increase the efficacy of naphthofluorescein, using the same *in vivo* mouse model. Mice were treated as before and allowed to develop unstable plaques over the course of 5 weeks. For these studies, four treatment groups were tested, with each group receiving two injections of the material two weeks apart: naphthofluorescein-loaded nanoparticles containing T-peptide and a Cy3 imaging dye,

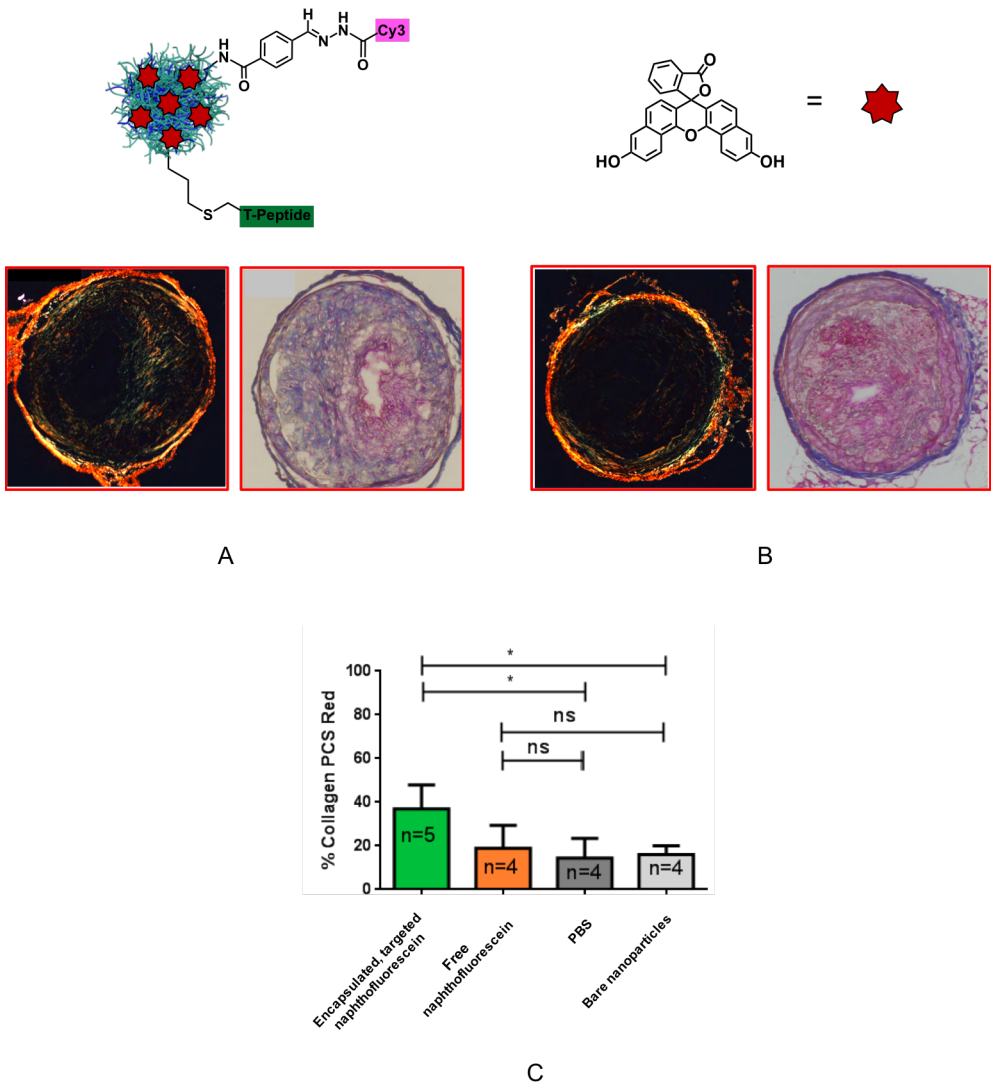

Figure IV-6. A) Mice treated with naphthofluorescein encapsulated in the T-peptide labeled nanoparticle system have plaques that exhibit a higher collagen content than B) those treated with free naphthofluorescein as evidenced by both Picrosirius Red (left panels) and Masson's Trichrome (right panels) tissue staining. C) Quantification of the collagen content using imaging software and the images from the Picrosirius Red staining shows an almost two-fold increase in collagen content in those plaques treated with the targeted drug construct. Plaques treated with free drug show no significant increase in collagen content as compared to the negative controls.

nanoparticles alone, PBS, and free naphthofluorescein. Following this treatment, the mice were killed and their plaques were harvested and subsequently stained for collagen content using both Picrosirius Red and Masons Trichrome staining. In the Picrosirius Red staining, thicker collagen

fibers are stained red, and thinner collagen fibers appear in green. In the Masons Trichrome staining, the collagen is stained blue. The amount of collagen in each plaque was then quantified using an image analysis program and compared to the other groups. Specifically, the percent collagen was calculated using the ratio of collagen present in the intima layer of the plaque to the total plaque area. An increased collagen content in the plaque can be correlated to the MMP14 inhibitory action of naphthofluorescein and is associated with an increased stability in the plaque, making it less likely to rupture. Figure 6 shows the results of the tissue staining, and the quantification of collagen content based upon the Picrosirius Red stain. As can be seen in Figure 6C, plaques from those mice treated with the naphthofluorescein entrapped within the targeted nanoparticle construct exhibit an almost 2-fold higher collagen content than those treated with the free drug. There is no significant increase in collagen content observed in those mice treated with either PBS or nanoparticles alone, as to be expected. What this indicates is that the efficacy and specific action of the naphthofluorescein can be significantly improved by encapsulating it within this targeted nanoparticle system.

Conclusions

In collaboration with the Hagemeyer group, we have developed a nanoparticle delivery system that can deliver naphthofluorescein specifically to unstable plaques, thereby increasing the efficacy of the drug almost 2-fold. A synthesis scheme has been developed to attach both a collagen-IV targeting peptide and an imaging dye, and particles have been post-loaded successfully with naphthofluorescein to a loading capacity of 14%. The activity of the peptide has been shown to be unaffected both *in vitro* and *in vivo* upon attachment to the particle surface. This work shows that this construct has the potential to be utilized as a targeted delivery system

for the delivery of MMP inhibitors that have previously been limited in their applicable use because of off-target effects. By delivering these drugs within this targeted nanoparticle system, we can widely expand the range of options for the treatment of unstable plaques and the prevention of myocardial infarction.

Experimental

Materials

N-succinimidyl-p-formylbenzoate was custom synthesized by Chem-Impex International (Wood Dale, IL). The T-peptide and the naphthofluorescein were provided by the Hagemeyer group. The cyanine3 hydrazide dye was obtained from GE Healthcare Life Sciences (Marlborough, MA). Spectra/Por® dialysis membrane was purchased from Spectrum Laboratories Inc. m-CPBA (<77%) was purified as previously described in the literature, and **δ**-valerolactone was purified after receipt by vacuum distillation. All other reagents were obtained from Sigma Aldrich (St. Louis, MO) and used as received unless otherwise specified.

Characterization

All NMR spectra of polymer precursors and attachments to the particle surface were obtained using a Bruker AV-I 400 MHz, a Bruker DRX 500 MHz, or a Bruker AV-III 600 MHz spectrometer. TEM imaging was performed using an FEI Technai Osiris Transmission Electron Microscope.

Synthesis of α-allyl-δ-valerolactone

This reaction was performed as previously described in the literature[26] with the following exceptions: vacuum distilled **δ**-valerolactone was used in place of the purchased purity, and an equivalent amount of diisopropylamine (DIPA) was used in place of diisopropylethylamine (DIPEA). ^{1}H NMR (300 MHz, $CDCl_3$) **δ**: 1.51-2.17 (4H, m, CH2), 2.33 (1H, m, CH2), 2.59 (2H, m, CH2, CH), 4.31 (2H, m, CH2), 5.07 (2H, m, CH2), 5.80 (1H, m, CH).

General Procedure for Synthesis of a VL/AVL Polymer

A 25 mL round-bottom flask was flame-dried and purged with nitrogen. A catalytic amount (2.5 mg, 6.1 μmol, 3.2 x 10^{-4} eq/total monomer) of tin triflate was added to the bottom of the round-bottom flask, and then the flask was again purged with nitrogen. The 3-methyl-1-butanol initiator (72.64 μL, 0.67 mmol) was added to the flask, along with the DCM (0.96 mL), and the mixture was stirred for 30 minutes to allow the catalyst to coordinate to the alcohol group on the initiator. The **δ**-valerolactone (1.56 mL, 16.77 mmol, 7.3 eq) and the **α**-allyl-**δ**-valerolactone (0.30 mL, 2.29 mmol, 1.0 eq) were added to the reaction mixture and the reaction was allowed to stir for 16-18 hours at room temperature. The product was purified by precipitation in cold methanol. ^{1}H NMR (400 MHz, $CDCl_3$) **δ**: 0.92 (6H, d, CH3), 1.47-1.78 (8H, m, CH2), 1.86 (1H, m, CH), 2.14-2.52 (5H, m, CH2, CH), 3.65 (2H, t, CH2), 4.08 (4H, m, CH2), 5.04 (2H, m, CH2) 5.73 (1H, m, CH).

General Procedure for Synthesis of a VL/AVL/EVL Polymer

To a 25 mL round-bottom flask equipped with a stir bar, the VL/AVL polymer (0.200 g, 0.1828 mmol allyl) was added along with m-CPBA (22.3 mg, 0.129 mmol, 0.7 eq/allyl). Dichloromethane was added to a final epoxide concentration of 0.065 M. The flask was capped with a septum and

then allowed to stir at room temperature for 48 hours. Oxidized polymer was purified by washing three times with an equal volume of saturated sodium bicarbonate followed by an extraction of the product three times in dichloromethane. ^{1}H NMR (400 MHz, $CDCl_3$): The significant change seen in the ^{1}H NMR is a reduction of the allylic peaks at 5.3 and 5.9 ppm and the emergence of small broad peaks at 2.47, 2.76, and 2.94 ppm due to the epoxide ring.

General Procedure for Synthesis of a VL/EVL Polymer

To a 25 mL round-bottom flask equipped with a stir bar, the VL/AVL polymer (0.200 g, 0.1773 mmol allyl) was added along with m-CPBA (43.2 mg, 0.250 mmol, 1.4 eq/allyl). Dichloromethane was added to a final epoxide concentration of 0.065 M. The flask was capped with a septum and then allowed to stir at room temperature for 48 hours. Oxidized polymer was purified by washing three times with an equal volume of saturated sodium bicarbonate followed by an extraction of the product three times in dichloromethane. ^{1}H NMR (400 MHz, $CDCl_3$): The significant change seen in the ^{1}H NMR is the disappearance of the allylic peaks at 5.3 and 5.9 ppm and the emergence of small broad peaks at 2.47, 2.76, and 2.94 ppm due to the epoxide ring.

General Procedure for Synthesis of Polyester Nanoparticles

To a 100 mL round-bottom flask, the VL/AVL/EVL linear polymer (154.5 mg, 0.0726 mmol epoxide) was added and then dissolved in dichloromethane to a final epoxide concentration of 0.00324 M. The 2,2' (ethylenedioxy) diethylamine (8.0 μL, 1.5 amines/epoxide) was added to the vigorously stirring flask via microsyringe, and the solution was refluxed at 46°C for 12 hours. The resulting nanoparticles were purified by dialysis using Snakeskin Dialysis tubing (MWCO = 10,000) against DCM for 72 hours and then passed through a 0.45μm syringe filter. Particle size

and uniformity were determined by transmission electron microscopy. ^{1}H NMR (400 MHz, d-DMSO) **δ**: 0.92 (6H, d, CH3), 1.47-1.78 (8H, m, CH2), 1.86 (1H, m, CH), 2.14-2.52 (5H, m, CH2, CH), 3.50-3.65 (14H, m, CH2), 4.08 (4H, m, CH2), 5.04 (2H, m, CH2), 5.73 (1H, m, CH).

Attachment of N-succinimidyl-p-formylbenzoate to Polyester Nanoparticles

A 1-dram vial equipped with stir bar and septum was flamed dried and purged with nitrogen. Polyester nanoparticles (4.6% AVL, 4.9% EVL, 80.0 mg, 5.33 x 10^{-7} mol, 1.0 eq) were added to the vial, and the vial was again purged with nitrogen. Particles were dissolved by adding a minimal amount of dimethyl sulfoxide through the septum via syringe. A stock solution of N-succinimidyl-p-formylbenzoate was prepared in DMSO, and the linker (4.0 mg, 1.60 x 10^{-5} mol, 30.0 eq) was added through the septum via syringe. The reaction was then allowed to stir at room temperature overnight. The resulting mixture was purified by dialysis against dichloromethane using Snakeskin tubing (10K MWCO) for 24 hours. ^{1}H NMR (400 MHz, d-DMSO) **δ**: 0.92 (6H, d, CH3), 1.47-1.78 (8H, m, CH2), 1.86 (1H, m, CH), 2.14-2.52 (5H, m, CH2, CH), 3.50-3.65 (14H, m, CH2), 4.08 (4H, m, CH2), 5.04 (2H, m, CH2) 5.73 (1H, m, CH), 7.90-8.10 (4H, m, CH), 10. 06 (1H, s, CH)

Attachment of T-Peptide to Polyester Nanoparticles

A 1-dram vial equipped with stir bar and septum was flame-dried and purged with nitrogen. Polyester nanoparticles (4.6% AVL, 4.9% EVL, 50.0 mg, 3.33 x 10^{-7} mol, 1.0 eq) and T-peptide (21.2 mg, 3.33 x 10^{-6} mol, 0.15 eq/allyl) were added to the vial, and the vial was again purged with nitrogen. Particles and peptide were dissolved by adding d-DMSO through the septum. A stock solution of 2,2-dimethoxy-2-phenylacetophenone was prepared in d-DMSO, and the photoinitiator

(1.12 mg, 4.37 x 10^{-6} mol, 0.2 eq/allyl) was added to the reaction mixture via syringe. The reaction vial was placed under long wave UV light and allowed to stir at room temperature overnight. Percent attachment of the peptide was calculated using the reduction in the allyl peaks at 5.04 and 5.73 ppm seen in the crude NMR spectrum.

Attachment of Cyanine3 Hydrazide Dye to Polyester Nanoparticles

To a 1-dram vial equipped with a stir bar, polyester nanoparticles previously functionalized with an N-succinimidyl-p-formylbenzoate aldehyde linker (50.0 mg, 3.33 x 10^{-7} mol, 1.0 eq) were added. Particles not functionalized with T-peptide were added as a dry powder, whereas particles functionalized with T-peptide were transferred back to the original reaction vial from the NMR tube. A stock solution of Cy3 mono hydrazide was prepared in DMSO and the dye (1.58 mg, 2.90 x 10^{-6} mol, 8.7 eq) was added to the reaction vial via syringe. The reaction was allowed to stir in the absence of light at room temperature overnight. The resulting mixture was purified by dialysis against a 50:50 v/v mixture of acetonitrile and methanol using Snakeskin tubing (10K MWCO) for 48 hours. Successful attachment of the dye was verified by the absence of the aldehyde peak at 10.06 ppm.

Loading of Polyester Nanoparticles with Naphthofluorescein

To an Eppendorf tube, D-**α**-tocopherol polyethylene glycol 1000 succinate (0.0125 mg, 0.59 μL), naphthofluorescein (0.17375 mg, 2.60 μL), and fully functionalized polyester nanoparticles (1.06375 mg, 31.9 μL), all previously dissolved in DMSO, were added. The solution was mixed well until a homogeneous mixture was achieved. Cell culture water (1.00 mL) was added to the

tube, and the resulting solution was mixed well. The resulting solution was frozen and then lyophilized to obtain the drug-loaded particles.

Testing the Activity of T-Peptide Conjugated Nanoparticles in vitro using HT1080 Cells

HT1080 cells were cultured by Mei Choy in the Hagemeyer lab. Briefly, cells were treated with an aliquot of nanoparticles labeled with both T-peptide and cyanine3 dye and then incubated overnight at 37^{o}C and 5% CO_2. The following day, the cells cytoplasm was stained green and cells were imaged using live cell confocal microscopy. Images were taken using both the FITC and TRITC channels at 60x magnification.

Studying the Targeting Ability of T-Peptide Conjugated Nanoparticles to Unstable Plaques *in vivo*

In vivo studies were performed by Mei Choy in the Hagemeyer lab. ApoE knock out mice had sutures placed at the right carotid artery after 7 weeks of high fat diet to induce the formation of unstable plaques. After five weeks, mice were injected with one of two constructs: nanoparticles with T-peptide and Cy3 dye attached, or nanoparticles with only Cy3 dye attached. Plaques were then harvested and analyzed by fluorescence microscopy in the TRITC channel.

Studying the Efficacy of Naphthofluorescein Encapsulated in a Targeted Nanoparticle Delivery System *in vivo*

Mice were prepared as for the *in vivo* targeting study by Mei Choy. Mice received two injections each, two weeks apart of one of four treatment groups: naphthofluorescein-loaded nanoparticles containing T-peptide and a Cy3 imaging dye (1.25 mg particles, 14.0 wt% naphthofluorescein),

nanoparticles alone (1.06 mg), PBS, and free naphthofluorescein (0.17 mg). Mice were then killed and their plaques were harvested and subsequently stained for collagen content using both Picrosirius Red and Masons Trichrome staining.

References

1. Go, A. S.; Mozaffarian, D.; Roger, V. L.; Benjamin, E. J.; Berry, J. D.; Blaha, M. J.; Dai, S. F.; Ford, E. S.; Fox, C. S.; Franco, S.; Fullerton, H. J.; Gillespie, C.; Hailpern, S. M.; Heit, J. A.; Howard, V. J.; Huffman, M. D.; Judd, S. E.; Kissela, B. M.; Kittner, S. J.; Lackland, D. T.; Lichtman, J. H.; Lisabeth, L. D.; Mackey, R. H.; Magid, D. J.; Marcus, G. M.; Marelli, A.; Matchar, D. B.; McGuire, D. K.; Mohler, E. R.; Moy, C. S.; Mussolino, M. E.; Neumar, R. W.; Nichol, G.; Pandey, D. K.; Paynter, N. P.; Reeves, M. J.; Sorlie, P. D.; Stein, J.; Towfighi, A.; Turan, T. N.; Virani, S. S.; Wong, N. D.; Woo, D.; Turner, M. B.; Comm, A. H. A. S.; Subcomm, S. S., Heart Disease and Stroke Statistics-2014 Update A Report From the American Heart Association. *Circulation* **2014,** *129* (3), E28-E292.

2. Gaziano, T. A.; Bitton, A.; Anand, S.; Abrahams-Gessel, S.; Murphy, A., Growing epidemic of coronary heart disease in low- and middle-income countries. *Current Problems in Cardiology* **2010,** *35* (2), 72-115.

3. Gersh, B. J.; Sliwa, K.; Mayosi, B. M.; Yusuf, S., Novel therapeutic concepts: the epidemic of cardiovascular disease in the developing world: global implications. *European Heart Journal* **2010,** *31* (6), 642-8.

4. Lafont, A., Basic aspects of plaque vulnerability. *Heart* **2003,** *89* (10), 1262-1267.

5. Falk, E., Pathogenesis of atherosclerosis. *Journal of the American College of Cardiology* **2006,** *47* (8 Suppl), C7-12.

6. Bentzon, J. F.; Otsuka, F.; Virmani, R.; Falk, E., Mechanisms of plaque formation and rupture. *Circulation Research* **2014,** *114* (12), 1852-66.

7. Nadkarni, S. K.; Bouma, B. E.; de Boer, J.; Tearney, G. J., Evaluation of collagen in atherosclerotic plaques: the use of two coherent laser-based imaging methods. *Lasers in Medical Science* **2009,** *24* (3), 439-45.

8. Miller, J. D., Arterial calcification: Conscripted by collagen. *Nature Materials* **2016,** *15* (3), 257-8.

9. Schneider, F.; Sukhova, G. K.; Aikawa, M.; Canner, J.; Gerdes, N.; Tang, S. M.; Shi, G. P.; Apte, S. S.; Libby, P., Matrix-metalloproteinase-14 deficiency in bone-marrow-derived cells promotes collagen accumulation in mouse atherosclerotic plaques. *Circulation* **2008,** *117* (7), 931-9.

10. Suh, W. M.; Seto, A. H.; Margey, R. J.; Cruz-Gonzalez, I.; Jang, I. K., Intravascular detection of the vulnerable plaque. *Circulation: Cardiovascular Imaging* **2011,** *4* (2), 169-78.

11. Peeters, W.; Moll, F. L.; Vink, A.; van der Spek, P. J.; de Kleijn, D. P.; de Vries, J. P.; Verheijen, J. H.; Newby, A. C.; Pasterkamp, G., Collagenase matrix metalloproteinase-8 expressed in atherosclerotic carotid plaques is associated with systemic cardiovascular outcome. *European Heart Journal* **2011,** *32* (18), 2314-25.

12. Cheng, C.; Tempel, D.; van Haperen, R.; van Damme, L.; Algur, M.; Krams, R.; de Crom, R., Activation of MMP8 and MMP13 by angiotensin II correlates to severe intra-plaque hemorrhages and collagen breakdown in atherosclerotic lesions with a vulnerable phenotype. *Atherosclerosis* **2009,** *204* (1), 26-33.

13. Johnson, J. L.; Sala-Newby, G. B.; Ismail, Y.; Aguilera, C. M.; Newby, A. C., Low tissue inhibitor of metalloproteinases 3 and high matrix metalloproteinase 14 levels defines a subpopulation of highly invasive foam-cell macrophages. *Arteriosclerosis, Thrombosis, and Vascular Biology* **2008,** *28* (9), 1647-53.

14. Ishibashi, M.; Sayers, S.; D'Armiento, J. M.; Tall, A. R.; Welch, C. L., TLR3 deficiency protects against collagen degradation and medial destruction in murine atherosclerotic plaques. *Atherosclerosis* **2013,** *229* (1), 52-61.

15. Newby, A. C., Metalloproteinases promote plaque rupture and myocardial infarction: A persuasive concept waiting for clinical translation. *Matrix Biology* **2015,** *44-46*, 157-66.

16. Johnson, J. L.; Jenkins, N. P.; Huang, W. C.; Di Gregoli, K.; Sala-Newby, G. B.; Scholtes, V. P.; Moll, F. L.; Pasterkamp, G.; Newby, A. C., Relationship of MMP-14 and TIMP-3 expression with macrophage activation and human atherosclerotic plaque vulnerability. *Mediators of Inflammation* **2014,** *2014*, 276457.

17. Overall, C. M.; Kleifeld, O., Towards third generation matrix metalloproteinase inhibitors for cancer therapy. *British Journal of Cancer* **2006,** *94* (7), 941-6.

18. Pavlaki, M.; Zucker, S., Matrix metalloproteinase inhibitors (MMPIs): the beginning of phase I or the termination of phase III clinical trials. *Cancer and Metastasis Reviews* **2003,** *22* (2-3), 177-203.

19. Netta Sela-Passwell, A. T., Achim Kruger, and Irit Sagi, New opportunities in drug design of metalloproteinase inhibitors: combination between structure-function experimental approaches and systems biology. *Expert Opinion on Drug Discovery* **2011,** *6* (5), 527-542.

20. Newby, A. C.; George, S. J.; Ismail, Y.; Johnson, J. L.; Sala-Newby, G. B.; Thomas, A. C., Vulnerable atherosclerotic plaque metalloproteinases and foam cell phenotypes. *Thrombosis and Haemostasis* **2009,** *101* (6), 1006-11.

21. Jiao, G. S.; Cregar, L.; Wang, J.; Millis, S. Z.; Tang, C.; O'Malley, S.; Johnson, A. T.; Sareth, S.; Larson, J.; Thomas, G., Synthetic small molecule furin inhibitors derived from 2,5-dideoxystreptamine. *Proceedings of the National Academy of Sciences USA* **2006,** *103* (52), 19707-12.

22. Lockhart, J. N.; Stevens, D. M.; Beezer, D. B.; Kravitz, A.; Harth, E., Dual drug delivery of tamoxifen and quercetin: Regulated metabolism for anticancer treatment with nanosponges. *Journal of Controlled Release* **2015**.

23. Stevens, D. M., Gilmore, K. A., Harth, E., An assessment of nanosponges for intravenous and oral drug delivery of BCS class IV drugs: Drug delivery kinetics and solubilization. *Polymer Chemistry* **2014,** *5* (11), 3551-3554.

24. van der Ende, A. E.; Sathiyakumar, V.; Diaz, R.; Hallahan, D. E.; Harth, E., Linear release nanoparticle devices for advanced targeted cancer therapies with increased efficacy. *Polymer Chemistry* **2010,** *1* (1), 93-96.

25. Mueller, J.; Gaertner, F. C.; Blechert, B.; Janssen, K. P.; Essler, M., Targeting of tumor blood vessels: a phage-displayed tumor-homing peptide specifically binds to matrix metalloproteinase-2-processed collagen IV and blocks angiogenesis in vivo. *Molecular Cancer Research* **2009,** *7* (7), 1078-85.

26. van der Ende, A. E.; Kravitz, E. J.; Harth, E., Approach to formation of multifunctional polyester particles in controlled nanoscopic dimensions. *Journal of the American Chemical Society* **2008,** *130* (27), 8706-13.

CHAPTER V

IMPROVING THE TREATMENT OF CANCER USING A POLYGLYCIDOL FORMALDEHYDE PRODRUG

Introduction

Combination drug therapy is becoming increasingly widely used for the treatment of multiple ailments including cancer,[1] hypertension,[2] and multiple sclerosis,[3] to name a few. The benefits to combination therapy are numerous, including increased efficacy and reduced dosage requirements and toxicity.[4] Recently, small molecules such as carbon monoxide, nitric oxide, hydrogen sulfide, and formaldehyde have emerged as useful agents for synergistic combination therapy.[5-10] Oftentimes these small molecules are able to open a previously unavailable pathway for action when administered with another therapeutic, leading to increased efficacy of the administered drug.

One of these small molecules, formaldehyde, has been shown to effectively increase the efficacy of the class of anthracycline drugs for cancer therapy.[11-13] It is hypothesized that this is due to a conjugate formed between the formaldehyde and the anthracycline drug which is taken up into cancer cells much more readily than the anthracycline alone. As formaldehyde is a toxic small molecule, it cannot be delivered in high doses as a pure compound. It is necessary therefore, for successful combination therapy, to deliver the formaldehyde in a vehicle that will allow for sustained release. Previous work in this field has led to the development of an array of biocompatible materials that can be used to deliver these small molecules slowly over time. For example, carbon monoxide has been successfully delivered in a sustained way using Prussian

Blue nanoparticles,[7] while hydrogen sulfide has been co-delivered with paclitaxel for efficient chemotherapy using a prodrug based on aspirin.[8]

In this work, we will utilize a polyglycidol-based prodrug for the sustained release of formaldehyde for use in synergistic therapy. Polyglycidol is a polymer that has been shown to be useful for biomedical applications and has been used to construct materials such as nanogel carriers,[14-15] adhesives,[16] and anti-fouling coatings.[17] Most of these applications utilize a hyperbranched form of polyglycidol, which has limitations for use as a prodrug due to the limited number of functional groups present on the surface of the hyperbranched structure. Our group has previously developed a method for constructing semi-branched polyglycidol, which contains many more reactive handles than hyperbranched polyglycidol, and therefore allows for a much higher loading capacity of a conjugated small molecule. Formaldehyde can be successfully conjugated to the backbone of this polymer via an acetal linkage and then subsequently released from the polymer backbone in a sustained manner. A conjugate formed between an amino-oxy functionalized polyglycidol and formaldehyde via an oxime bond and its potential as a polymeric prodrug will also be considered here.

An additional advantage to the semi-branched polyglycidol is that the polymer itself acts as an excellent matrix material for the suspension of other drugs or macromolecular structures. The successful clinical use of this polyglycidol based prodrug will require the co-administration of an anthracycline for the intended synergistic effect. Our lab has previously demonstrated that polyglycidol can be used successfully as a matrix to suspend drug-loaded polyester nanoparticles.[18] We expect that by utilizing doxorubicin-loaded polyester nanoparticles suspended in a matrix of the polyglycidol based formaldehyde prodrug, we can create a delivery

system that is capable of sustained delivery of both therapeutics for enhanced synergistic effects (Figure 1).

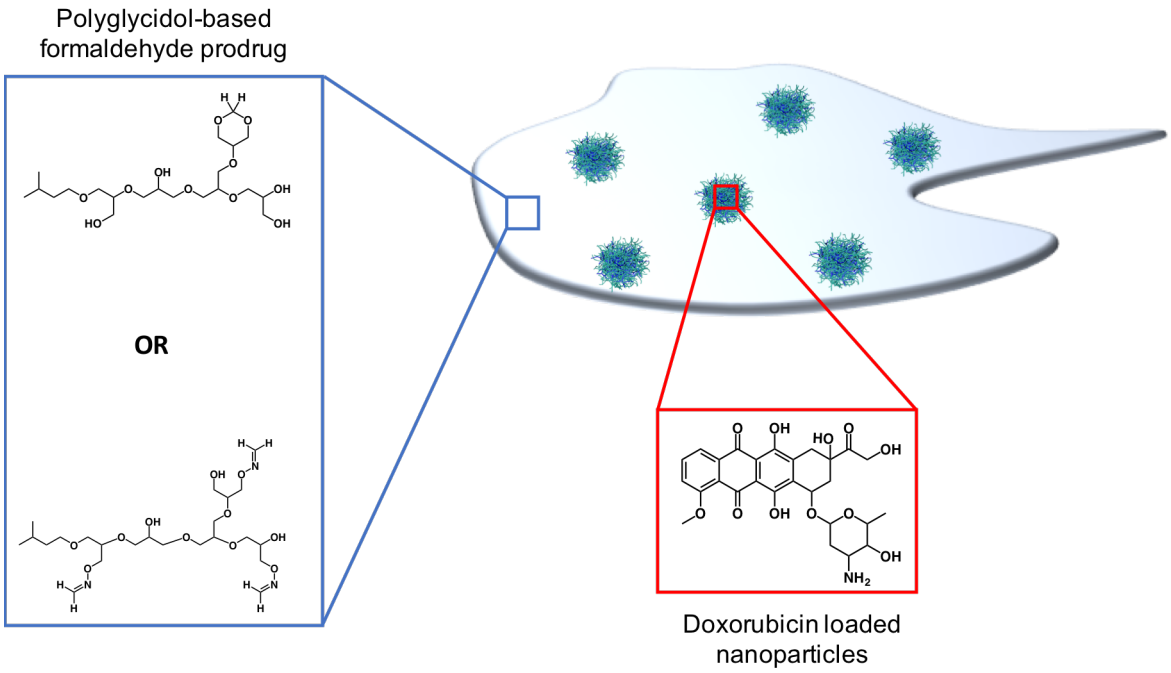

Figure V-1. The proposed dual delivery system providing a sustained release of both doxorubicin and formaldehyde for the improved treatment of cancer.

Results and Discussion

A polyglycidol formaldehyde prodrug was synthesized by conjugating formaldehyde to the semi-branched polymer via an acetal linkage. The release of formaldehyde from this prodrug was studied using a dialysis based method and found to be pH-dependent. The polyglycidol prodrug was also demonstrated to increase the efficacy of doxorubicin in the destruction of 4T1 cancer cells. Another conjugate using amino-oxy functionalized polyglycidol was also explored and found to successfully form a prodrug construct. Preliminary studies on the release rate of formaldehyde from this prodrug were conducted.

Synthesis of Polyglycidol Formaldehyde Prodrug

Formaldehyde has been shown to form oligomers in solution, as well as adducts with water and methanol. In this work, we wished to take advantage of this reaction of a primary alcohol with formaldehyde to form a polymeric prodrug. The structure of semi-branched polyglycidol is made of a number of distinct branching units as illustrated in Figure 2. The T_2 branching unit contains two adjacent primary alcohols that could serve as a potential site for formation of an acetal adduct with formaldehyde.

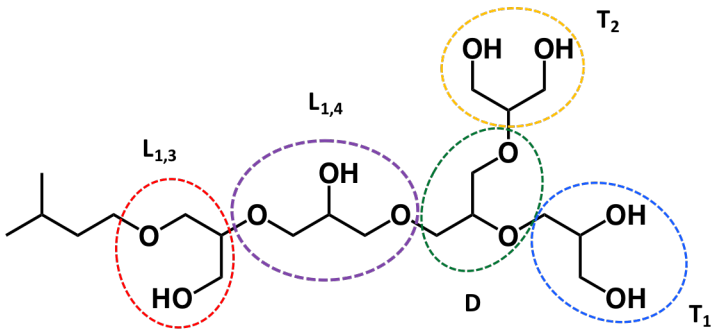

Figure V-2. The structure of semi-branched polyglycidol, with all types of branching units identified.

To investigate this possibility, we performed reactions of semi-branched polyglycidol with solutions of formaldehyde and monitored the results of the reaction by NMR. Figure 3 shows the ^{1}H and ^{13}C-IG spectra of the resulting product of the reaction. The proton spectrum of the product, when compared with that of the precursor polyglycidol, shows new peaks at 4.55, 4.65, and 4.74 ppm. The broad peak at 4.74 ppm is indicative of the acetal protons, while the peaks at 4.55 and 4.65 ppm are from an adduct of formaldehyde with methanol (CH_3O**CH2CH2**OH). The inverse gated carbon spectrum of the prodrug product shows three new peaks that emerge upon conjugation of the polyglycidol to the formaldehyde at 90.56, 91.07, and 91.14 ppm. The two peaks at 91.07 and 91.14 are the result of formaldehyde adducts with methanol, while the peak at

90.56 ppm is the acetal carbon. The HSQC spectrum helps to confirm these assignments (Figure 4). The presence of the adducts of formaldehyde with methanol in the NMR are a sign that formaldehyde that is not bound to the polyglycidol is present in the product. We postulate that

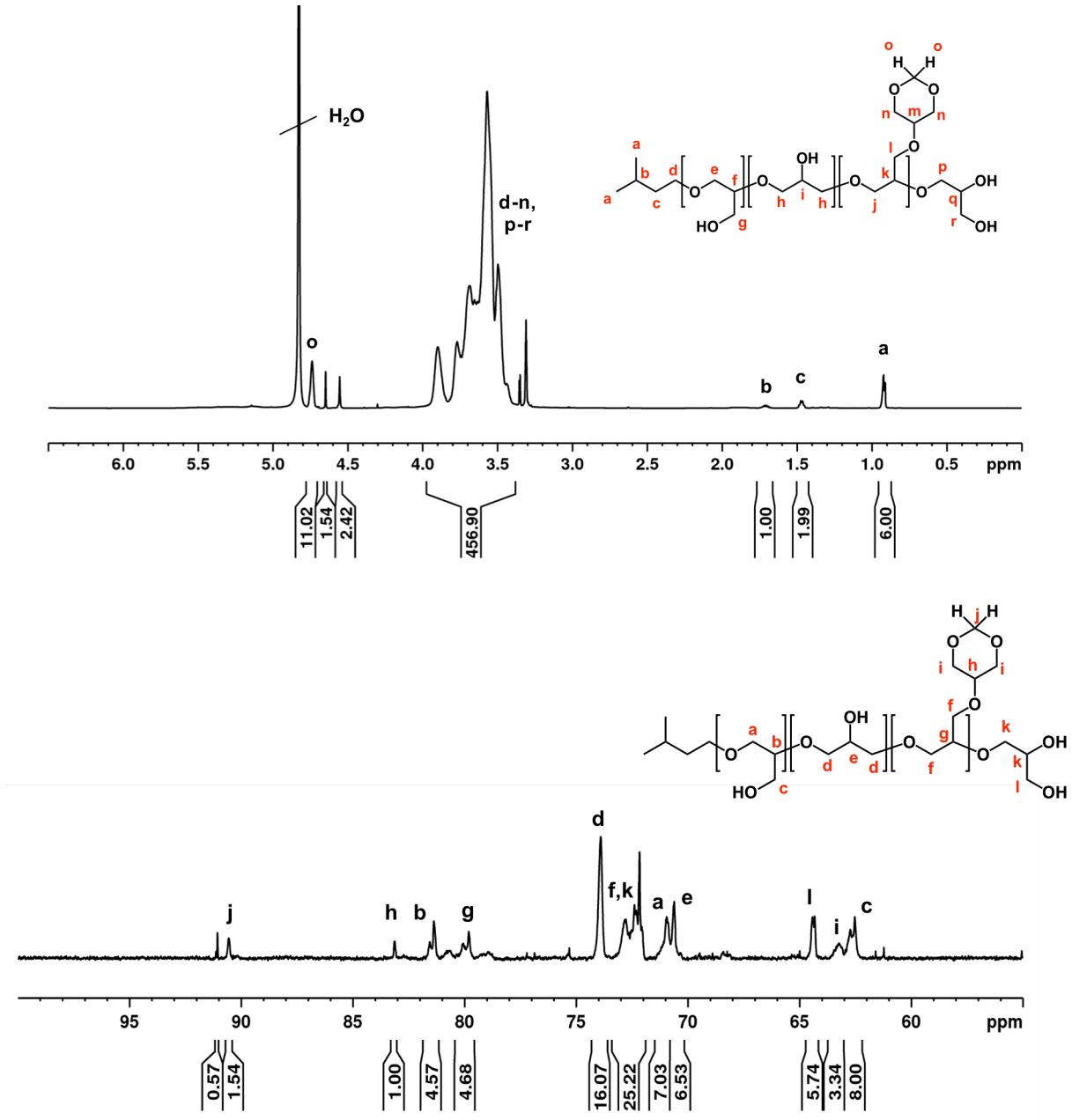

Figure V-3. ^{1}H NMR (top) and ^{13}C-IG (bottom) NMR spectra of the polyglycidol formaldehyde prodrug.

this is the result of free formaldehyde from the reaction becoming trapped in the viscous polyglycidol matrix upon drying of the product, making it difficult to remove. Integration of the peaks in the inverse gated carbon spectrum reveals a 1.54:1 ratio of T_2 carbons to acetal carbons. Full conversion of the T_2 units would theoretically give a perfect 1:1 ratio of the two peaks, but it is possible that this increased ratio is the result of intermolecular acetal formation between primary hydroxyl groups on adjacent polyglycidol chains.

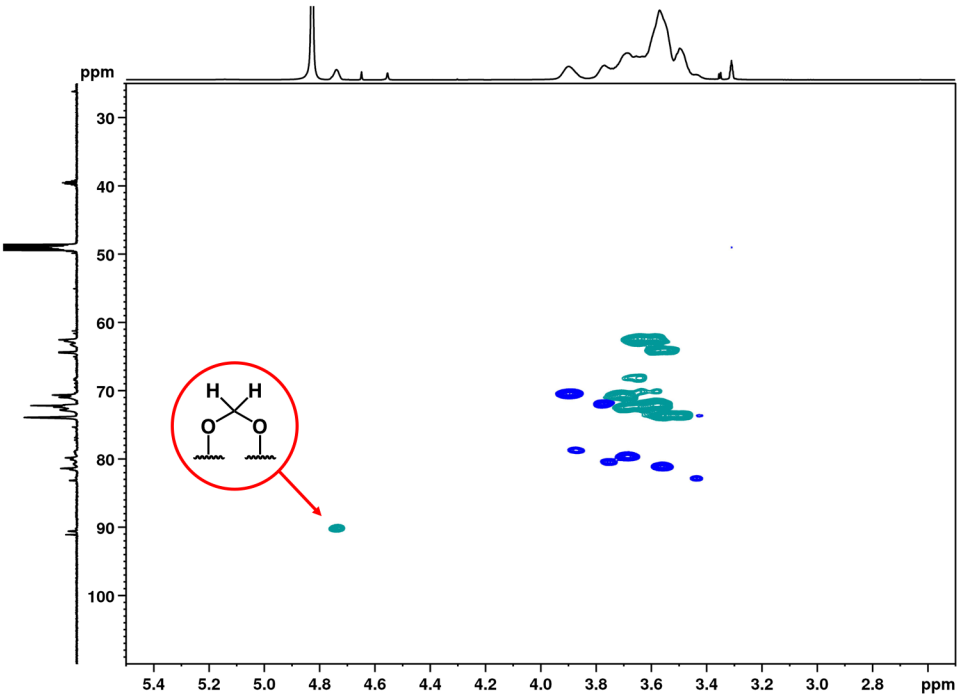

Figure V-4. HSQC spectrum of the polyglycidol-acetal formaldehyde prodrug in MeOD showing the crosspeak for the acetal protons and carbon.

Studying the Release Kinetics of a Polyglycidol Formaldehyde Prodrug

The next step in characterizing this prodrug was to determine rate of hydrolysis of formaldehyde from the backbone of the polymer scaffold over time. As described above, ^{13}C-IG NMR data was used to determine the formaldehyde loading percentage of the prodrug, along with the amount of formaldehyde present as part of a solvent adduct (calculation in Figure 5).

Semibranched polyglycidol precursor (from ^{13}C-IG NMR)

Branching Unit	Number of Units
T_2	1.00
$L_{1,3}$	4.62
D	2.92
$L_{1,4}$	5.81
T_1	4.52

$Sum\ of\ units = 18.87$

$$MW\ of\ one\ \text{“repeat unit”} = 18.87 * 74.08\frac{g}{mol} = 1397\frac{g}{mol}$$

$$\#\ of\ acetals\ per\ \text{“repeat unit”} = 1.5448$$

$$MW\ of\ acetal - formaldehyde\ per\ \text{“repeat unit”} = 1.5448 * 30.026\frac{g}{mol} = 46.38\frac{g}{mol}$$

$$\#\ of\ formaldehdye\ molecules\ in\ MeOH\ adducts\ per\ \text{“repeat unit”} = 0.5725$$

$$MW\ of\ MeOH\ adducted\ formaldehyde\ per\ \text{“repeat unit”} = 0.5725 * 30.026\frac{g}{mol} = 17.19\frac{g}{mol}$$

$$\%\ prodrug\ formaldehdye = \frac{46.38\frac{g}{mol}}{1397\frac{g}{mol} + 46.38\frac{g}{mol} + 17.19\frac{g}{mol}} * 100\% = 3.2\%\ wt$$

$$\%\ MeOH\ adducted\ formaldehdye = \frac{17.19\frac{g}{mol}}{1397\frac{g}{mol} + 46.38\frac{g}{mol} + 17.19\frac{g}{mol}} * 100\% = 1.2\%\ wt$$

$$\%\ \boldsymbol{Available\ T_2\ units\ functionalized} = \frac{1.00}{1.00}\ \boldsymbol{x\ 100\% = 100.0\%}$$

$$\%\ \boldsymbol{other\ primary\ OH\ groups\ functionalized} = \frac{0.5448}{4.62+4.52}\ \boldsymbol{x\ 100\% = 6.0\%}$$

Figure V-5. Example calculation for determining the loading of formaldehyde on the polyglycidol prodrug and the amount of formaldehyde found in MeOH adducts that must be accounted for during the release studies. The T_2 integral is used as a calibration standard between the prodrug product and the polyglycidol precursor.

The release of formaldehyde from the prodrug was studied using a dialysis release method wherein the sink outside of the dialysis tubing was sampled every few days for formaldehyde concentration. To determine the concentration of formaldehyde in the sink, a Purpald® colorimetric detection assay was used. Briefly, an oxidizing agent (sodium periodate) was added to the sample to release any formaldehyde trapped in adducts with the aqueous buffer. An aliquot of 4-amino-3-hydrazino-5-mercapto-1,2,4-triazole (Purpald®) was then added to the solution to react with the formaldehyde. Upon addition of more oxidizing agent, this Purpald-formaldehyde

complex is transformed into a purple-colored complex, which can be analyzed via UV-Vis to determine formaldehyde concentration. The release curves generated for the prodrugs were corrected for this "free" formaldehyde that is detected in the assay by subtracting the amount present from the total detected formaldehyde and setting the zero point of release at the point when all of the free methanol adducted formaldehyde has been detected. This correction method makes the assumption that all of the formaldehyde attached to methanol will pass into the sink and be detected before any formaldehyde that is attached to the polyglycidol backbone, which is a reasonable assumption based upon the principles of the dialysis method used here.

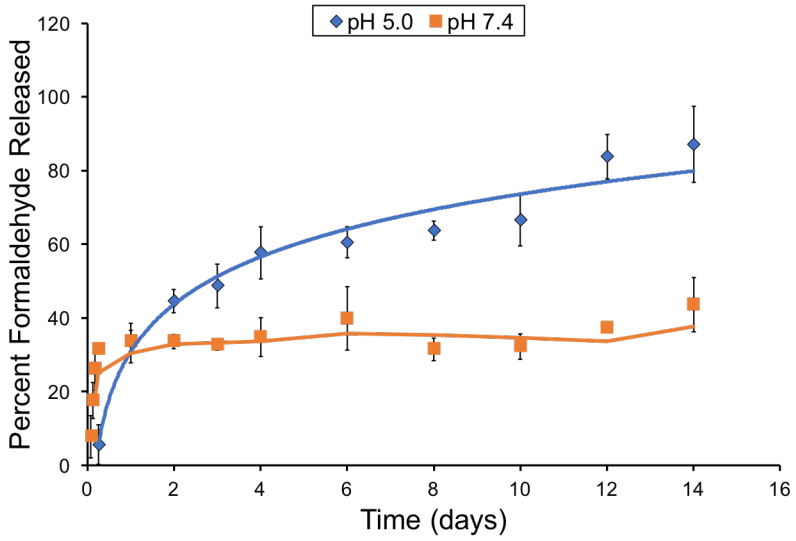

Figure V-6. Release profile of formaldehyde from a polyglycidol formaldehyde prodrug. The release follows a logarithmic pattern at pH 5.0 while at pH 7.4 the prodrug remains relatively stable after releasing only 30% of its attached payload.

Because these prodrugs are intended for applications in the treatment of cancer, releases were run at both pH 7.4 and at pH 5.0, to simulate both physiological pH, and the lower pH associated with a tumor environment. As can be seen in Figure 6, the polyglycidol formaldehyde prodrug exhibits a sustained release of the formaldehyde that is pH dependent. At pH 5.0, the

formaldehyde is hydrolyzed at a sustained rate over a period of 14 days. However, at pH 7.4, the prodrug remains stable after releasing only 30% of the attached payload.

Improving the Efficacy of Doxorubicin against 4T1 Cells using a Polyglycidol Formaldehyde Prodrug

As this prodrug is intended for use along with an anthracycline drug for synergistic therapy, the action of this construct on 4T1 mouse breast cancer cells was tested in combination with free doxorubicin. Free doxorubicin was used here as a starting point to test whether an increase in apoptosis of the cancer cells could be observed by the addition of the prodrug. 4T1 cells were seeded into a 96-well plate and then incubated for 24 hours with either free doxorubicin, doxorubicin plus free formaldehyde (formalin solution), or doxorubicin plus the polyglycidol formaldehyde prodrug. The concentration of doxorubicin was 0.1 μg/mL and the concentration of formaldehyde was 0.01 μg/mL for all cases. After 24 hours of treatment, the

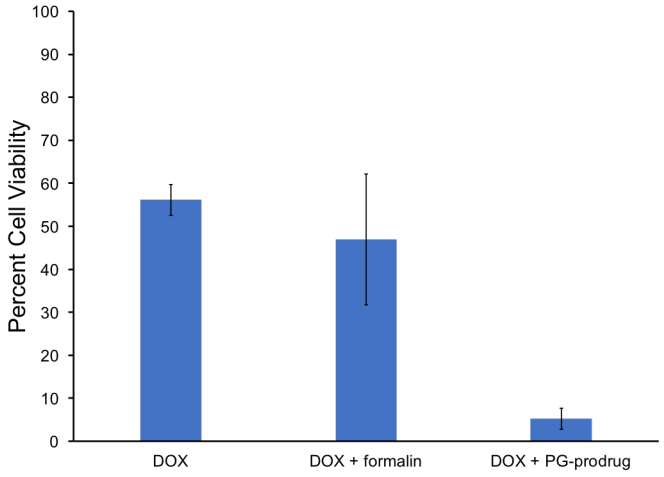

Figure V-7. Results of an MTT assay using 4T1 cells to test the efficacy of the polyglycidol formaldehyde prodrug as compared to doxorubicin administered alone. Administration of the prodrug with the doxorubicin is able to increase the efficacy of the drug by almost 11-fold, indicating that the prodrug is able to successfully release the formaldehyde conjugated to the backbone *in vitro*.

viability of the cells was then tested using an MTT assay. The efficacy of the combination used can be directly correlated to the viability of the cells following treatment, with the most efficacious combination exhibiting the lowest viability, or the highest kill rate of the cancer cells. The results of the MTT assay shown in Figure 7 demonstrate that the combination of doxorubicin with the polyglycidol formaldehyde prodrug is in fact the most efficacious combination for the killing of the cancer cells. Next steps for *in vitro* testing of this prodrug construct will involve the administration of the prodrug and doxorubicin-loaded nanoparticles to the 4T1 cells to closer match the intended delivery method as described previously. Nanoparticles have been successfully loaded with doxorubicin to a loading capacity of 10.2% and are poised to be tested in conjunction with the polyglycidol formaldehyde prodrug for action against cancer cells.

Synthesis of an Amino-oxy Polyglycidol Formaldehyde Prodrug

In light of the positive results from the polyglycidol formaldehyde prodrug described above, we became interested in investigating another potential formaldehyde prodrug using a functionalized polyglycidol. In addition to forming adducts with primary alcohols, formaldehyde is also expected to react with amino-oxy groups to form an oxime bond. Work in our lab has led to the development of an amino-oxy functionalized polyglycidol that can be synthesized to contain anywhere from 15-70% amino-oxy functionality.[19] Amino-oxy polyglycidol containing 67% amino-oxy functionality was reacted with a solution of formaldehyde and the resulting product was again analyzed by NMR as with the first prodrug construct. Figure 8 shows the ^{1}H and ^{13}C-IG NMR spectra of the amino-oxy polyglycidol formaldehyde prodrug. Here the proton peaks for the oxime protons are very clearly defined and well separated from the rest of the

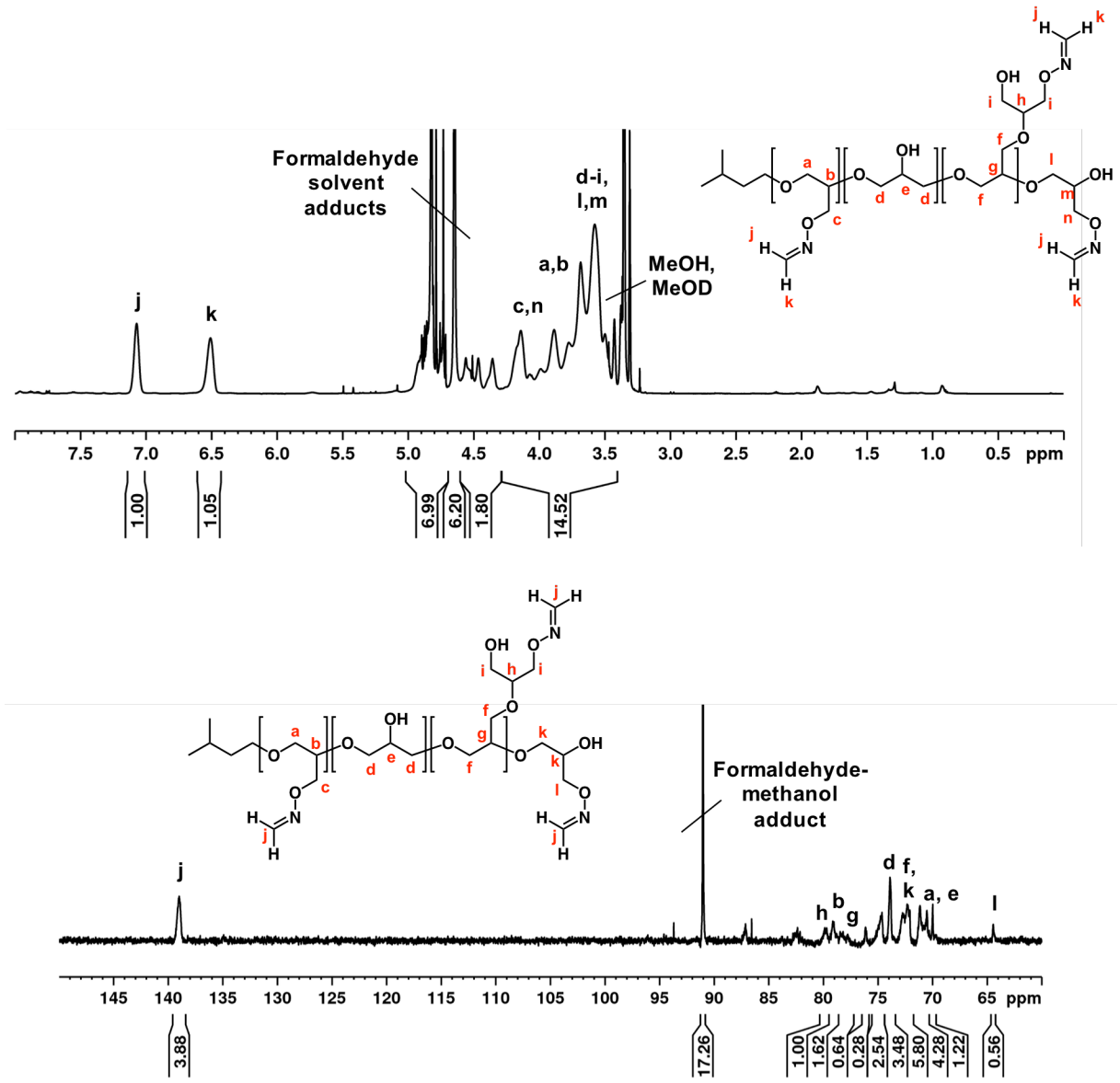

Figure V-8. ^{1}H NMR (top) and ^{13}C-IG (bottom) NMR spectra of the amino-oxy polyglycidol formaldehyde prodrug in MeOD.

peaks in the spectrum. The peaks for the diastereotopic protons are seen at 6.52 and 7.07 ppm. The carbon spectrum shows similar results, with the peak for the oxime carbon at 140 ppm being the most downfield of all the other signals. Just as for the polyglycidol formaldehyde prodrug, the HSQC spectrum helps to confirm the initial assignments (Figure 9).

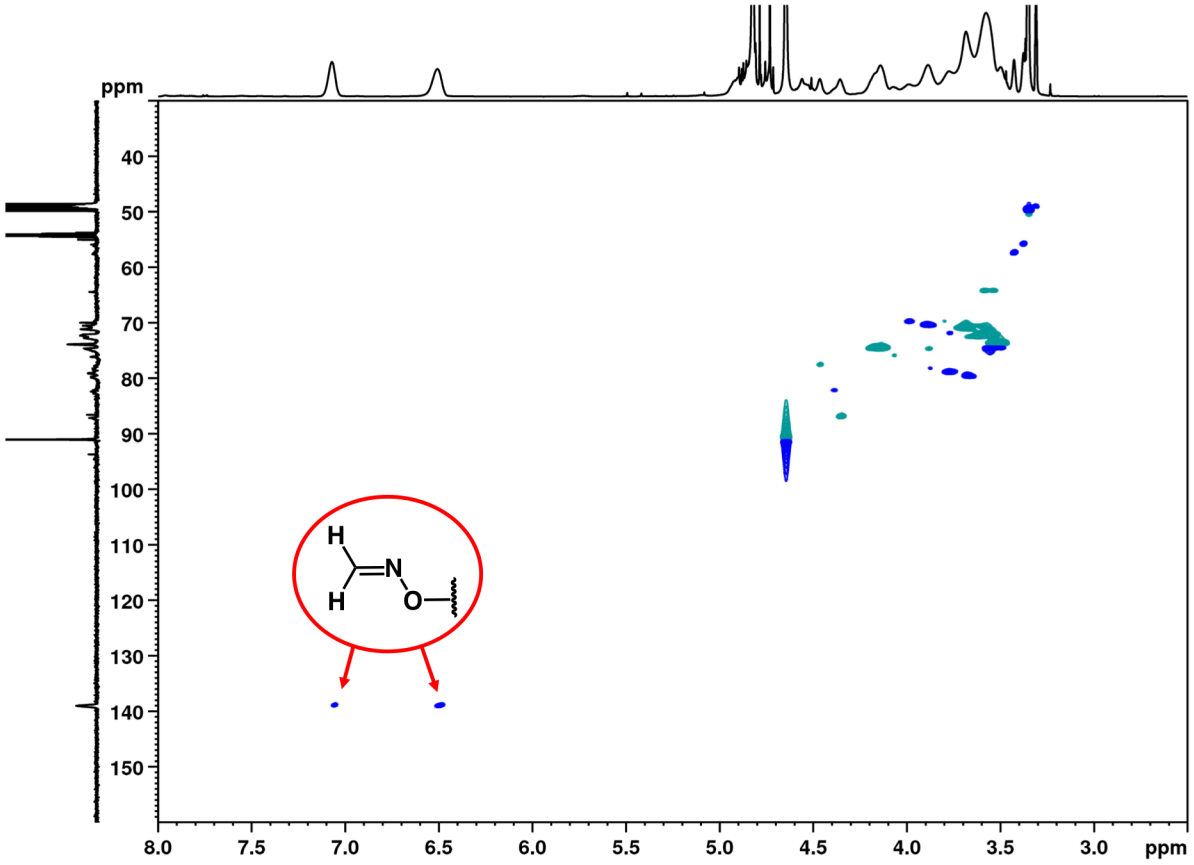

Figure V-9. HSQC spectrum of the amino-oxy polyglycidol formaldehyde prodrug in MeOD showing the crosspeak for the oxime protons and carbon.

Calculations from the ^{13}C-IG NMR show that this material contains 6.6 wt% formaldehyde bound as an oxime adduct (see Figure 10), and that 35.7wt% of the product is the result of formaldehyde adducted to methanol, which as before will be an important practical consideration when studying the release rate of the formaldehyde from this prodrug construct. As multiple branching units in this polymer will have amino-oxy functional groups, there is no standard in the ^{13}C-IG NMR as there was for the acetal linked prodrug to determine a reaction efficiency. However, the ^{1}H NMR can provide an estimate by comparing the signal for the backbone protons to that of the oxime protons. Comparison of these integrals shows a 35.2 mol%

AOPG precursor (from ^{13}C-IG NMR)

Branching Unit	Number of Units
T_2	2.13
$L_{1,3}$	5.91
D	5.52
$L_{1,4}$	3.45
T_1	3.14

$Sum\ of\ units = 20.15$

$$MW\ of\ one\ \text{“}repeat\ unit\text{”} = 20.15 * 74.08\frac{g}{mol} = 1493\frac{g}{mol}$$

$$\#\ of\ oxime\ bonds\ per\ \text{“}repeat\ unit\text{”} = 5.67$$

$$MW\ of\ oxime - formaldehyde\ per\ \text{“}repeat\ unit\text{”} = 5.67 * 30.026\frac{g}{mol} = 170.25\frac{g}{mol}$$

$$\#\ of\ formaldehdye\ molecules\ in\ MeOH\ adducts\ per\ \text{“}repeat\ unit\text{”} = 30.82$$

$$MW\ of\ MeOH\ adducted\ formaldehyde\ per\ \text{“}repeat\ unit\text{”} = 30.82 * 30.026\frac{g}{mol} = 925.40\frac{g}{mol}$$

$$\%\ prodrug\ formaldehdye = \frac{170.25\frac{g}{mol}}{1493\frac{g}{mol} + 170.25\frac{g}{mol} + 925.40\frac{g}{mol}} * 100\% = 6.6\%\ wt$$

$$\%\ MeOH\ adducted\ formaldehdye = \frac{925.40\frac{g}{mol}}{1493\frac{g}{mol} + 170.25\frac{g}{mol} + 925.40\frac{g}{mol}} * 100\% = 35.7\%\ wt$$

$$\boldsymbol{\%\ Amino - oxy\ groups\ functionalized = \frac{35.2\ mol\%}{67.0\ mol\%} * 100\% = 52.6\%}$$

Figure V-10. Example calculation for determining the loading of formaldehyde on the amino-oxy polyglycidol prodrug and the amount of formaldehyde found in MeOH adducts that must be accounted for during the release studies.

loading of the formaldehyde onto the backbone. As the precursor was calculated to have a 67 mol% content of amino-oxy groups, this indicates a reaction efficiency of 52.6%. Future work will focus on optimizing the efficiency of this reaction in order to obtain a higher loading of the active molecule formaldehyde.

Because of the reactive nature of amino-oxy groups towards ketones and aldehydes, this amino-oxy polyglycidol backbone could also be utilized to create a prodrug of doxorubicin via the ketone in the drug. This construct could potentially be used in place of the nanoparticle encapsulation of doxorubicin as an alternate method of controlled release. Synthesis of such a construct will be included in future research.

Studying the Release Kinetics of an Amino-oxy Polyglycidol Formaldehyde Prodrug

Initial attempts to study the release kinetics of formaldehyde from this oxime-linked prodrug was met with several challenges. Following formation and removal of solvent, the remaining amino-oxy groups not functionalized with formaldehyde form strong hydrogen bonds

with each other, resulting in a substance that can only be solubilized through the addition of strong acid. The need for acid addition led to the rapid hydrolysis of formaldehyde off of the backbone, and therefore the destruction of the prodrug construct. Future work with this material will focus on increasing the reaction efficiency, thereby reducing the potential for the formation of an insoluble hydrogen bonded material, and eliminating the need for acid addition to solubilize.

Conclusions

We have shown that two types of polyglycidol based prodrugs can be synthesized using either semi-branched polyglycidol or amino-oxy polyglycidol as precursors. Both constructs have been extensively characterized by NMR spectroscopy. The formaldehyde prodrug made via an acetal linkage has been shown to release the formaldehyde in a sustained and pH dependent manner. This prodrug has also been shown to increase the efficacy of doxorubicin by almost 11-fold using 4T1 cells. Future work will focus on exploring the release kinetics of formaldehyde from this amino-oxy polyglycidol prodrug and on its efficacy towards 4T1 cells in combination with doxorubicin.

Experimental

Materials

All reagent materials were purchased from Sigma-Aldrich (St. Louis, MO) and were used as received unless otherwise specified. Materials used for the MTT assay were purchased from Life Technologies. Spectra/Por® dialysis membrane was purchased from Spectrum Laboratories Inc. Glycidol was purified after receipt by vacuum distillation.

Synthesis of Polyglycidol

A 25 mL round-bottom flask was flame-dried and purged with nitrogen. A catalytic amount (9.0 mg, 2.16 x 10^{-5} mol, 3.2 x 10^{-4} eq.) of tin triflate was added to the bottom of the round-bottom flask, and then the flask was again purged with nitrogen. The flask was equipped with a nitrogen balloon, and the 3-methyl-1-butanol initiator (136.0 μL, 1.25 mmol, 1.0 eq.) was then added to the flask and the mixture was allowed to stir at room temperature for 30 minutes. The reaction flask and the distilled glycidol monomer were then cooled to 0ºC. The glycidol monomer (4.50 mL, 67.5 mmol, 54.0 eq) was added to the reaction mixture at 0ºC dropwise over the course of 20 minutes. After monomer addition was complete, the reaction was allowed to come to room temperature and then stirred overnight. The reaction was quenched with excess methanol and then purified by precipitation into ethyl acetate. ^{1}H NMR (600 MHz, MeOD) δ: 0.92 (6H, d, CH3), 1.48 (2H, q, CH2), 1.72 (1H, m, CH), 3.39-3.98 (5H, m, CH_2CHCH_2). ^{13}C-IG NMR (150 MHz, MeOD) δ: 61.3, 61.8, 63.0, 69.3, 69.6, 70.5-71.9, 72.6, 78.6, 80.1, 81.8.

Synthesis of Polyglycidol Formaldehyde Prodrug

Polyglycidol (500 mg, 0.480 mmol, 1.0 eq) was dissolved in methanol to a concentration of 250 mg/mL and transferred to a 6-dram vial equipped with a stir bar. A 37% formaldehyde solution (214 μL, 2.881 mmol, 6.0 eq) was added to the reaction vial, and the mixture was stirred at room temperature for 1 hour. Methanol was removed via rotary evaporation and water was removed via lyophilization. ^{1}H NMR (600 MHz, MeOD) δ: 0.92 (6H, d, CH3), 1.48 (2H, q, CH2), 1.72 (1H, m, CH), 3.39-3.98 (5H, m, CH_2CHCH_2), 4.74 (2H, s, CH2). ^{13}C-IG NMR (150 MHz, MeOD) δ: 61.3, 61.8, 63.0, 69.3, 69.6, 70.5-71.9, 72.6, 78.6, 80.1, 81.8, 90.6.

In-vitro Release of Formaldehyde from Polyglycidol Formaldehyde Prodrug

The in-vitro release of formaldehyde from the prodrugs was determined using Float-A-Lyzer® dialysis tubing (MWCO: 0.1K-0.5K). A sample of the polyglycidol formaldehyde prodrug (50.0 mg, 2.18 mg formaldehyde total) was suspended in 1.0 mL of either acetate buffer (Sodium acetate/acetic acid, pH 5.0) or PBS (pH 7.4) and transferred to a Float-A-Lyzer® dialysis pod. The pod was then placed in a 50-mL Falcon tube containing 18.0 mL of the corresponding buffer solution. Falcon tubes were placed in an oil bath at 37^{o}C and media was stirred constantly using a magnetic stir bar. Samples of 100 μL were withdrawn from the sink at specified intervals. An equal amount of fresh media was added to the sink after each withdrawal to maintain sink conditions. The amount of formaldehyde released at each time point was quantified using a colorimetric assay as described below.

Colorimetric Analysis of Formaldehyde Concentration

A 50 μL aliquot of sample was placed in the well of a 96-well plate and 50 μL of 2mM $NaIO_4$ in 0.2M NaOH was added to the sample. The plate was then incubated for 20 minutes at room temperature in the dark. After 20 minutes, 100 μL of a 34mM solution of 4-amino-3-hydrazino-5-mercapto-1,2,4-triazole (Purpald®) in 2M NaOH was added to the sample and incubated at room temperature for 20 minutes. Final color development was achieved via the addition of 33mM $NaIO_4$ in 0.2M NaOH, and absorbance was read at 550 nm using a plate reader. All reagent solutions were made with cell culture grade water.

Studying the Effect of Doxorubicin and Polyglycidol Formaldehyde Prodrugs using 4T1 Cells

4T1 cells were trypsinized and then resuspended in full culture medium (RPMI Medium 1640, 10% bovine serum, 1% penicillin/streptomycin) to a concentration of 425,000 cells/mL. Cells were then seeded onto a 96-well plate at a concentration of 10,200 cells/well and incubated at 37^{o}C, 5% CO_2 for 3 hours to allow for attachment to the surface. After 3 hours, media was aspirated and cells were treated with either free doxorubicin (0.1 μg/mL), doxorubicin (0.1 μg/mL) and formalin (0.01 μg/mL formaldehyde), or doxorubicin (0.1 μg/mL) and a polyglycidol formaldehyde prodrug (0.01 μg/mL formaldehyde) and then incubated for 24 hours. After 24 hours, the drug solutions were carefully aspirated and cells were washed with 150 μL of PBS. 150 μL of MTT reagent (500 μg/mL) was then added to each well and cells were incubated for 3 hours. Following the incubation period, all but 25 μL of the MTT reagent was removed, and 50 μL of DMSO was added to each well to solubilize the formazan crystals. The absorbance of the plate was then read at 540 nm using a Synergy Biotek plate reader.

Encapsulation of Doxorubicin into Polyester Nanoparticles

Polyester nanoparticles (8.5% EVL, 4.4% AVL, 58.1 mg) and doxorubicin (10.1 mg) were mixed with 100 μL of DMSO in an Eppendorf tube until a homogenous solution was formed. A solution of 1.0% D-α-Tocopherol polyethylene glycol 1000 succinate (290.5 mg) was prepared by dissolving it into 29.05 mL of cell culture grade water. The DMSO mixture was then precipitated into the rapidly vortexing aqueous solution, and the mixture was transferred to a Falcon tube. The mixture was centrifuged for 20 minutes at 7830 rpm and then decanted. The pellet was washed with cell culture water, and then centrifuged again at 7830 rpm for 20

minutes. Again the solution was decanted and the pellet was resuspended in 5.0 mL of cell culture grade water and lyophilized to obtain doxorubicin-loaded nanoparticles. The loading of doxorubicin in the nanoparticles was determined by UV-Vis.

Synthesis of Phthalimide Functionalized Polyglycidol

A 100 mL round-bottom flask was flame-dried and purged with nitrogen, then equipped with a nitrogen balloon. Purified polyglycidol (4.43 g, 2.22 x 10^{-3} mol, 1.0 eq) was dissolved in anhydrous DMF to a concentration of 0.0444 M, and then added to the reaction flask via syringe. N-hydroxyphthalimide (6.99 g, 0.0425 mol, 19.2 eq.) and triphenylphosphine (11.24 g, 0.0425 mol, 19.2 eq.) were added to the reaction flask sequentially. Diisopropyl azodicarboxylate (8.35 mL, 0.0425 mol, 19.2 eq.) was then added dropwise through the septum and the reaction mixture was allowed to stir at room temperature overnight. After reaction completion, DMF was removed via high vacuum rotary evaporator. The concentrated reaction mixture was resuspended in dichloromethane and precipitated twice into a 50/50 (v/v) mixture of ethyl acetate and diethyl ether. Percent functionalization of the polyglycidol was calculated by comparing the integration of the polyglycidol backbone peaks from 3.08-4.29 ppm to the aromatic proton peak from the phthalimide at 7.72 ppm. ^{1}H NMR (400 MHz, d-DMSO) δ: 0.92 (6H, d, CH3), 1.48 (2H, q, CH2), 1.72 (1H, m, CH), 3.08-4.29 (5H, m, CH_2CHCH_2), 4.29-5.09 (1H, m, OH), 7.51-7.88 (4H, m, CH).

Synthesis of Amino-oxy Polyglycidol

A 200 mL round-bottom flask was flame-dried and purged with argon, then equipped with an argon balloon. The phthalimide functionalized polyglycidol (7.24 g, 3.62 x 10^{-3} mol, 1.0 eq.) was dissolved in anhydrous tetrahydrofuran and added to the reaction flask through the septum. An

equivalent volume of anhydrous methanol was then added to the reaction flask. An excess of hydrazine (7.32 mL, 64.3 eq) was then added to the flask dropwise and the reaction was allowed to stir overnight. Unreacted hydrazine was removed via high vacuum rotary evaporator. The phthalimide byproduct was removed by filtration through a 0.45 micron syringe filter followed by dialysis against distilled water, and then methanol using Spectra/Por Dialysis Tubing with a 1,000 MWCO. ^{1}H NMR (600 MHz, MeOD) δ: 0.87 (6H, d, CH3), 1.42 (2H, q, CH2), 1.66 (1H, m, CH), 3.45-4.28 (5H, m, CH_2CHCH_2). ^{13}C-IG NMR (150 MHz, MeOD) δ: 63.8, 69.3, 70.2, 71.7, 73.2, 76.3, 77.5, 78.2, 79.1

Synthesis of Amino-oxy Polyglycidol Formaldehyde Prodrug

Amino-oxy polyglycidol (180 mg, 81.4 μmol, 1.0 eq) was dissolved in methanol to a concentration of 180 mg/mL and transferred to a 6-dram vial equipped with a stir bar. A 37% formaldehyde solution (3.45 mL, 46.3 mmol, 25 eq/oxime) was added to the reaction vial, and the mixture was stirred at room temperature for 1.5 hours. Methanol was removed via rotary evaporation and water was removed via lyophilization. ^{1}H NMR (600 MHz, MeOD) δ: 0.87 (6H, d, CH3), 1.42 (2H, q, CH2), 1.66 (1H, m, CH), 3.45-4.28 (5H, m, CH_2CHCH_2), 6.51 (1H, s, CH2), 7.07 (1H, s, CH2). ^{13}C-IG NMR (150 MHz, MeOD) ^{13}C-IG NMR (150 MHz, MeOD) δ: 64.5, 70.0, 70.6, 71.2, 72.5, 73.9, 74.7, 76.1, 77.9, 79.1, 79.8, 139.0

References

1. Melero, I.; Berman, D. M.; Aznar, M. A.; Korman, A. J.; Perez Gracia, J. L.; Haanen, J., Evolving synergistic combinations of targeted immunotherapies to combat cancer. *Nature Reviews Cancer* **2015,** *15* (8), 457-72.

2. Richards, T. R.; Tobe, S. W., Combining other antihypertensive drugs with beta-blockers in hypertension: a focus on safety and tolerability. *Canadian Journal of Cardiology* **2014,** *30* (5 Suppl), S42-6.

3. Stuart, W. H., Combination therapy for the treatment of multiple sclerosis: Challenges and opportunities. *Current Medical Research and Opinion* **2007,** *23* (6), 1199-1208.

4. Lehar, J.; Krueger, A. S.; Avery, W.; Heilbut, A. M.; Johansen, L. M.; Price, E. R.; Rickles, R. J.; Short, G. F., 3rd; Staunton, J. E.; Jin, X.; Lee, M. S.; Zimmermann, G. R.; Borisy, A. A., Synergistic drug combinations tend to improve therapeutically relevant selectivity. *Nature Biotechnology* **2009,** *27* (7), 659-66.

5. Wegiel, B.; Gallo, D.; Csizmadia, E.; Harris, C.; Belcher, J.; Vercellotti, G. M.; Penacho, N.; Seth, P.; Sukhatme, V.; Ahmed, A.; Pandolfi, P. P.; Helczynski, L.; Bjartell, A.; Persson, J. L.; Otterbein, L. E., Carbon monoxide expedites metabolic exhaustion to inhibit tumor growth. *Cancer Research* **2013,** *73* (23), 7009-21.

6. Sciorati, C.; Buono, R.; Azzoni, E.; Casati, S.; Ciuffreda, P.; D'Angelo, G.; Cattaneo, D.; Brunelli, S.; Clementi, E., Co-administration of ibuprofen and nitric oxide is an effective experimental therapy for muscular dystrophy, with immediate applicability to humans. *British Journal of Pharmacology* **2010,** *160* (6), 1550-60.

7. Li, W. P.; Su, C. H.; Tsao, L. C.; Chang, C. T.; Hsu, Y. P.; Yeh, C. S., Controllable CO Release Following Near-Infrared Light-Induced Cleavage of Iron Carbonyl Derivatized Prussian Blue Nanoparticles for CO-Assisted Synergistic Treatment. *ACS Nano* **2016,** *10* (12), 11027-11036.

8. Cai, L.; He, L.; Wang, Y.; Zhong, J.; Zhao, C.; Zeng, S.; Yu, J.; Bian, Y.; Wei, Y.; Cai, W.; Long, E.; Jiao, P.; Yan, J.; Xu, Q., Efficient cocktail chemotherapy by co-delivery of a

hydrogen sulfide-releasing aspirin prodrug and paclitaxel via single nanoparticles. *RSC Advances* **2017,** *7* (22), 13458-13466.

9. Fan, W.; Lu, N.; Huang, P.; Liu, Y.; Yang, Z.; Wang, S.; Yu, G.; Liu, Y.; Hu, J.; He, Q.; Qu, J.; Wang, T.; Chen, X., Glucose-Responsive Sequential Generation of Hydrogen Peroxide and Nitric Oxide for Synergistic Cancer Starving-Like/Gas Therapy. *Angewandte Chemie International Edition* **2017,** *56* (5), 1229-1233.

10. Tesei, A.; Brigliadori, G.; Carloni, S.; Fabbri, F.; Ulivi, P.; Arienti, C.; Sparatore, A.; Del Soldato, P.; Pasini, A.; Amadori, D.; Silvestrini, R.; Zoli, W., Organosulfur derivatives of the HDAC inhibitor valproic acid sensitize human lung cancer cell lines to apoptosis and to cisplatin cytotoxicity. *Journal of Cellular Physiology* **2012,** *227* (10), 3389-96.

11. Evison, B. J.; Bilardi, R. A.; Chiu, F. C.; Pezzoni, G.; Phillips, D. R.; Cutts, S. M., CpG methylation potentiates pixantrone and doxorubicin-induced DNA damage and is a marker of drug sensitivity. *Nucleic Acids Research* **2009,** *37* (19), 6355-70.

12. Swift, L. P.; Rephaeli, A.; Nudelman, A.; Phillips, D. R.; Cutts, S. M., Doxorubicin-DNA adducts induce a non-topoisomerase II-mediated form of cell death. *Cancer Research* **2006,** *66* (9), 4863-71.

13. Swift, L. P.; Cutts, S. M.; Nudelman, A.; Levovich, I.; Rephaeli, A.; Phillips, D. R., The cardio-protecting agent and topoisomerase II catalytic inhibitor sobuzoxane enhances doxorubicin-DNA adduct mediated cytotoxicity. *Cancer Chemotherapy and Pharmacology* **2008,** *61* (5), 739-49.

14. Sisson, A. L.; Haag, R., Polyglycerol nanogels: highly functional scaffolds for biomedical applications. *Soft Matter* **2010,** *6* (20), 4968.

15. Lockhart, J. N.; Beezer, D. B.; Stevens, D. M.; Spears, B. R.; Harth, E., One-pot polyglycidol nanogels via liposome master templates for dual drug delivery. *Journal of Controlled Release* **2016,** *244* (Pt B), 366-374.

16. Koehler, J.; Kuehne, A. J. C.; Piermattei, A.; Qiu, J.; Keul, H. A.; Dirks, T.; Keul, H.; Moeller, M., Polyglycidol-based metal adhesion promoters. *Journal of Materials Chemistry B* **2015,** *3* (5), 804-813.

17. Lukowiak, M. C.; Wettmarshausen, S.; Hidde, G.; Landsberger, P.; Boenke, V.; Rodenacker, K.; Braun, U.; Friedrich, J. F.; Gorbushina, A. A.; Haag, R., Polyglycerol coated polypropylene surfaces for protein and bacteria resistance. *Polymer Chemistry* **2015,** *6* (8), 1350-1359.

18. de la Croix Ndong, J.; Stevens, D. M.; Vignaux, G.; Uppuganti, S.; Perrien, D. S.; Yang, X.; Nyman, J. S.; Harth, E.; Elefteriou, F., Combined MEK inhibition and BMP2 treatment promotes osteoblast differentiation and bone healing in Nf1Osx -/- mice. *Journal of Bone and Mineral Research* **2015,** *30* (1), 55-63.

19. Beezer, D. B.; Harth, E., Post-Polymerization Modification of Branched Polyglycidol with N-Hydroxy Phthalimide to Give Ratio-Controlled Amino-Oxy Functionalized Species. *Journal of Polymer Science Part A: Polymer Chemistry* **2016,** *54* (17), 2820-2825.

APPENDIX I

OPTIMIZATION EXPERIMENTS

Synthesis of Poly (VL/OPD)

Initial attempts at synthesis of this polymer were met with challenges, mainly achieving a high incorporation of the OPD monomer into the backbone chain concurrently with a molecular weight comparable to the target. Table 1 shows the results of the first synthesis attempts.

Table AI-1. Initial Results of Synthesis of Poly (VL/OPD)

Monomer feed ratio (VL:OPD)	Target M_n (Da)	Monomer concentration (M)	Length of dialysis purification	Polymer composition (VL:OPD)	M_n NMR (Da)	Yield (%)
80:20	3000	3.3	2.5 days	90:10	2094	22.8
90:10	3000	3.3	2.5 days	95:5	2579	9.0
80:20	3000	neat	1 day	91:9	2472	42.2
60:40	3000	neat	1 day	90:10	1339	27.7

*All reactions were run in dichloromethane at room temperature.

The first two entries in this table show that under the chosen starting conditions, only 50% of the OPD monomer is successfully incorporated into the chain, resulting yields are low, and molecular weights are below target values. Entry 3 shows an attempt to both increase the incorporation of the OPD and increase the yield by eliminating the solvent and reducing the purification time. The reduced purification time does lead to a higher yield, however concentrating the reaction does not aid in the OPD incorporation. Attempts at increasing the monomer feed ratio to incorporate more of the OPD monomer are unsuccessful (entry 4) and only serve to reduce both the molecular weight of the resulting polymer and the reaction yield.

Failure to increase the incorporation by increasing the monomer feed ratio suggest the presence of competing reactions that are responsible for consuming the OPD monomer before it can participate in the polymerization. The initial synthesis procedure included dissolving the 2-oxepane-1,5-dione (OPD) monomer in the **δ**-valerolactone (VL) prior to addition to the reaction. NMR analysis of this mixture after 45 minutes of mixing shows clear signs of spontaneous ring opening polymerization before addition to the reaction vessel (Figure 1). The sequestration of the

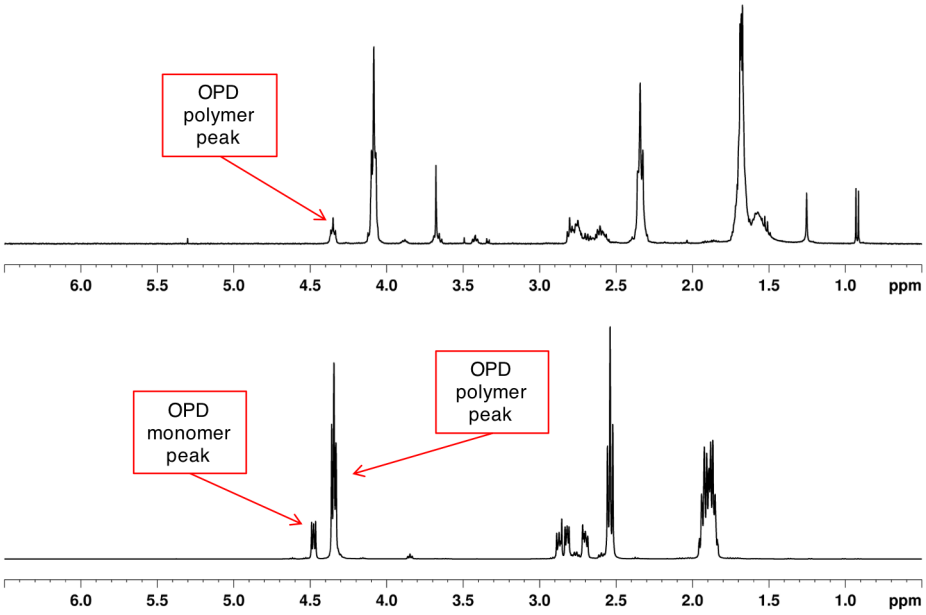

Figure AI-1. A representative ^{1}H NMR spectrum of a VL/OPD polymer (top), and an ^{1}H NMR spectrum of a mixture of VL and OPD before addition to the reaction (bottom). Polymer peaks and monomer peaks are indicated by arrows.

OPD monomer into these short chains prior to the reaction is a likely cause of both the low incorporation and of the below target molecular weights.

Additional NMR analysis of the crude product of a polymerization of VL and OPD shows a second side reaction that is contributing to the low incorporation of the OPD and the low observed molecular weights. Allyl peaks in the crude spectrum indicate degradation of polymer chains ending in an OPD unit, leading to chain scission and formation of shorter molecular

weight polymers or oligomers (Figure 2). This observation in addition to the spontaneous polymerization are the two likely reasons for the challenges seen in initial syntheses of this polymer.

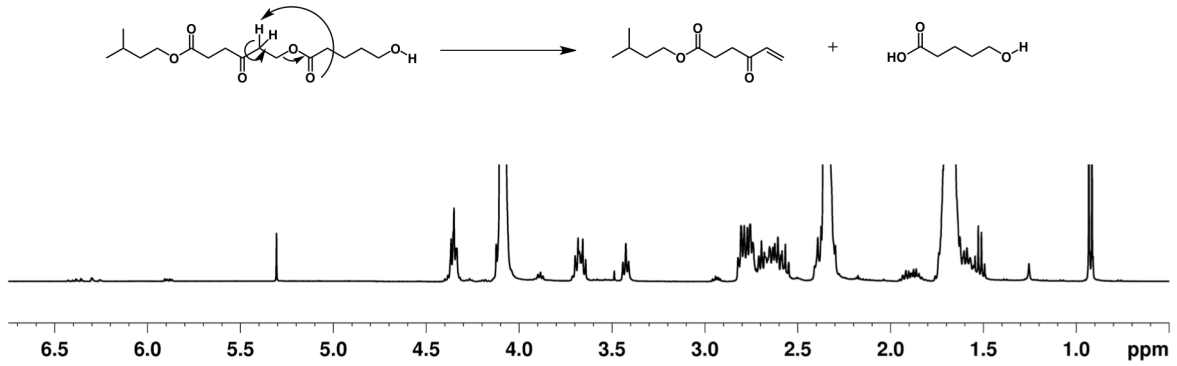

Figure AI-2. Reactions run at room temperature lead to the heat-induced degradation of polymer chains containing OPD units. This degradation gives rise to the allylic peaks seen at 5.9 and 6.35 ppm in the NMR spectrum.

To combat both of these obstacles, reactions were performed at lower temperature (0^{o}C), and monomers were added separately to the reaction vessel. Both measures together led to an increase in the incorporation of the OPD monomer from 50 to 66%, as well as an increase in the molecular weight of the polymer significant enough to now be comparable to the targeted molecular weight (Table 2).

Table AI-2. Results of Synthesis of Poly (VL/OPD) with Implemented Improvements

	% VL	% OPD	M_n (Da)
Targeted	80.0	2.0	4000
Observed	86.7	13.3	4131

Final optimization of this synthesis was performed by analysis of the purification time. As seen in Table 1, dialysis performed over a period of one day was able to achieve a yield of just over 40%. It may be that one day is not the minimum time needed to achieve acceptable

purity of the polymer, and yield may be increased by decreasing the dialysis time. To study this, a reaction was performed using an 80:20 monomer feed ratio (VL/OPD) at a monomer concentration of 5.6M in DCM beginning at 0^{o}C and then dialyzed in two hour intervals upon completion and analyzed by GPC. The results of this analysis are outlined in Table 3. As an acceptable PDI is reached after 6 hours, along with an acceptable yield, this purification time was used for all further polymerizations.

Table AI-3. Optimization of Dialysis Purification Time

Hours of dialysis	Yield (mg)	PDI
0	850 (85%)	1.33
2	725 (72.5%)	1.15
4	650 (65%)	1.14
6	600 (60%)	1.10

LIVE/DEAD Staining of 3T3 Cells on an Oxime Click Hydrogel

The original experimental design for testing the biocompatibility of the oxime click hydrogel structures involved seeding the cells directly onto the hydrogel material. Initial tests found that these hydrogels exhibit auto-fluorescence in the red channel, making direct seeding of the cells impossible if LIVE/DEAD staining is to be used as a characterization technique for

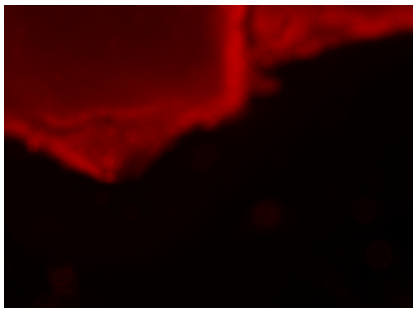

Figure AI-3. Oxime click hydrogels exhibit auto-fluorescence in the red channel.

determining biocompatibility. Figure 3 shows the fluorescence image of an oxime click hydrogel in the red channel. As direct seeding onto the surface was not possible, biocompatibility experiments were performed by overlaying the hydrogel structure with cells growing on TCPS for a set amount of time and then removing the gel structure before imaging.

Determination of Formaldehyde Concentration using a Purpald Assay

Past literature indicates that the Purpald assay can be used to determine the concentration of formaldehyde in a solution and can be run either with or without an oxidizing agent present, depending on sensitivity needs. Using formalin as a model for released formaldehyde, solutions of known concentration were subjected to the Purpald assay both with and without the additional oxidizing step to determine the benefit, if any, of adding this additional measure to the assay. The results of these tests are outlined in Table 4. Values shown in the body of the table are absorbance values at 550 nm. Samples subjected to oxidation before treatment with the Purpald reagant were treated with 2 mM sodium periodate for 20 minutes.

Table AI-4. Determination of Optimum Conditions for Purpald Analysis of Formaldehyde Concentration

Formaldehyde concentration (M)	(-) oxidation step	(+) oxidation step
0.01	0.223	0.458
0.025	0.211	0.666
0.05	0.248	1.28
0.1	0.222	2.832
0.25	0.471	3.207
0.4	3.679	Out of range

As can be seen from Table 4, absorbance values for the set of samples pretreated with an oxidizing agent are both higher and more consistent with the expected linear trend. As such, this

oxidation step was chosen to be included as part of the analysis of all formaldehyde samples from release studies.